ELECTROCHEMICAL IMMUNOSENSORS

KOH GUIWAN

B.Sc. (Hons), NUS

A THESIS SUBMITTED

FOR THE DEGREE OF MASTERS OF SCIENCE

DEPARTMENT OF CHEMISTRY

NATIONAL UNIVERSITY OF SINGAPORE

2008

ACKNOWLEDGEMENTS

I thank God for strength and wisdom. I am grateful to Dr Toh Chee-Seng for his invaluable guidance and opportunities given to participate in various international conferences. In addition, I would like to thank Professor Ng Mah Lee, Mary for providing the West Nile Virus domain III protein and particles for the research. I am indebted to the National University of Singapore and its staffs for providing the facilities, assistance, and funding for the research as well as my scholarship. I also would like to express my gratitude to the following people: Yin, Binh, Dr Yuan Hong, Pui Sze, Ridha, He Lin, Shuchi and Hui Si. Finally, I would like to thank my mother and my sister for their support and prayers.

TABLE OF CONTENTS

SUMMARY

The development of a membrane-based electrochemical immunosensor is described in this thesis. Nanoporous alumina was directly fabricated onto the tip of a home-made platinum disk electrode using a novel pipette anodization technique. Immunoglobulin G (IgG) and bovine serum albumin (BSA) was next immobilized along the porous alumina nanochannel walls and the alumina-modified platinum disk electrode was subsequently used for glucose oxidase (GOx) detection, in the presence of a redox probe, ferrocenemethanol. Upon binding the complementary GOx to IgG, formation of the antigen–antibody complexes blocked the approach of ferrocenemethanol towards the exposed platinum surface beneath the alumina layer, resulting in a signal-off immunosensor. The constructed immunosensor proved to be highly sensitive and selective and has a low detection limit of 100 ng L^{-1} for GOx. The same sensor configuration was used for determination of West Nile Virus domain III protein (WNV D-III) and particles by immobilising it with immunoglobulin M (IgM) and BSA. Again, the prepared immunosensor was highly sensitive and low detection limits of 7 ng L^{-1} and 3 particles mL^{-1} was achieved for WNV-DIII and viral particles, respectively. The potential of the immunosensor for real sample detection was evaluated by conducting WNV particles detection in blood serum.

Finally, the activity of IgG-bound GOx adsorbed on glass and gold substrates was studied using scanning electrochemical microscopy (SECM). Feedback curves were obtained and the data were fitted to calculate the apparent heterogeneous rate constants as well as turnover numbers of IgG-bound GOx.

LIST OF TABLES

Table 1. Comparison of total pore areas (1- θ) calculated from equation (2) and maximum total pore areas (1- θ)$_{max}$ determined from SEM measurements of pore size and pore density of alumina films.

Table 2. K and r^2 values obtained from Langmuir plots of WNV-DIII protein calibration plots obtained upon variation of different parameters investigated.

Table 3. Average apparent rate constants and turnover number for heterogeneous glucose oxidase-mediator reaction at different concentrations of mediator and IgG.

LIST OF FIGURES

buffered solution of 1 mM ferrocenemethanol (pH 6.8). Average background noise of 3 consecutive DPV after each step of the experiment was in the range of ± 0.1 to ± 1.6 nA.

Figure 20. DPV signal response towards the redox probe, ferrocenemethanol for an immunosensor prepared using 0.4 mg L^{-1} anti-GOx and 200 mg L^{-1} BSA over varying concentrations of GOx. Immunosensors were derived from alumina electrodes etched for 0, 30 and 60 min in 3% phosphoric acid solutions. Concentration of ferrocenemethanol used was 1 mM and all experiments were conducted at 297 K.

Figure 21. Scanning electron micrographs of side profiles of alumina overlayers etched in 3% phosphoric acid for (A) 15, (B) 30, (C) 45 and (D) 60 min. The pores of the outer films show extensive merging with poorly defined shapes. Pore sizes of the inner film estimated from SEM micrographs were (A) 20–50 nm (B) 25–70 nm (C) 30–75 nm and (D) 30–100 nm. Pore densities of inner films range from 5.9×10^9 to 7×10^9 pores cm^{-2} for (B), (C) and (D).

Figure 22. Plots of $(\delta i)_{\max}$ against $(1 - \sigma)/(1 + \sigma)$ obtained by varying DPV pulse amplitude from 10 to 130 mV with a pulse width of 50 ms in an unstirred solution containing 1mM ferrocenemethanol at 297 K. Relative standard deviation of $(\delta i)_{\max}$ ranges from ± 4.2% for 10 mV pulse amplitude to ± 22.7% for 130 mV pulse amplitude. Inset: variation of $AD^{1/2}$ with respect to types of alumina electrodes immobilized with IgG, IgG/BSA or IgG/BSA/antigen, derived from slopes and slope errors of best-fit lines through the plots presented in this figure.

Figure 23. A 17 Å structure of West Nile virus determined by cryo-EM. (**A**) A surface shaded view of the virus. (**B**) A central cross section showing the concentric layers of density [7]. From Mukhopadhyay S., Kim B.-S., Chipman P. R., Rossmann M. G., Kuhn R. J., *Science* **2003**, 302, 248. Reprinted with permission from AAAS.

Figure 24. (A) DPV signal response obtained at a 60 min etched alumina electrode immersed in 1 mM ferrocenemethanol, after each step of the sensor preparation procedure. (B) DPV signal response of an immunosensor towards ferrocenemethanol in increasing concentration of WNV-DIII protein, with corresponding decrease in signal response for an immunosensor prepared similarly as in (A).

Figure 25. DPV signal responses of four different alumina electrodes prepared using IgM (IgM-alumina electrode), BSA (BSA-alumina electrode) and IgM/ BSA (IgM-BSA-alumina electrode) or no adsorbed biomolecule (alumina electrode). Controls were studied over the antigen concentration range of 0.007 to 0.053 ng mL^{-1} in 1 mM ferrocenemethanol solution at pH 6.8 and an ionic strength of 1.7 M. All alumina electrodes used were etched in 3% phosphoric acid for 60 min. 0.2 µg mL^{-1} IgM solution and 200 mg mL^{-1} BSA solution were used for immobilisation of either or both proteins for the alumina electrodes. All experiments were conducted at 297 K.

Figure 26. Plots of normalised current against (A) concentration and (B) log of concentration of WNV-DIII protein for different concentrations of IgM used. When a high concentration of 0.4 µg mL^{-1} IgM was used, a lower limit of detection and a narrow linear range was obtained. At lower concentration of 0.1 µg mL^{-1} IgM, a higher limit of detection and a wide linear range was achieved. Thus, to have a

compromise between these two figures of merit, 0.2 μg mL^{-1} IgM was utilised. Sensing solution was 1 mM ferrocenemethanol in 100 mM phosphate buffer (pH 6.8) with an ionic strength of 1.7 M. All alumina electrodes used were etched in 3% phosphoric acid for 60 min.

Figure 27. (A) Percentage decrease in observed current upon IgM immobilization at various pH values. The larger decrease in observed current indicates higher loading of IgM molecules onto the surface of the alumina membrane and within the alumina nanopores. (B) DPV signal responses towards redox probe in the presence of increasing antigen concentration using alumina electrode adsorbed with IgM from solutions of different pH and in sensing solutions of different pH. 1 mM ferrocenemethanol, prepared in 100 mM phosphate buffer with 1.7 M ionic strength solutions were used as the sensing solution.

Figure 28. DPV signal responses towards redox probe, prepared in phosphate buffers of different ionic strengths, in the presence of increasing antigen concentration using alumina electrode adsorbed with IgM from solutions of different ionic strengths. 1 mM ferrocenemethanol, prepared in 100 mM phosphate buffer (pH 6.8) was used as the sensing solution. Sodium chloride salt was employed to control of ionic strengths of the prepared buffers.

Figure 29. DPV signal response towards the redox probe for an immunosensor prepared using 0.2 μg L^{-1} IgM and 200 mg L^{-1} BSA over varying concentrations of WNV-DIII protein. Immunosensors were derived from alumina electrodes etched for 0, 30 and 60 min in 3% phosphoric acid solutions. Sensing solution was 1 mM ferrocenemethanol, prepared in pH 6.8 phosphate buffer with ionic strength of 1.7 M.

Figure 30. DPV signal response towards the redox probe for an immunosensor prepared using 0.2 μg L^{-1} IgM and 200 mg L^{-1} BSA over varying concentrations of WNV particles. Immunosensors were derived from alumina electrodes etched for 0, 30 and 60 min in 3% phosphoric acid solutions. Sensing solution was 1 mM ferrocenemethanol, prepared in pH 6.8 phosphate buffer with ionic strength of 1.7 M.

Figure 31. Reproducibility (A) across different batches of sputtered electrodes and (B) within a single batch of electrodes sputtered with aluminum simultaneously. Standard deviations in the range of 2% to 10% and a low limit of detection of 7 ng mL^{-1} were obtained.

Figure 32. Reproducibility of the prepared IgM-BSA-alumina electrodes applied in the detection of WNV particles. Standard deviations in the range of 2% to 6% and a low limited of detection of ca. 3 viral particles mL^{-1} were obtained.

Figure 33. Plots of the normalized DPV signal response against logarithmic function of WNV-DIII protein concentration (A) within a single batch and (B) across different batches of fabricated electrodes. Calibration plots were obtained using alumina modified electrodes etched for 60 min in 3% phosphoric acid. Sensing solution was 1 mM ferrocenemethanol, prepared in pH 6.8 phosphate buffer with ionic strength of 1.7 M.

LIST OF SYMBOLS

α	Electrochemical transfer coefficient
ΔE_p	Peak to peak separation in a cyclic voltammogram
$\Delta \mathrm{E}$	Pulse amplitude
Λ	$k'_f d/D_R$
Γ_{enz}	Surface coverage of the enzyme
σ	$\exp(-nF\Delta E/2RT)$
θ	Surface coverage of the blocking film in Chapter II and the fraction of filled effective binding sites in Chapter V
κ	$k'_f a/D$
$(\tau - \tau')$	Pulse duration
$(\delta i)_{max}$	Maximum peak height or DPV signal response
a	Radius of ultramicroelectrode
A	Electrode area
C	Concentration of redox species
C_{bulk}	Bulk concentration of ferrocenemethanol
d	Probe tip-substrate separate
D	Diffusion coefficient of ferrocenemethanol
D_R	Diffusion coefficient of the reduced mediator in water
E^0	Formal potential for a reversible redox couple
$E^{0'}$	Standard formal potential for a reversible redox couple
$E_{1/2}$	Observed mid potential between oxidation and reduction peaks for a reversible redox couple
$E_{p,a}$	Anodic peak potential

F	Faraday constant
$\mathrm{F}(L, \Lambda)$	$(11/\Lambda + 7.3)/(110-40L)$.
i_{p}	Peak current
$i_{\mathrm{p,a}}$	Anodic peak current
$i_{\mathrm{p,c}}$	Cathodic peak current
$I_{\text{anti-GOx}}$	Signal response of electrode in the presence of anti-GOx
I_{GOx}	Signal response of electrode in the presence of GOx
$I_{\mathrm{GOx}}/I_{\text{anti-GOx}}$	Signal response normalised against signal response of electrode immobilised with only anti-GOx
$I_{\mathrm{GOx}}/I_{\text{anti-GOx/BSA}}$	Signal response normalised against signal response of electrode immobilised with only anti-GOx
I_{IgM}	Signal response of electrode in the presence of IgM
$I_{\mathrm{T}}^{\mathrm{c}}(L)$	Normalized ultramicroelectrode probe currents on a conducting substrate
$I_{\mathrm{T}}^{\mathrm{ins}}(L)$	Normalized ultramicroelectrode probe currents on a insulating substrate
$I_{\mathrm{s}}^{\mathrm{k}}$	Substrate current
v	Scan rate
k	Heterogeneous rate constants in Chapter II and k is the proportionality constant in Chapter V
k'_{f}	Apparent heterogeneous rate constant
k^0	Standard rate constant for ferrocenemethanol
k_{cat}	Maximal turnover number

k_d	Diffusion rate constant of mediator comprising the solution diffusion ($k_{d,soln}$) and diffusion within the IgG-GOx multi-layer film ($k_{d,film}$)
k_s	Homogeneous rate constant
K_b	Equilibrium binding constant between IgM and WNV-DIII
K_M	Michaelis-Menten constants
n	Number of electrons transferred at electrode surface
R	Ideal gas constant
t	Time in seconds
T	Temperature in Kelvins

LIST OF ABBREVIATIONS

Ag-Ab	Antigen–antibody complexes
BSA	Bovine serum albumin
C	Nucleocapsid protein
CNT	Carbon nanotubes
CV	Cyclic voltammetry
DPV	Differential pulse voltammetry
E	Envelope protein
EDX	Energy dispersive X-ray analyzer
ELISA	Enzyme-linked immunoassay analysis
FAD	Flavin adenine dinucleotide
FeMeOH	Ferrocenemethanol
GOx	Glucose oxidase
GST	Glutathione S-transferase
IgG	Immunoglobulin G
IgM	Immunoglobulin M
ITO	Indium titanium oxide
LOD	Limit of detection
M	Lipid membrane protein
O	Oxidized species of a redox species
PFU	Plauge forming unit
PSS-PANI	Poly(styrene sulfonate)-polyaniline
QCM	Quartz crystal microbalance
R	Reduced species of a redox species

RSD	Relative standard deviation
RT-PCR	Reverse transcriptase polymerase chain reaction
S/N	Signal-to-noise ratio
SECM	Scanning electrochemical microscopy
SEM	Scanning electron microscopy
UME	Ultramicroelectrode
WNV	West Nile virus
WNV-DIII	West Nile virus domain III

CHAPTER I

INTRODUCTION

According to the IUPAC Compendium of Chemical Terminology, a biosensor is “a device that uses specific biochemical reactions mediated by isolated enzymes, immunosystems, tissues, organelles or whole cells to detect chemical compounds usually by electrical, thermal or optical signals” [8]. In general, a biosensor consists of a biorecognition layer, immobilized onto a suitable substrate and integrated with a transducer that converts biological or biochemical changes detected into readable electrical data [9, 10]. In the construction of biosensors, it is often aimed to enhance a sensor’s performance in one or more of the following figures of merit: sensitivity, selectivity, reproducibility and stability.

When antibodies or antigens are used for biomolecular recognition in bioaffinity-based biosensors, the sensors are known as immunosensors. The fundamental basis for immunosensors is the specific coupling of an antibody to its antigen or vice versa, to form a stable immunocomplex. This is similar to immunoassay methodology, except that modern transducer technology and novel sensing methodologies applied in immunosensors can allow label-free detection and quantification of the detected antigen or antibody [11]. Immunosensors are usually classified by the type of integrated transducer, which are generally electrochemical, optical, thermal or piezoelectric devices [9]. Among the different types, electrochemical immunosensors are particularly attractive due to their specificity, simplicity, low cost, high sensitivity and potential for miniaturization. Electrochemical immunosensors can be further categorized into amperometric, voltammetric or potentiometric sensors depending on whether current is monitored with respect to time or potential, or potential is measured with respect to time, respectively.

Many developed electrochemical immunosensors have already been commercialized and are widely applied in clinical, industrial, environmental and agricultural analyses [12]. Current research and development of electrochemical immunosensors thus focused on innovations and development of novel sensing configurations or strategies to improve specificity, sensitivity, and response time of the sensors.

In this thesis, the development and application of an alumina membrane-based electrochemical immunosensor is described. Electrochemical studies of the fabricated immunosensor and a glucose biosensor, utilising a simple enzyme immobilisation method, are also discussed. Chapter I provides the brief background to the topic of electrochemical immunosensors. Detailed introduction on each sub-topic is provided at the beginning of each following chapter.

Chapter II describes the fabrication of alumina on home-made platinum disk electrodes, via anodization of aluminum. The fabricated nanoporous alumina acts as the substrate onto which the biorecognition elements are immobilised upon. A novel method of aluminum anodization developed in our laboratory is illustrated and explained. Electrochemical and scanning electron microscopy (SEM) studies of the constructed alumina modified platinum disk electrodes are also discussed.

In chapter III, the application of these alumina modified platinum disk electrodes in the detection of glucose oxidase (GOx) enzyme is demonstrated. In the following chapter, the developed immunosensor is further applied for the determination of West Nile Virus (WNV) domain III (D-III) protein as well as WNV particles. Optimisations of the experimental conditions for detection of WNV D-III protein are also discussed. In addition, the potential of the prepared immunosensor for real sample detection is evaluated.

In chapter V, scanning electrochemical microscopy (SECM) studies of immunoglobulin (IgG)-bound glucose oxidase (GOx) enzyme is described and kinetic parameters such as apparent heterogeneous rate constants and turnover numbers were calculated. The subsequent application of the IgG-bound GOx monolayer in a glucose biosensor has also been demonstrated, thus confirming the kinetic calculations.

In the final chapter, the thesis is concluded and further possible research and development of the work described is evaluated.

CHAPTER II

CHARACTERIZATION OF THE BARRIER LAYER OF NANOPOROUS ALUMINA FILMS PREPARED USING TWO DIFFERENT CONTACT CONFIGURATIONS

1. Introduction

1.1. Formation and Structure of Alumina

Nanoporous alumina comprising uniform and regularly spaced pores of nanometer dimension (Figure 1), has attracted great interest as a template material for the fabrication of various nanostructures [13-15]. Its features of uniform pore sizes, high pore density and high aspect ratio, are relatively easy and inexpensive to achieve by comparison to conventional lithographic techniques.

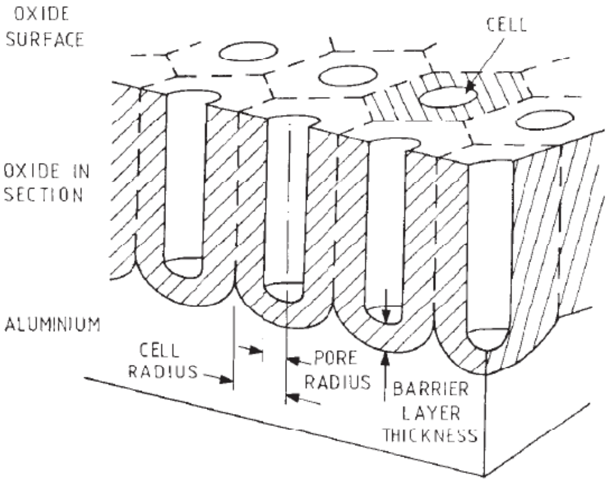

Figure 1. Schematic diagram of porous alumina film formed by anodization of aluminum [1]. Reprinted with permission from Furneaux R. C., Ribgy W. R., Davidson A. P., Nature 1989, 337, 147. Copyright 1989, Nature.

When aluminum films are exposed to air, they react with oxygen in the atmosphere and a thin layer of alumina is formed on the surface of the films. This reaction is driven by the potential difference of ca. 3 V between aluminum and oxygen. However, the layer of alumina form naturally has a limiting thickness and its growth can be artificially extended. This is usually achieved by anodizing aluminum in acidic solutions such as sulfuric acid, phosphoric acid, or oxalic acid [16, 17] and applying a constant voltage in the range of 10 to 100 V or a constant current. In this process, a highly ordered hexagonal prismatic structure with a pore at the centre of each hexagon is formed. Beneath this regular structure is a non-porous alumina barrier layer (Figure 2). Variation in the electrochemical and etching conditions can lead to alumina films of different pore density and pore diameter [16].

The high voltage applied during anodization generates an electric field, which drives aluminum and oxygen ions through the oxide surface layer on the aluminum film and leads to a flow of ionic current. Oxide anions migrate towards the aluminum/oxide interface to react with aluminum, forming alumina:

$$2Al + 3O^{2-} \rightarrow Al_2O_3 + 6e^-$$

Aluminum cations move towards the oxide/electrolyte interface to react with the water, forming alumina as well:

$$2Al^{3+} + 3H_2O \rightarrow Al_2O_3 + 6H^+$$

The circuit is completed by the reduction of hydrogen ions to form hydrogen gas at the cathode, which is usually a platinum mesh or wire electrode:

$$2H^+ + 2e^- \rightarrow H_2$$

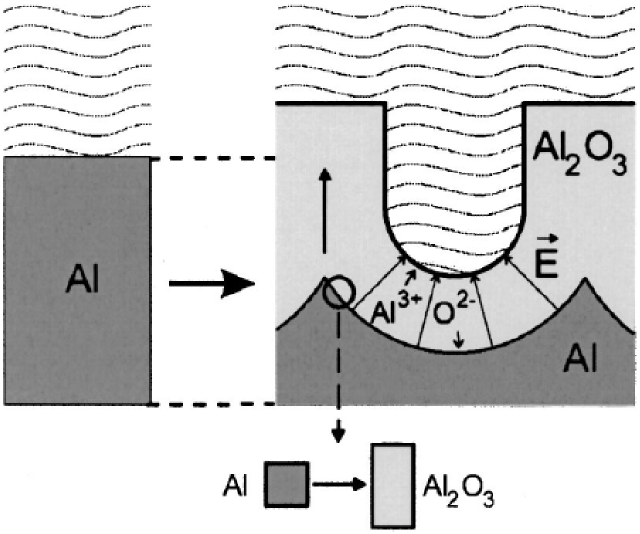

Figure 2. Schematic diagram of alumina film growth. Nanoporous alumina with a thin barrier layer is formed during anodization [2]. Reprinted with permission from Knaack S. A., Redden M., Onelliona M., The American Journal of Physics 2004, 72, 856-9. Copyright 2004, American Institute of Physics.

1.2. Barrier Layer Removal

The necessary formation of the non-porous alumina layer during anodization of aluminum limits several applications in which direct electrodeposition of materials in the alumina pores is required, as the underlying conductive electrode is separated from the solution species by the insulating barrier layer. One method to remove the barrier layer is the chemical etching method [18]. Commonly, nanoporous alumina is first formed from anodization of aluminum metal films and subsequently removed by etching with $HgCl_2$ or $CuCl_2$. The barrier layer is removed from these free-standing films using acids [18]. In a second approach, first described by Furneaux and co-workers, the anodization voltage is stepped down progressively after the porous alumina layer is formed [1]. Another group described reduction of the thickness of the barrier layer by re-anodization of alumina under constant current conditions, which resulted in considerable reduction in the electrical resistance of the barrier layer [19]. These approaches of barrier layer removal were similarly found applicable when the alumina films were formed on conductive surfaces such as those of gold, platinum, carbon and indium titanium oxide (ITO) electrodes, other than base aluminum metal films.

In this work, aluminum coated platinum electrodes were anodized using a novel ‘pipette’ anodization technique (Figure 4), in which the aluminum surface in contact with the anodizing solution, was directly connected to the power supply. This is in contrast with the conventional and commonly used ‘sub-surface’ anodization technique (Figure 5), in which the aluminum overalyer of the electrode was anodized in the anodizing solution via electrical connection to the underside of the overlayer. The physical nature of the barrier layer formed at the alumina-platinum electrode interface was studied using cyclic voltammetry (CV) and scanning electron microscopy (SEM), for alumina modified electrodes prepared using both sub-surface and pipette anodization techniques.

1.3. Cyclic Voltammetry

Cyclic voltammetry (CV) is an electrochemical technique consisting of scanning the potential of a working electrode using a triangular waveform (Figure 3A) and measuring the current resulting from the applied potential [20]. Figure 3B illustrates the expected response of a reversible redox couple during a single potential cycle, assuming that only the oxidized form (O) of the redox species is present initially. A scan in the negative direction is initiated and the observed current will start increasing when the applied potential approaches the reduction potential, E^0 of the redox species. A maximum is reached when any oxidized species (O) that diffuses toward the electrode surface is instantaneously reduced. When the direction of the potential sweep is switched in the opposite direction, the reduced species (R) generated in the forward scan are oxidised back to O, resulting in an anodic peak.

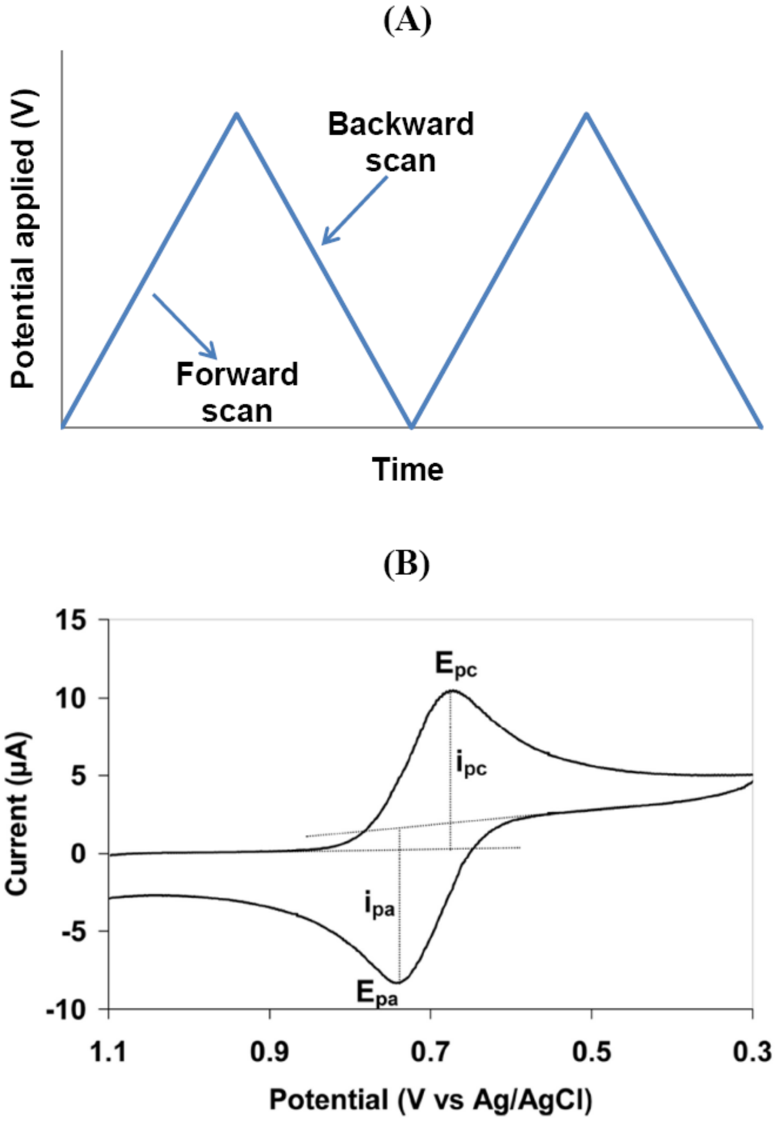

Figure 3. (A) Potential waveform applied during cyclic voltammetry. (B) Expected current response of a reversible redox couple during a single potential cycle, assuming that only the oxidized form (O) of the redox species is present initially [3].

The peak current, i_p for a reversible couple is related to square root of the scan rate, v in the Randles-Sevick equation:

$$i_p = (2.69 x 10^5) n^{3/2} A C D^{1/2} v^{1/2}$$

where n is the number of electrons, A is the electrode area, C is the concentration of redox species, D is the diffusion coefficient and v is the scan rate. The peak potential, E_p is related to the formal potential, E^0 of the redox process according to the equation:

$$E^0 = \frac{E_{p,a} + E_{p,c}}{2}$$

where $E_{p,a}$ is the anodic peak potential and $E_{p,c}$ is the cathodic peak potential. Separation between peak potentials for a reversible couple is given by:

$$\Delta E_p = E_{p,a} - E_{p,c} = \frac{0.059}{n}$$

Thus the peak separation can be used to determine the number of electrons, n, transferred and a rapid one electron redox process will exhibit an ΔE_p of about 59 mV.

Cyclic voltammetry is commonly used for acquiring qualitative information from electrochemical reactions. It is a technique that can provide adequate information on the thermodynamics of redox process, kinetics of heterogeneous electron transfer reactions and on coupled chemical reactions or adsorption processes [20].

2. Experimental

2.1. Materials and Instruments

Electrodes used were either commercial platinum disk electrodes (CH Instruments, 0.2 cm diameter) or home-made platinum disk electrodes (76 μm diameter, 99.99% platinum wire sealed in epoxy resin). Sub-micrometer thick aluminum films were sputter coated over the tip (ca. 3 mm diameter) of the platinum electrodes using high purity aluminum target (99.999%, JEOL Asia), Denton discovery® 18 Sputtering System with a sputtering power of 100 W in an atmosphere of research-grade Ar at 5×10^{-3} Torr for 1.5 hours. Anodization of aluminum coated electrodes was conducted using Apelex electrophoresis power supply model P304 minipac II.

Morphologies and microstructures of anodized specimens were observed using a field emission scanning electron microscope (FEI, XL30-FEG SEM) with an energy dispersive X-ray analyzer (EDX). Measurement of pore sizes and densities on alumina surfaces under varying etching times in 3% phosphoric acid were carried out on alumina coated glass substrates. The anodization set up for these alumina coated glass substrates is the same as that for sub-surface anodization of aluminum-coated electrodes further discussed below in methodology. The aluminium glass slide was connected directly to the positive output of the power supply. All scanning electron microscopy specimens were sputtered with about 20 nm thick gold before observations of morphologies, without which high charging current will caused imaging to be impossible.

Electrochemical behaviours of alumina-modified electrodes were characterized using the cyclic voltammetry technique (CHI440 potentiostat/galvanostat, data acquisition software) in the presence of the redox probe, ferrocenemethanol (FeMeOH, >99% Sigma Aldrich) in 1.0 mM in 0.1 M phosphate buffer solution, pH 6.8), using a three electrode system. All potentials were measured and reported with respect to the silver–silver chloride (saturated KCl) reference electrode and a platinum mesh electrode was used as the counter electrode. Scan rate used for all cyclic voltammograms obtained were 50 mV s^{-1}, unless otherwise stated.

2.2. Methodology

2.2.1. Fabrication of Platinum Disk Electrodes

Homemade electrodes were fabricated using epoxy resin (RS Components Pte Ltd), micropipette tips and 99.99% platinum wire (76 μm diameter, Sigma Aldrich). The platinum wire was aligned in the center of the micropipette tips and sealed within epoxy resin. The platinum wire was subsequently soldered to a copper wire and the connection was sealed with epoxy resin. The fabricated platinum wire electrodes were polished with 1.0 μm and 0.3 μm diameter alumina slurry and sonicated in ultrapure water with resistivity of more than 18 Ω (Barnstead Nanopure Ultrapure Water System), before aluminum was deposited onto the electrode tips.

2.2.2. Anodization of Aluminium Sputtered Electrodes

A general scheme for fabrication of nanoporous alumina modified electrodes using the pipette anodization technique is shown in Figure 4. In this method, anodization was carried out by positioning a glass pipette coated with ca. 40 nm thick platinum layer, above and in contact with the surface of the aluminum coated electrode (Figure 4).

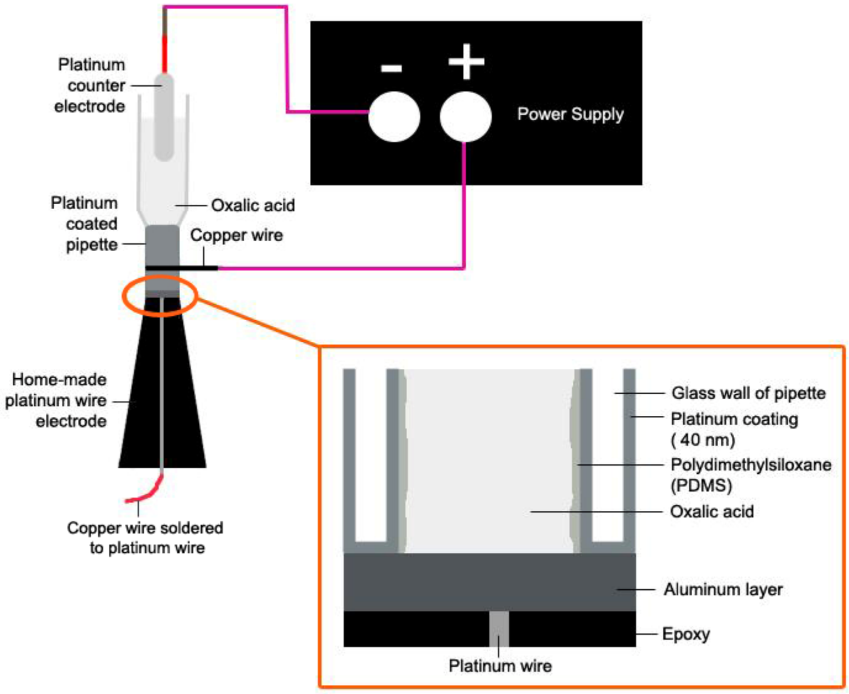

Figure 4. Schematic diagram of the fabrication procedure for alumina-modified electrodes, using the pipette anodization technique.

The pipette tip (2 mm internal diameter, 0.5 mm wall thickness) was coated with platinum and subsequently carefully positioned over the aluminum area overlaying the 76 μm diameter platinum disk electrode tip. 0.1 M oxalic acid solution was then added into interior portion of the platinum coated glass pipette. The contact junction between the platinum coated glass pipette and aluminum coated electrode was sealed using Teflon tape to prevent leakage of the anodizing solution. Prior to this arrangement, the interior rim of the platinum glass pipette was insulated with polydimethylsiloxane to prevent direct contact of solution with platinum. The positive output of a power supply was connected via the connecting copper wire, directly to the platinum coated pipette. Thus, the aluminum coating, which was exposed to the oxalic acid solution within the pipette and in contact with the platinum coated pipette, functioned as the anode. The negative output of the power supply was connected to a platinum mesh counter electrode, which functioned as the cathode and was immersed in the same oxalic acid solution (or anodizing solution) within the pipette. In this way, the area of aluminum coating which overlaid 76 μm dia. platinum wire at the centre of the electrode tip was subsequently anodized, when the anodizing voltage was applied. Whereas, the area of aluminum outside the pipette contacted region remain unanodized after the anodization procedure.

This was in contrast to the experimental set-up for conventional sub-surface anodization of aluminum coated electrodes, in which the entire aluminum overlayer above the electrode tip was anodized, when immersed in the anodizing solution together with counter electrode (Figure 5). In this case, the home-made electrode was placed ca. 3 cm away from the platinum mesh counter electrode and the anodizing solution was stirred at 240 rpm continuously through the process. In this study, both anodization procedures were carried out and the electrochemical behaviours of these alumina-coated electrodes in the presence of a redox probe were compared.

All the aluminum-coated electrodes were rinsed with ultrapure water before anodized potentiostatically in 0.1 M oxalic acid at 40 V. A two-step anodization process was adopted [16, 17] in which the aluminum was anodized at 40 V in oxalic acid solution, followed by immersion in 3% H_3PO_4 solution containing 0.2 M CrO_3 for 1 min and a second step anodization until the current decreased to zero. This two-step process ensures that a more uniform layer of alumina is formed and improves the overall pore arrangement [15]. Highly ordered pore arrangement is usually achieved in oxalic acid solutions [21] and hence the choice of this acidic medium for anodization in this investigation.

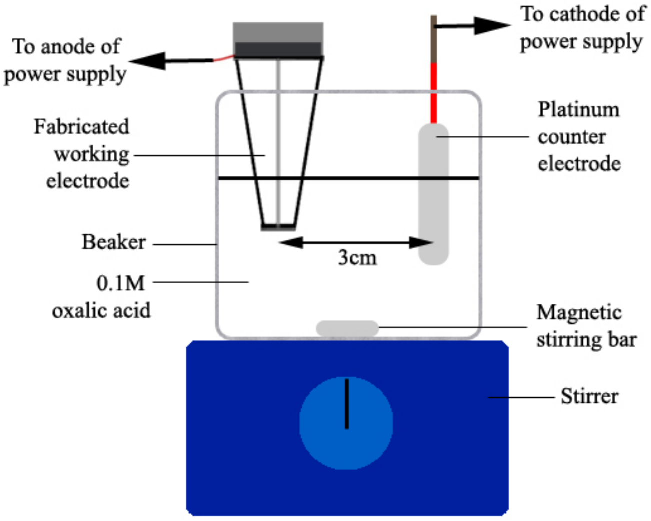

Figure 5. Schematic diagram of the fabrication procedure for alumina-modified electrodes, using the sub-surface anodization technique.

3. Results and Discussion

3.1. Electrochemical Investigations of Alumina Barrier Layer

In the following work, the physical nature of the barrier layer between the porous alumina structure and the underlying electrode prepared using the different sub-surface and pipette anodization procedures, was investigated. Several outer-sphere one electron redox couples have been employed to probe electron transfer and diffusion through thin films in solution, including ferrocenemethanol [22], hexacyanoferrate [23] and rutheniumhexaamine [24]. For these studies, ferrocenemethanol was employed as the redox probe and cyclic voltammetry studies in 1.0 mM solutions of ferrocenemethanol, prepared in 0.1 M phosphate buffer, (pH 6.8) were carried out.

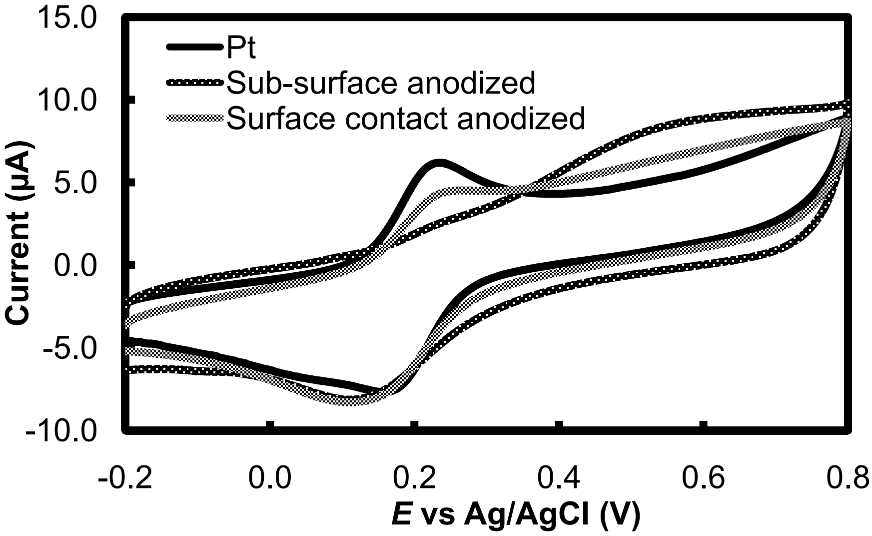

Figure 6. Cyclic voltammograms of sub-surface anodized electrode, pipette anodized electrode, bare platinum electrode obtained at 50 mV s^{-1} in 1 mM ferrocenemethanol solution, 0.1 M phosphate buffer solution (pH 6.8).

Figure 6 shows the cyclic voltammograms of a bare platinum electrode and alumina-modified electrodes prepared using the conventional sub-surface anodization and pipette anodization techniques. In the cyclic voltammogram of the bare platinum electrode, the peak-to-peak distance corresponded closely to 60 mV for the one-electron, reversible redox couple. Peak shape obtained during cyclic voltammograms of the pipette anodized electrode closely resembled that of the bare electrode, with a peak-to-peak separation of 133 mV. $E_{1/2}$ of ferrocenemethanol measured at the pipette-anodized electrode also corresponded closely with $E_{1/2}$ measured at the platinum electrode and these were consistent with that obtained at a gold electrode [22]. In contrast, cyclic voltammogram of the sub-surface anodized electrode exhibited electrochemically irreversible behaviour with a peak-to-peak distance of 640 mV, clearly differing from the pipette-anodized electrode.

The irreversible anodic peak clearly indicates a sluggish electron transfer process occurring at the sub-surface anodized electrode. The heterogeneous rate constants were derived by plotting ln i_p versus ($E_p - E^{0\prime}$) determined from the irreversible anodic peak at different scan rates, using the following Equation (1) derived for an irreversible one-step, one-electron process [25]:

$$i_{\mathrm{p,a}} = 0.227FACk^0 \exp\left[\frac{(1-\alpha)F(E_{\mathrm{p,a}} - E^{0\prime})}{RT}\right] \qquad (1)$$

where $i_{\mathrm{p,a}}$, $E_{\mathrm{p,a}}$ and $E^{0\prime}$ refers to the anodic peak current, anodic peak potential and formal potential respectively. The remaining parameters have their usual meanings in reference [25]. Using a value of 0.16 V for the formal potential determined at a bare platinum electrode, k and α were found to be 1.5 (± 0.9) × 10^{-6} cm s^{-1} and 0.60, respectively for the sub-surface anodized electrode. Anodization of aluminum is known to yield an anodization voltage-to-barrier layer thickness growth parameter of 1.2 nm V^{-1} [26], thus the voltage-dependent barrier layer thickness for the sub-surface anodized electrode prepared using an anodization voltage of 40 V, was expected close to 50 nm [27]. It is also well known that tunnelling currents are strongly damped for aluminum oxide films thicker than ca. 4 nm [27]. Therefore, the observable current response obtained at the sub-surface anodized electrode in Figure 6 was not expected. The conduction of current for the sub-surface anodized electrode probably occurred via intermediate states by means of resonance mechanisms [28]. These intermediate states could arise from defective sites due to interstitials, vacancies or surface states [29]. It is however, unlikely due to permeation of hydrophobic ferrocenemethanol into the barrier layer, which has been shown to consist of anion rich hydrophilic outer region [30, 31].

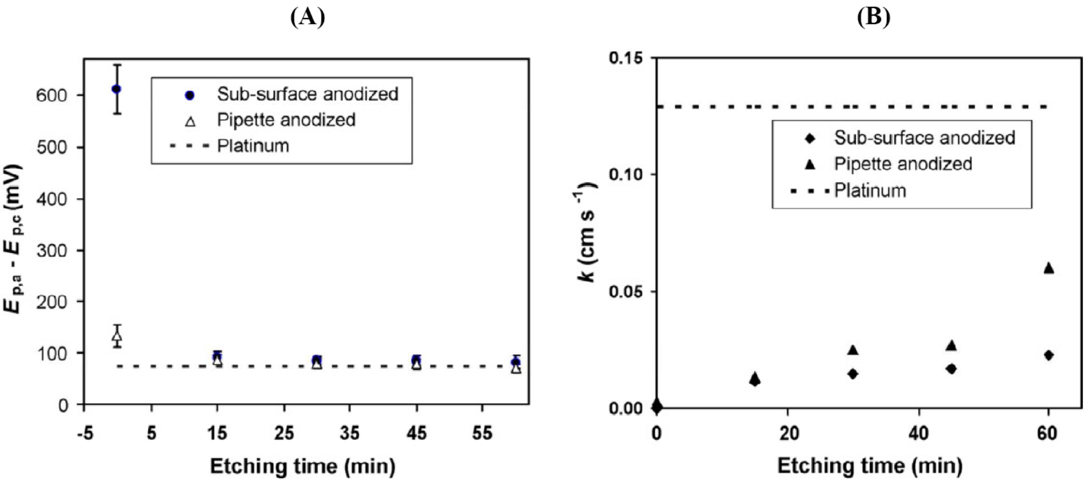

Figure 7. Effect of immersion duration in 3% phosphoric acid on the (A) peak-to-peak separation ΔE_p and (B) heterogeneous rate constant k for the electrochemical reaction of ferrocenemethanol at bare platinum and alumina-modified electrodes. ΔE_p were averaged over four different scan rates: 20, 50, 100 and 200 mV s^{-1} and error bars indicate the error range of values obtained at different scan rates. Heterogeneous rate constants k were calculated from the average ΔE_p values using the method of Nicholson for all voltammograms showing $\Delta E_p < 200$ mV; k value for unetched sub-surface anodized electrode was calculated using Equation (1), since $\Delta E_p > 200$ mV is beyond the quasi-reversible range.

The cyclic voltammograms of ferrocenemethanol at the pipette anodized electrode between scan rates of 20 and 200 mVs^{-1} showed quasi-reversible behaviour with peak-to-peak separation ranging from 133 to 155 mV. These data were analyzed using the method used by Nicholson to estimate the rate constant for quasi-reversible systems by analysis of the peak-to peak separation and using the working curve in Figure 3 of reference [32]. The peak-to-peak separation ΔE_p values as theoretically determined by Nicholson were nearly independent of α for $0.3 < \alpha < 0.7$ for small ΔE_p close to the reversible system ($60/n$ mV< $\Delta E_p < 200/n$ m V) [32]. From the symmetry of the redox peaks obtained for ferrocenemethanol at the pipette anodized electrode, α was estimated to be close to 0.5. Heterogeneous rate constant k values were then calculated from average values of ΔE_p obtained over different scan rates, using Equation (17) from the same reference [32]. The other parameters used for the calculation included the estimated α value at 0.5, diffusion coefficient of 1×10^{-5} cm^2 s^{-1} and assuming negligible difference in the diffusion coefficient values of reduced and oxidized ferrocenemethanol. The effect of uncompensated ohmic potential drop on ΔE_p was expected to be minimal in the 0.1 M phosphate buffer solution and a very low ferrocenemethanol concentration of 1 mM.

Using this method, the heterogeneous rate constant k for the electrochemical reaction of ferrocenemethanol at a pipette anodized electrode was determined to be 2.8×10^{-3} cm s^{-1}. This is ca. three orders of magnitude faster than the heterogeneous electron transfer rate occurring at a sub-surface anodized electrode. The substantially larger heterogeneous rate constant of ferrocenemethanol obtained at the pipette-anodized electrode suggests either a barrier layer with extensive number of defective sites or a very thin barrier layer. Overall, it is clear the insulating barrier layer in the sub-surface anodized electrode was kinetically unfavourable towards the electrochemical reaction of ferrocenemethanol. In contrast, the electrochemical behaviour of the redox probe at the pipette-anodized electrode was more similar to that observed at the bare platinum electrode which has a standard rate constant k^0 for ferrocenemethanol at 0.129 cm s^{-1}, estimated using the method employed by Nicholson.

In addition, the thickness of the barrier layer for the sub-surface anodized electrode was varied and compared with an electrode prepared using pipette anodization technique. Figure 7 shows the decrease in peak-to-peak separation ΔE_p in the cyclic voltammograms and increase in rate constant k after varying etching time in phosphoric acid for both sub-surface anodized and pipette-anodized electrodes. Various acids such as phosphoric acid, oxalic acid, sulfuric acid have been routinely used as chemical etchants for control of alumina pore sizes as well as removal of the barrier layer [33]. Etching rate of nanoporous alumina has been estimated to proceed at 9.4 nm min^{-1} in 5% phosphoric acid [34]. It is therefore expected the barrier layer to be completely removed at long etching times, so the redox probe was able to access the underlying platinum electrode. Under these conditions, ΔE_p would be close to 60 mV, the electrochemically reversible situation. As expected, Figure 7 shows an increase in electrochemical reversible behaviour as the insulating barrier layer was subsequently removed from the sub-surface anodized electrode.

Non-linear diffusion effects occurring at an electrode covered by a blocking film comprising large numbers of microscopic pores give rise to the following relation between the rate constant k at the insulated electrode and bare metal electrode [35]:

$$k = k^0(1 - \theta) \qquad (2)$$

where θ refers to the surface coverage of the blocking film. This relation holds when the average film thickness and pore diameters are smaller than the total diffusion layer thickness [35]. The thicknesses of the sputtered alumina films employed in the work were in the range of 2 μm and below, and the total diffusion layer thickness was ca. 40 μm, estimated using the relation $(\pi D t)^{1/2}$ for an experimental timescale of 0.5 s and diffusion coefficient D of 1×10^{-5} cm^2 s^{-1}. Thus, the three-dimensional porous structure of the alumina-modified electrode would have the same effect of a thin two-dimensional insulating film, comprising non-conducting and inert aluminum oxide, which partly covers the surface of a platinum electrode.

Equation (2) can be used to describe the alumina-modified electrodes and the term $(1-\theta)$ is equivalent to the total pore area, which exposes the platinum surface to the solution species. The fractions of exposed platinum surfaces $(1-\theta)$ at the alumina-modified electrodes etched for different time periods were determined from the rate constant values (see Table 1). These values calculated from rate constants were compared with actual physically available pore areas determined from scanning electron microscopy studies of alumina films coated on glass substrates. The maximum electrode area available for electron transfer $(1-\theta)_{\max}$ was determined by the total pore area along the alumina surface calculated from pore size and pore density, since the same area could become accessible to the underlying platinum electrode in the absence of a barrier layer.

For the pipette anodized electrode, the values of $(1-\theta)$ calculated from rate constants agreed very well with the values of $(1-\theta)_{\max}$ determined from surface pore areas measured using scanning electron microscopy. This strongly suggests the absence of a barrier layer for alumina-modified electrodes prepared using pipette anodization method. This was further supported by close agreement within experimental errors, of $(1-\theta)$ and $(1-\theta)_{\max}$ values for the sub-surface anodized electrode after 15 min etching, indicating the removal of barrier layer after an initial 15 min etch time was necessary to improve the heterogeneous electron transfer rate at the electrode. The similarity between the values of $(1-\theta)$ and $(1-\theta)_{\max}$ does not preclude the additional contribution of electron transfer occurring via electron tunnelling, which could be significant when the barrier layer was sufficiently thin.

Table 1. Comparison of total pore areas $(1-\theta)$ calculated from equation (2) and maximum total pore areas $(1-\theta)_{\max}$ determined from SEM measurements of pore size and pore density of alumina films.

Etching time/ min	**Pt electrode**	**Sub-surface anodized electrode**		**Pipette anodized electrode**		[b]**Pore size (nm)**	[b]**Pore density x 10^9 (pores cm^{-2})**	[c]**Maximum total pore area $(1-\theta)_{\max}$**
	[a]k^0 (cm s^{-1})	[a]k (cm s^{-1})	Total pore area $(1-\theta)$	[a]k (cm s^{-1})	Total pore area $(1-\theta)$			
0	0.129	1.5×10^{-6}	1.1×10^{-5}	0.003	0.022	30 ± 9	2.6 ± 0.3	0.02 ± 0.01
15	--	0.012	0.090	0.014	0.107	50 ± 10	5.1 ± 0.5	0.10 ± 0.03
30	--	0.015	0.118	0.025	0194	64 ± 14	5.9 ± 0.6	0.19 ± 0.06
45	--	0.017	0.133	0.027	0.209	75 ± 10	6.2 ± 0.5	0.27 ± 0.06
60	--	0.023	0.176	0.060	0.469	80 ± 12	7.0 ± 0.4	0.35 ± 0.06

See text for calculation of kinetic rate constants for electron transfer reaction of ferrocenemethanol at bare platinum, sub-surface anodized and pipette-anodized electrodes. Values of rate constant k are the same as those plotted in Figure 7B.

[a] Determined from cyclic voltammograms obtained at scan rates ranging from 20 to 200 mV s^{-1}.

[b] Determined from scanning electron micrographs of surface morphologies of alumina coated glass substrates, etched in 3% phosphoric acid over varying time duration.

[c] Calculated values based on the geometric area of a 0.2 cm diameter platinum electrode.

3.2. Reproducibility of Pipette Anodization Technique

To investigate the reproducibility of the pipette anodization technique, platinum electrodes (76 µm diameter) sealed in epoxy were prepared. Figure 8 shows the cyclic voltammograms of seven pipette-anodized electrodes in which the alumina modified electrodes were cycled between −0.2 and 0.8 V (versus silver-silver chloride reference electrode) in 1.0 mM ferrocenemethanol buffer solution. It was obvious the electrochemical behaviours of these alumina modified electrodes prepared using the pipette anodization technique were reproducible and consistent with the quasi-reversible behaviour of ferrocenemethanol observed at the pipette anodized commercial electrode using the larger platinum electrode of 0.2 cm diameter (Figure 6).

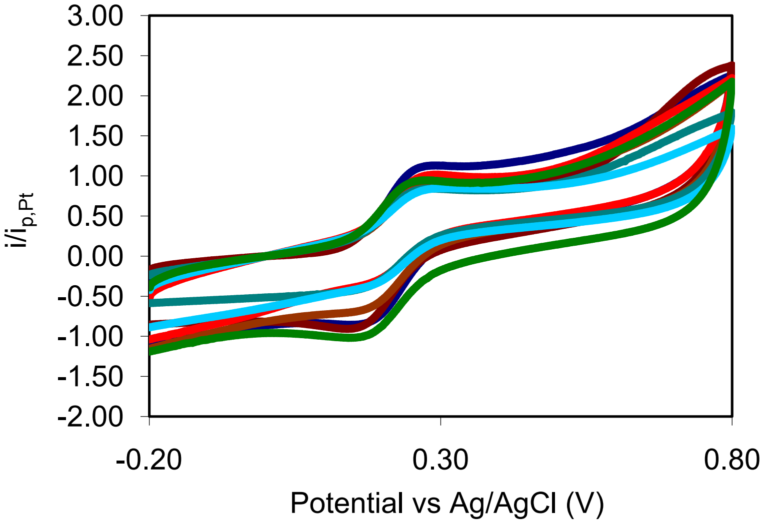

Figure 8. Cyclic voltammograms of seven pipette-anodized electrodes in 1.0 mM ferrocenemethanol buffer solutions. Currents were normalized to peak current responses towards 1.0mM ferrocenemethanol, at the respective bare platinum electrodes prior to deposition of aluminum overlayers. All electrodes used were home-made 76 µm diameter platinum disk electrodes.

3.3. Scanning Electron Microscopy Studies

Inspection of the scanning electron micrographs of the top surfaces of alumina overlayers obtained from pipette contact and sub-surface anodization techniques revealed similar morphologies (Figure 9A and B), with pore densities of 4.1 (± 0.1) $\times 10^9$ and 4.2 (± 0.1) $\times 10^9$ pores cm^{-2}, respectively. In contrast, the undersides of alumina overlayers obtained from the sub-surface anodized and pipette contact anodized electrodes prepared from the 76 μm diameter platinum electrode sealed in epoxy were clearly different in their morphologies. A non-porous barrier layer was observed at the side profile of the alumina overlayer of an unetched sub-surface anodized electrode (Figure 9C), unlike the roughened surface comprising microporous structures at the underside surface of the alumina overlayer obtained from a pipette-anodized electrode (Figure 9D). It is noteworthy to mention that removing the alumina films from the electrode tips using tape during the preparation process of obtaining scanning electron micrograph images of these samples could possibly have introduced observed artefacts of roughened surfaces.

The central symmetry of the pipette wall placed in contact with the aluminum/alumina overlayer was expected to give rise to a current distribution, which originated from the pipette wall and extend into the anodizing solution through the aluminum/ alumina overlayer during anodization. At and close to the central point of the pipette tip, the potential field must extend normally through the aluminum/alumina overlayer, generating a current distribution similar in the aluminum/alumina overlayer at a sub-surface anodized electrode during anodization. The absence of barrier layer was thus probably due to progressively increasing ohmic losses as growth of the non-conducting alumina at the pipette walls continued during anodization. This would be similar to the method of uniform barrier layer thinning [1] by gradually reducing an externally applied anodizing voltage during anodization. It was equally possible under the condition of limited volume of the anodizing solution during pipette contact anodization, pH changes were more significant and likely affected the kinetics of porous oxide layer formation and dissolution rate of the non-porous barrier layer.

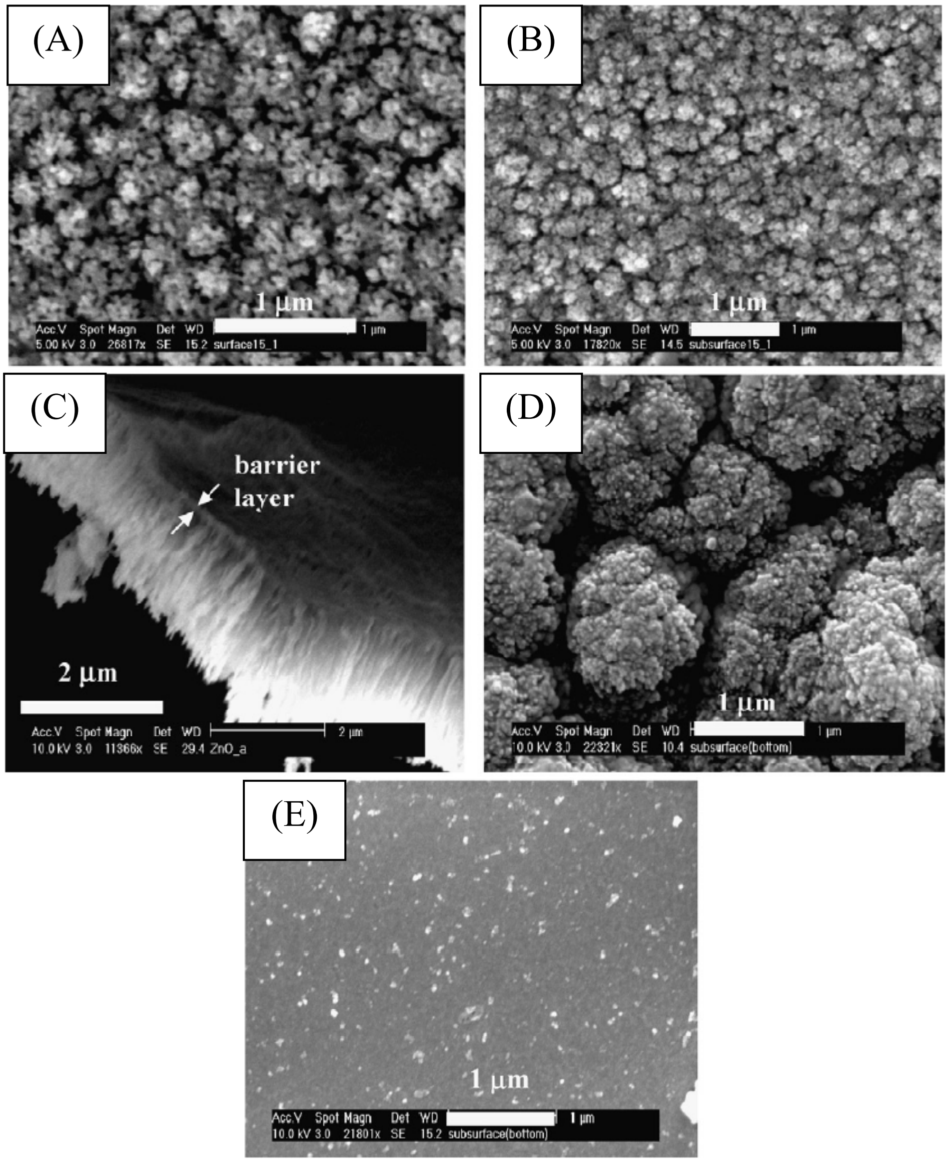

Figure 9. Scanning electron micrographs of the surfaces of alumina overlayers obtained from (A) pipette anodized and (B) sub-surface anodized electrodes.

Micrographs of (C) side profile of the alumina overlayer of an unetched sub-surface anodized electrode and undersides of the alumina overlayers of (D) pipette anodized and (E) sub-surface anodized electrodes. These samples were obtained from the central regions of the electrode tips, close to the platinum wire and all electrodes used were home-made 76 µm diameter platinum disk electrodes.

4. Conclusion

An alternative approach to fabrication of nanoporous alumina films with no barrier layer is described. Heterogeneous electron transfer rate constant for the oxidation of ferrocenemethanol at a sub-surface anodized electrode was found to be five orders of magnitude lower than that of a bare platinum electrode. In contrast, the electrochemical behaviour of redox probe ferrocenemethanol, at a pipette-anodized electrode was characteristically more similar to that observed at a bare platinum electrode, in which the heterogeneous electron transfer rate constant was about 50 times lower than that observed at a bare platinum electrode. Scanning electron microscopy studies supported the conclusion of a “barrier layer-free” alumina structure, when fabricated using the pipette anodization technique. This novel preparation method of “barrier layer-free” is foreseen to be useful in these applications in which direct access of solution species to the underlying conductive electrode is highly desirable, such as for electrochemical sensors, membrane electrodes and preparation of sensors of nanometer dimension using the template synthesis approach.

The structural differences of alumina fabricated from sub-surface and pipette anodization methods may be due to the differences in placement of cathode and direction of the applied potential. In the former method, current flows from the soldered copper wire, through the platinum wire to the underside of the aluminium layer, while in the latter method, current flows from the platinum coating to the top of the aluminium layer. This, together with the difference in placement of the cathode will most likely lead to a difference in the flow and direction of electric field, which in turn may result in changes in the growth mechanism of the alumina film. Material growth mechanism studies can be undertaken to further probe into these observed differences.

CHAPTER III

MEMBRANE-BASED ELECTROCHEMICAL BIOSENSOR – DETECTION OF GLUCOSE OXIDASE

1. Introduction

Development of immunosensors with capability for rapid, sensitive and selective detection of infectious diseases continues to be an important subject for research and development [36-39]. It is equally desirable to have fast response sensing capability towards other analytes, including proteins, DNAs and haptens in environmental studies, pharmaceutical applications and biomedical diagnostics, as long as their complementary binding immunoglobulins can be produced. Current methods used by *in vitro* immunoassay such as enzyme-linked immunosorbent assay (ELISA) incorporates immunoglobulins or antigens tagged with markers into appropriate biorecognition materials and coupled to a transducer such as optical [40], fluorescence [41] or electrochemical sensor [42-44]. Typically, these techniques give a linear response of 10 μg L^{-1} to 150 mg L^{-1} and have a detection limit of 10 μg L^{-1} [45].

Herein, a method for measuring the amount of protein antigen based on monitoring the magnitude of diffusion limited faradiac current of a redox probe diffusing within narrow channels of a nanoporous alumina matrix is described. Nanoporous alumina is a highly regular, rigid and dense porous material with nominal pore sizes ranging from 10 to 200 nm pore density of about 1×10^{10} pores cm^{-2} [46, 47] and is chemically and thermally stable [48]. It is reasoned that these same features can be used to trap specific-binding antibody such as immunoglobulin G within the confined spaces of the vertical channels of an alumina matrix. In addition, these immunoglobulin G coated channels could function as diffusion paths for a redox probe, ferrocenemethanol, chosen for its neutral charge and electrochemically reversible behaviour.

Sensors based on similar scheme of detection had been constructed based on porous polymer films or aligned carbon nanotubes. Shan et al. developed a glucose biosensor by entrapping glucose oxidase into porous poly(acrylonitrileco-acrylic acid [49]. The use of the porous film increased the stability and sensitivity of the sensor, resulting in a low limit of detection, as well as enabled a rapid rate of detection. Similar sensor behaviour was also observed by Kanungo et al., who developed protein sensors based on poly(styrene sulfonate)-polyaniline (PSS-PANI) composites tubules [50]. To allow maximum access of nanotubes surface, there had been efforts to align carbon nanotubes (CNT). This approach had enabled high loading of thionine onto an aligned CNT electrode, which subsequently allowed highly sensitive detections of nitrite [51]. However, these methods involve more complicated and tedious film fabrication processes, whereas our direct method of alumina film fabrication from anodization of aluminium is simpler and do not require a long formation time.

Recently, Nematollahi et. al. had studied catalytic oxidation of thiourea at an alumina modified platinum electrode using cyclic voltammetry [52]. However, their electrode was modified by polishing a bare platinum electrode with alumina powder. This method of modification renders the alumina film on the electrode surface to be unstable. Other groups [53, 54] made used of alumina as a template and sputter metal into the pores to fabricate a nanoarray sensor. Instead, our work made use of alumina, produced from anodization of sputtered aluminium, as a substrate to immobilise antibodies in the development of an electrochemical immunosensor. This method of preparation of alumina modified electrodes provided alumina films of high stability and strong adhesion to the electrode surface.

Figure 10 shows the basic design of our immunosensor which explains its scheme of operation. A layer of aluminum (ca. 400 nm thick) was sputtered onto a home-made platinum disk electrode tip and anodized to alumina using a pipette anodization method, which yields barrier-free alumina [55]. A sub-monolayer or monolayer of immunoglobulin G was then immobilized along the nanochannel walls of the porous alumina, followed by immobilization of bovine serum albumin (BSA) to block the unspecific adsorption sites. The alumina-modified platinum disk electrode was subsequently used for antigen detection, in the presence of the redox probe, ferrocenemethanol. Upon binding the complementary antigen to the immunoglobulin G, formation of the antigen–antibody (Ag–Ab) complexes blocked the approach of ferrocenemethanol towards the exposed platinum surface beneath the porous alumina layer. The developed sensor is thus a signal-off immunosensor, where the signal response decreases as the concentration of analyte increases.

Differential pulse voltammetry (DPV) was employed to monitor the faradiac current limited by the diffusion rate of the redox probe diffusing towards the underlying platinum electrode. The feasibility of using this scheme of operation for antigen detection is demonstrated, by choosing glucose oxidase (GOx) and anti-glucose oxidase (immunoglobulin G) as our model antigen-antibody system. The antigen GOx system was chosen because GOx is a well-studied protein with known molecular mass, size and shows high binding specificity for its immunoglobulin G antibody. Descriptions of immunoglobulin G antibody and glucose oxidase enzyme are provided below.

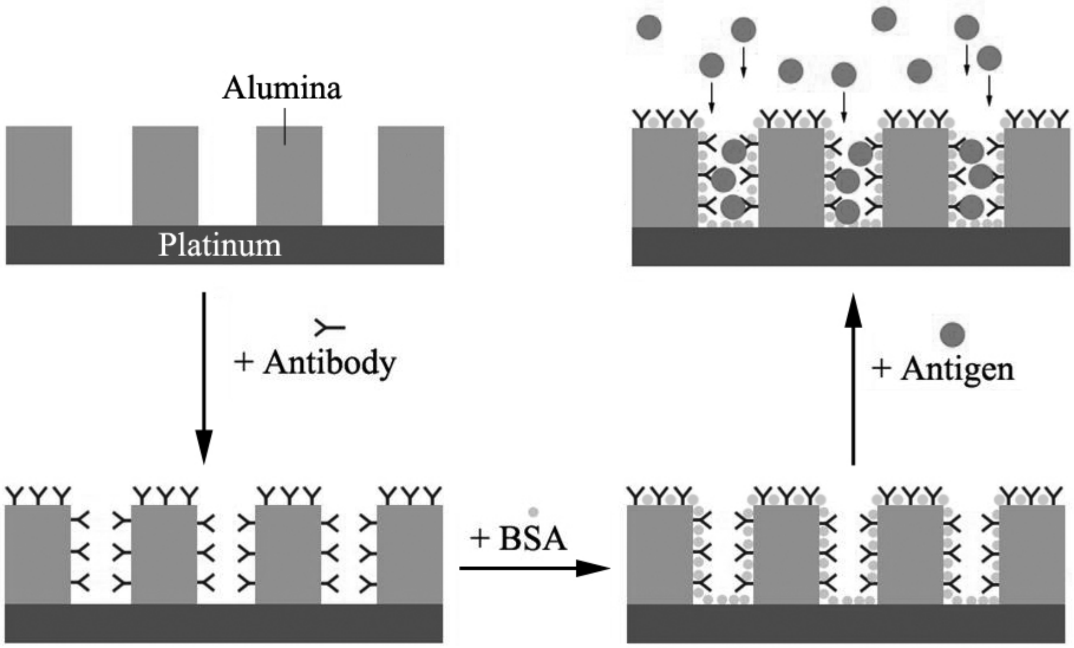

Figure 100. Scheme of antigen detection. A monolayer or submonolayer of antibody was physically adsorbed onto the channel walls of the nanosized alumina pores, followed by blocking of non-specific adsorption sites with BSA and finally the alumina-modified electrode was used for antigen detection. Formation of the Ab–Ag complex resulted in the narrowing and blocking of the nanosized pores and the subsequent decrease in signal response towards a redox probe measured using differential pulse voltammetry.

1.1. Structure of Immunoglobulin G

Immunoglobulin G (IgG) is a major antibody in the blood and has a molecular weight of about 150 kDa [56]. X-ray diffraction analysis of IgG molecules revealed that it consists of three subunits – two identical fragment antigen binding arms known as the Fab arms and a short constant stem region known as the Fc domain [57] (Figure

11). The Fab arms are connected to the Fc domain via hinges, which enable rotation of the Fab arms. Though the structure of IgG molecule is frequently referred to as Y-shape, the Fab-Fc angle can extend from 66º to 123º and the Fab-Fab angle ranges from 115º to 172º [58]. This flexibility allows the IgG molecules to bind to any specific antigen located within its rotation region and thus increases the probability of antibody-antigen binding.

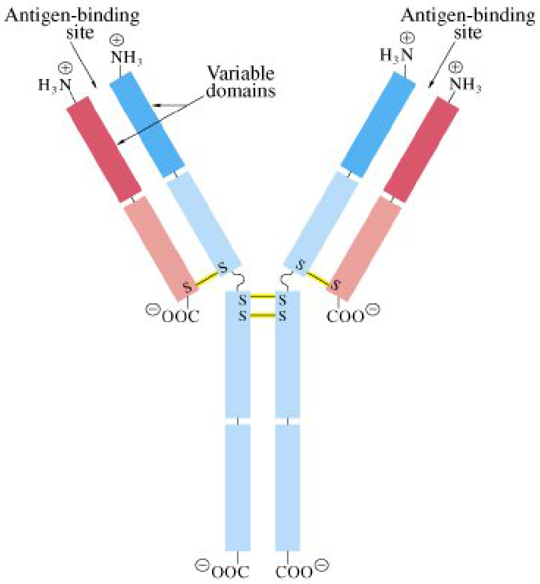

Figure 11. Schematic diagram of an IgG molecule [4].

Self assembly studies of IgG molecules on substrate surfaces has shown that IgG molecules adsorb via different configurations, which include end-on with contracted Fab fragments, end-on with intermediate Fab fragments, end-on with highly repelling Fab fragments or side-on or face-on orientation [59-61]. The preference for the IgG molecule to bind end-on via the Fc domain is likely due to higher tendency for the Fc domain to unfold, compared to the Fab arms [61]. This orientation is highly favourable, since the Fab arms will be left free to bind to its specific antigen.

1.2. Structure of Glucose Oxidase

Glucose oxidase (GOx) exists as a dimeric protein with a molecular weight of 160 kDa (Figure 12). Each monomer consists of a flavin adenine dinucleotide (FAD) unit, which acts as the redox carrier during catalytic reactions. The enzyme catalyses the oxidation of β-D-glucose to D-glucono-1,5-lactone and hydrogen peroxide, using molecular oxygen as the electron acceptor. Details of the catalytic reaction are further discussed in the introduction of Chapter V as the enzyme was not used for catalysis in the development of the immunosensor, but as an analyte.

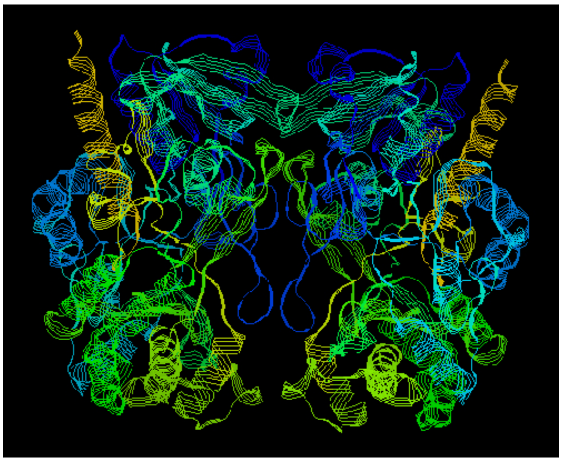

Figure 12. Three dimensional structure of glucose oxidase created using RasMol Version 2.6.

1.3. Differential Pulse Voltammetry

Differential pulse voltammetry (DPV) is commonly used for measuring trace levels of analytes due to its higher limit of detection, compared to cyclic voltammetry. In this technique, fixed magnitude pulses, superimposed on a linear potential ramp, are applied to the working electrode (Figure 13A). The current is sample twice, just before the pulse application (at 1) and again at just before the end of the pulse (at 2), when the charging current has decayed. The first current is subsequently subtracted from the second current by the instrument and this current difference is plotted against the applied potential (Figure 13B) [20].

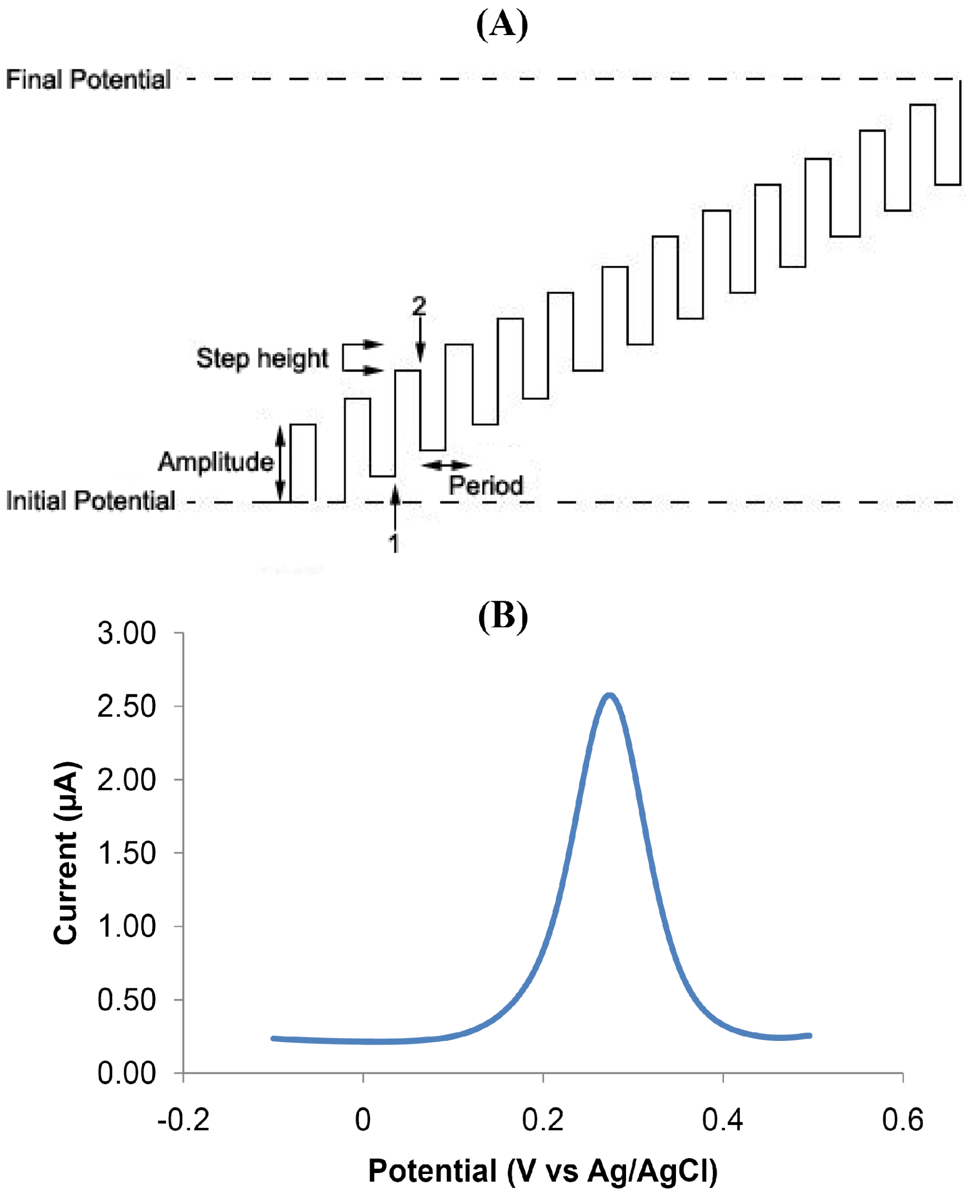

Figure 13. (A) Potential waveform applied during differential pulse voltammetry. Adapted from reference [6]. (B) Current response of a redox species during a potential scan from -0.1 to 0.5 V.

The resulting differential pulse voltammogram consists of a peak current, i_p, which is directly proportional to the concentration of the corresponding analytes according to the equation:

$$i_{\mathrm{p}} = \frac{nFAD^{1/2}C_{\mathrm{bulk}}}{\pi^{1/2}(\tau - \tau')^{1/2}}\left[\frac{(1-\sigma)}{(1+\sigma)}\right]$$

where i_p is the maximum peak height or DPV signal response, n is the number of electrons transferred, F is the Faraday constant, D is the diffusion coefficient of redox species, C_{bulk} is the bulk concentration of the redox species, (τ- τ') is the pulse duration, ΔE is the pulse amplitude and σ = exp (-nFΔE/2RT).

2. Experimental

2.1. Reagents and Materials

Monoclonal anti-glucose oxidase (anti-GOx) provided as mouse ascites fluid with 0.1% sodium azide as preservative, glucose oxidase (GOx) from *Aspergillus Niger*, bovine serum albumin (BSA, >98%), ferrocenemethanol (FeMeOH, >99%) and phosphoric acid (85%) were purchased from Sigma Aldrich (Singapore). All proteins solutions were prepared in phosphate buffered saline (PBS; containing 100 mM sodium phosphate and 1.7 M sodium chloride; pH 6.8). All chemicals and solvents of analytical grade were used as received. Ultrapure water (Barnstead Nanopure Ultrapure Water System) was used for all preparations, unless otherwise stated. Glutathione S-transferase (GST) was supplied by BST Scientific Pte Ltd. in the form of a 1 mg mL^{-1} solution in phosphate buffered saline containing 0.02% Tween 20 and 0.02% sodium azide. Mouse monoclonal antibody (IgG2b-kappa, clone GST 3-4C) raised against 26 kDa GST protein from *S. japonica* was supplied by ZYMED laboratories Inc. as a 200 mL aliquot at a concentration of 0.5 mg mL^{-1} in PBS, pH 7.4, containing 0.1% sodium azide (NaN_3)

2.2. Electrode Fabrication

Home-made electrodes were fabricated using epoxy glue, micropipette tips and platinum wire (0.076 mm diameter) as in Chapter I. The electrode tip was polished with 1.0 and 0.3 μm diameter alumina powder and sonicated in ultrapure water, before being sputter-coated with aluminum metal film. Sub-micrometer thick aluminum films in the thickness range of 300–500 nm were sputter-coated onto the platinum electrodes using 99.999% purity aluminum target, Denton discovery® 18 Sputtering System and sputtering power of 100W in an atmosphere of research-grade Ar at 5×10^{-3} Torr. Anodization of aluminum-coated electrodes was conducted using Apelex electrophoresis power supply model P304 minipac II. All aluminum-coated electrodes were rinsed with ultrapure water before anodized potentiostatically in 0.1 M oxalic acid at 40 V. Anodization using the surface contact anodization method described in Chapter I and in reference [55], was carried out by positioning a platinum coated glass pipette in contact with the surface of the aluminum-coated electrode. A two-step anodization process was used in which the aluminum was first anodized at 40 V in 0.1 M oxalic acid solution, followed by immersion in 3% H_3PO_4 solution containing 0.2 M CrO_3 for one minute and a second anodization step until the current decreased to zero. Electrochemical behaviours of the alumina-modified electrodes were characterized using cyclic voltammetry and differential pulse voltammetry techniques (CHI440 potentiostat/ galvanostat, data acquisition software) in the presence of 1.0 mM ferrocenemethanol in 0.1M phosphate buffer solution, pH 6.8. All potentials were measured with respect to the silver–silver chloride (saturated KCl) reference electrode.

2.3. Preparation of Immunosensor

Figure 14 shows the signal responses of the membrane-based electrochemical immunosensor electrode obtained by DPV technique towards the redox probe, during each step of the sensor preparation procedure carried out consecutively as follows. A sub-monolayer to monolayer of immunoglobulin G was first immobilized via physical adsorption onto the alumina by immersing the alumina-modified electrode in 5 μL of 0.4 mg L^{-1} anti-GOx IgG solution for 1 hr, followed by rinsing in 0.1 M phosphate buffer solution (pH 6.8). The DPV signal response of this alumina-IgG electrode towards ferrocenemethanol was measured in a solution containing 1 mM ferrocenemethanol, 0.1 M phosphate buffer (pH 6.8). The electrode was subsequently transferred to and physically adsorbed with BSA in a solution containing 200 mg L^{-1} BSA for 30 min, followed by rinsing, transferring to a 1 mM ferrocenemethanol solution and measurement of immunosensor response towards the redox probe using DPV. Adsorption of IgG and BSA onto the alumina electrode reduced the signal response towards ferrocenemethanol (Figure 14).

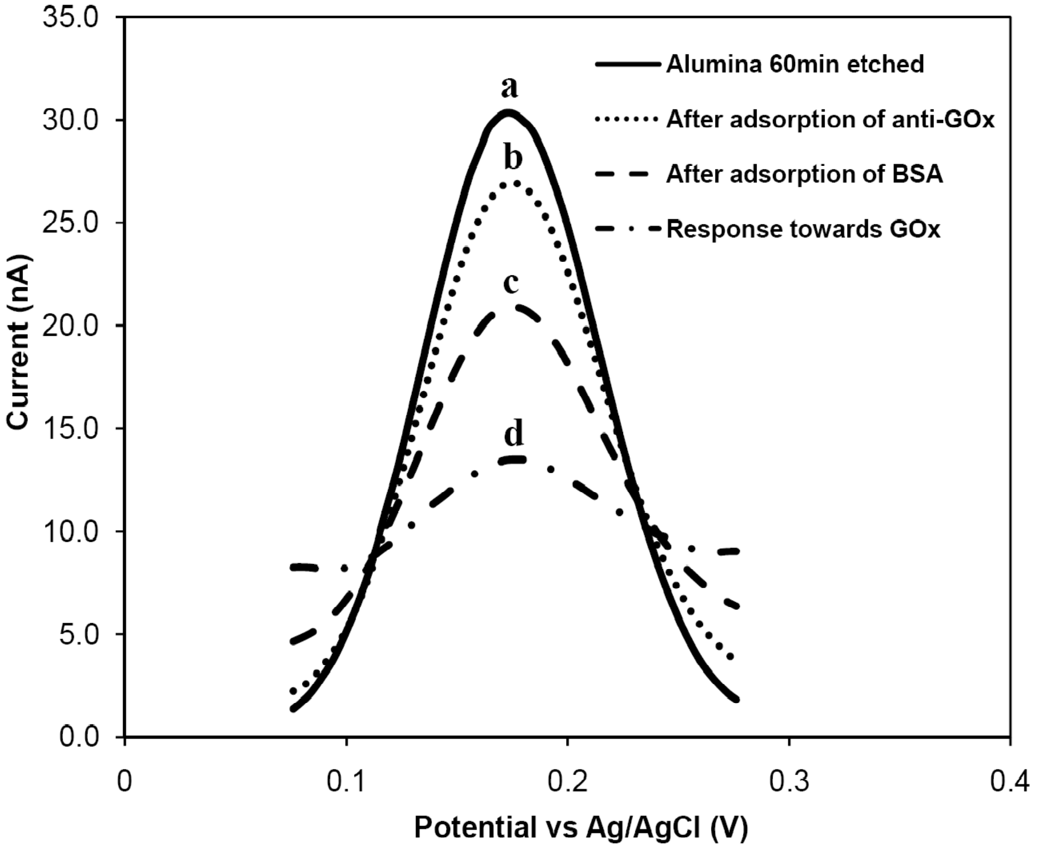

Figure 14. DPV signal response obtained at a 60 min etched alumina electrode immersed in 1 mM ferrocenemethanol, after each step of the sensor preparation procedure: (a) before adsorption of IgG, (b) after adsorption of anti-GOx IgG, (c) after adsorption of BSA and (d) after formation of IgG-GOx complex. Experimental conditions were described in text. Average background noise determined from standard deviations of three consecutive DPV scans of all the experiments was ± 0.5 nA.

The immunosensor was stable, with no significant change (± 2%) in the DPV signal response towards redox probe in the absence of antigen over a period of 2 hr (Figure 15). A precautionary measure that had been taken to establish this stability was to immerse the immunosensor in the redox probe solution for 30 min before commencing measurement of antigen concentrations in order for the redox probe to infiltrate the nanochannels of the alumina layer. Without this preparative step, the electrode showed erratic behaviour during measurement of the first one or two antigen concentrations.

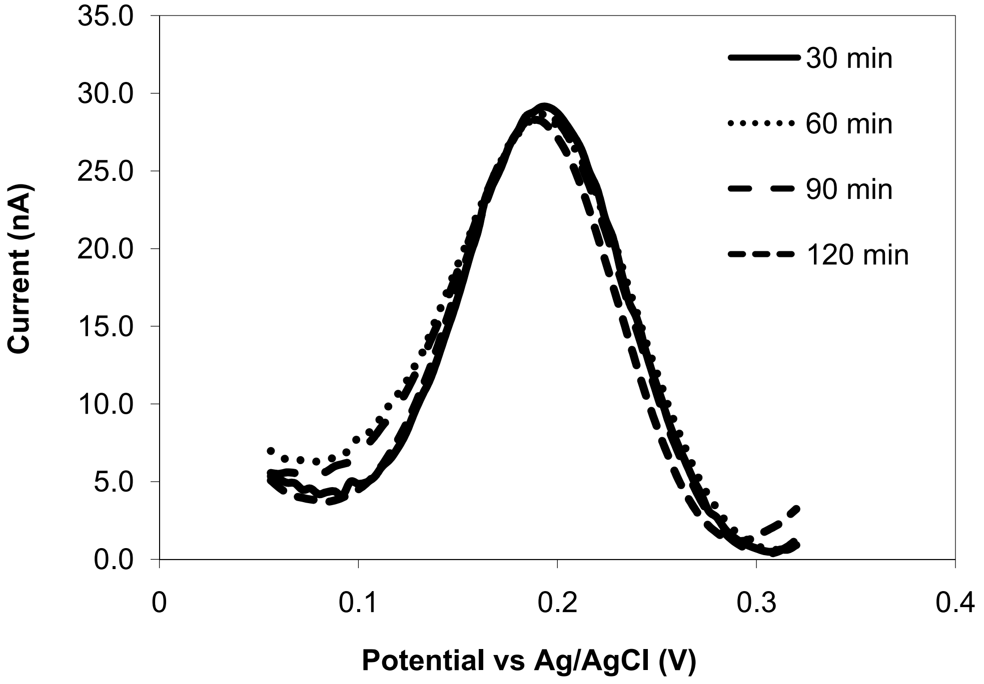

Figure 15. Relatively constant DPV signal responses (± 2%) of a 60 min etched alumina electrode immobilised with IgG and BSA obtained in a solution of 1 mM ferrocenemethanol in the absence of antigen, GOx over a period of 2 hr indicate stability of the IgG-BSA monolayer.

2.4. Glucose Oxidase Detection

Detection of the GOx antigen was carried out using a batch system in which the prepared immunosensor (alumina-IgG BSA electrode) was kept immersed in 15 mL of a buffered solution containing 1mM ferrocenemethanol, pH 6.8. Concentration of GOx in the solution was varied by addition of aliquots of a 10 mg L^{-1} GOx stock solution containing 1 mM ferrocenemethanol. Further quartz crystal microbalance (QCM) experiments coupled to cyclic voltammetry using an alumina coated gold quartz crystal revealed that significant antigen–antibody binding occurred within the first 2 min of immersing the alumina-modified electrode in the antigen solution while near equilibrium was reached after ca. 30 min, when the observed current in cyclic voltammetry coupled to QCM stabilized. In a separate study, continuous differential pulse voltammetric signal response obtained at intervals of 2 min during this immersion time in the antigen solution between 2–30 min, similarly decreased over time and stabilized after 20–30 min (Figure 16).

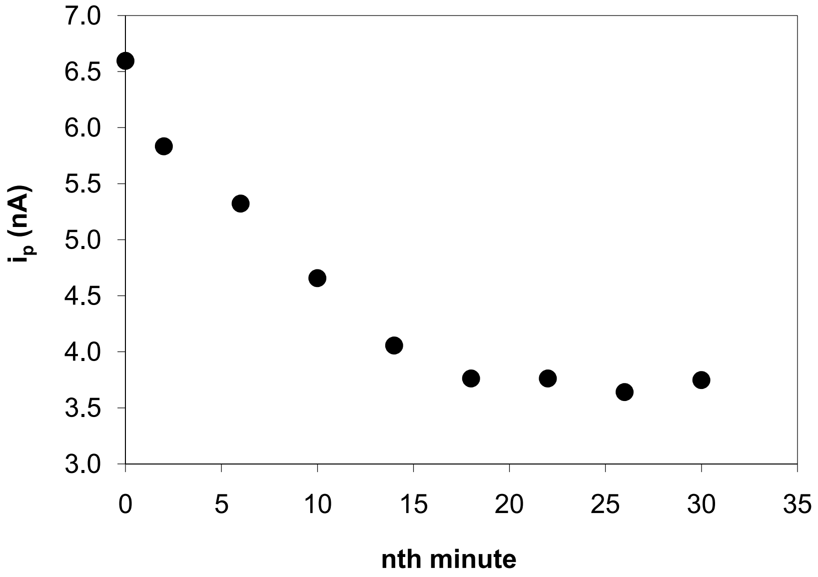

Figure 16. Measurement of DPV current responses of a 60 min etched alumina electrode immobilised with IgG and BSA, used for detection of GOx over time. Current responses decreased over time and stabilised after ca. 20 min.

Detection of antigen was thus, carried out after immersion times of immunosensor in the antigen solution for 30 min. Figure 17 shows the decreasing signal responses of the immunosensor towards the redox probe, during successive additions of increasing concentrations of the GOx, using differential pulse voltammetry.

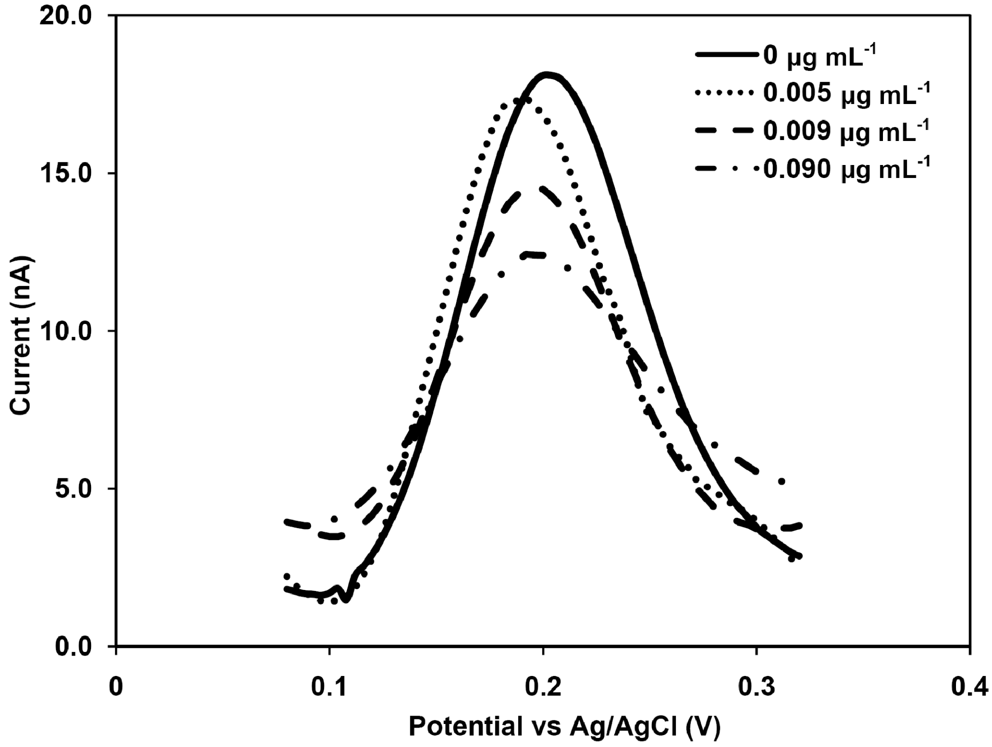

Figure 17. DPV signal response of an immunosensor towards the redox probe in increasing concentration of GOx, with corresponding decrease in signal response. Average background noise determined from standard deviations of three consecutive DPV scans of all the experiments was ± 0.4 nA.

All differential pulse voltammetry (DPV) experiments were conducted using the prepared electrode as the working electrode, a platinum disk electrode as the auxiliary electrode and a silver-silver chloride reference electrode. Parameters used for DPV were as follows: amplitude of 50 mV, pulse width of 0.05 s, sample width of 0.0167 s and scan range from −0.2 to 0.8 V.

3. Results and Discussion

3.1. Control Experiments

Several control studies were carried out using a high concentration of 0.1 mg L^{-1} GOx antigen concentration. First, a bare platinum electrode was prepared under identical immunosensor preparation procedure, but without the alumina overlayer, indicated high constant signal response towards the redox probe, at different antigen concentrations. In the second control experiment, a 60 min etched alumina-modified electrode was prepared under the same conditions as the working immunosensor, immobilized with BSA, but without IgG (alumina-BSA electrode). The third control used a 60 min etched alumina modified electrode immobilized with IgG, but without BSA (alumina-IgG electrode). Figure 18 shows the differential pulse voltammograms obtained for the three controls before and after the addition of glucose oxidase antigen into the sensing solution. Both the alumina-BSA and alumina-IgG electrodes showed decrease in signal response in the presence of antigen GOx (Figure 18B and C).

It was expected the presence of BSA in the alumina-BSA electrode prevented non-specific adsorption along the BSA coated alumina channel walls. The observed decrease in signal response was likely the result of displacement of the BSA molecules (65 kDa) by the bulkier GOx molecules (180 kDa). It was unclear whether the decrease in signal response of the alumina-IgG electrode in the presence of GOx was due to specific or non-specific binding. However, it is obvious from Figure 18D, the decreases in signal responses in the presence of GOx for both alumina-BSA and alumina-IgG control electrodes were not cumulative, but were significantly less than that obtained at the alumina-IgG-BSA electrode.

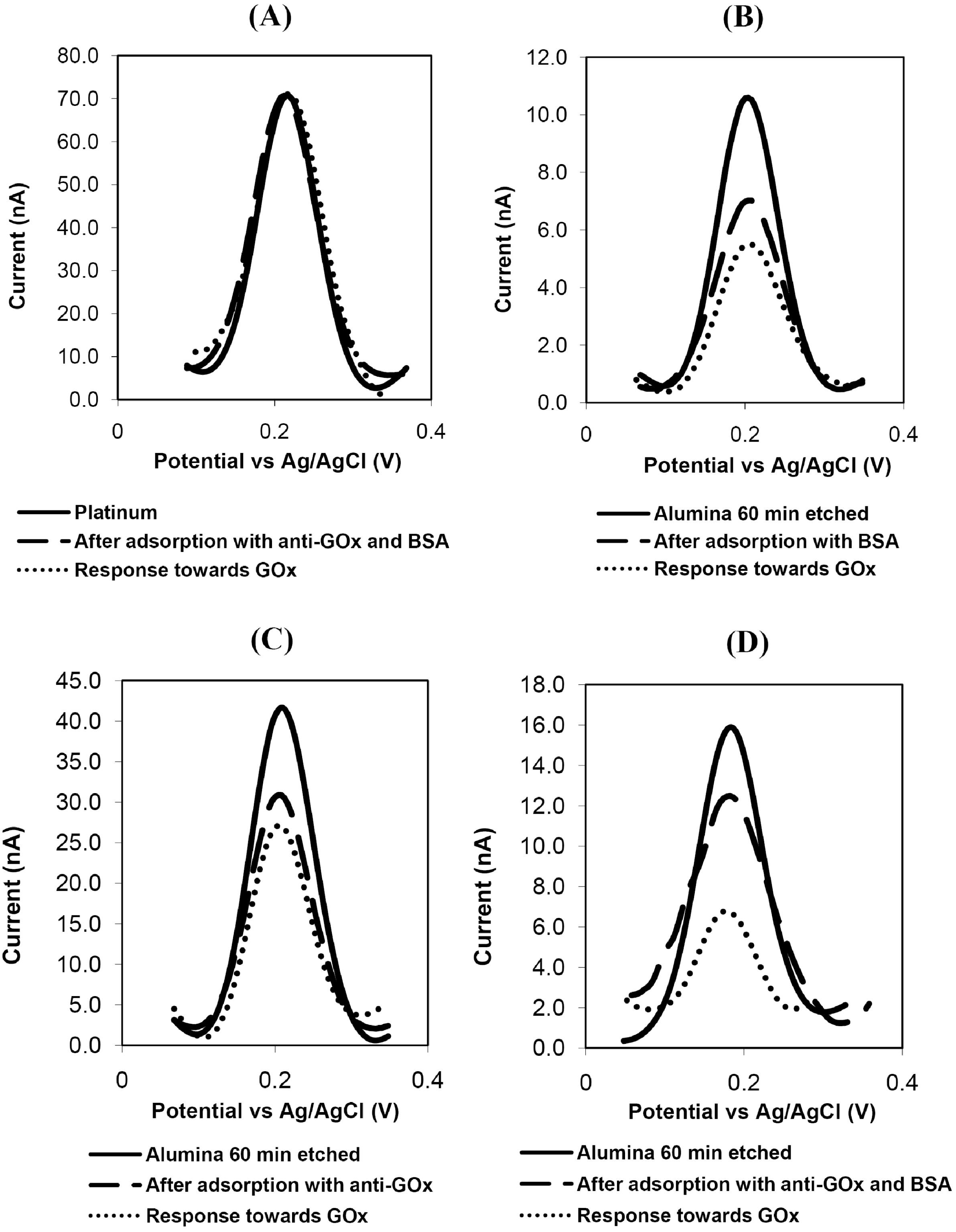

Figure 18. DPV signal responses of (A) platinum disk electrode, (B) alumina-BSA electrode, (C) alumina-IgG electrode and (D) alumina-IgG-BSA electrode obtained for the various control studies. Average background noise of three consecutive DPV for the control experiments was in the range of ± 0.1 to ± 2 nA.

The signal responses of these electrodes towards the redox probe obtained in the presence of antigen GOx were compared to the signal responses towards the redox probe by their respective bare platinum electrodes before coating with alumina overlayers. It was found that in the presence of 0.1 mg L^{-1} GOx, the alumina-BSA control electrode showed 74% (± 7%) reduction and the alumina-IgG electrode a similar 65% (± 5%) reduction with respect to the signal responses obtained at their respective uncoated platinum electrode. In contrast, the alumina-IgG-BSA electrode showed a significantly larger signal reduction of 82% (± 1%) which indicated the channels within the alumina-IgG-BSA electrode were blocked more effectively compared to the alumina-BSA and alumina-IgG electrodes. This suggests specific binding which yields a larger size immunocomplex probably occurs to greater extent in the alumina-IgG-BSA electrode, compared to the alumina-IgG electrode.

3.2. Selectivity Studies

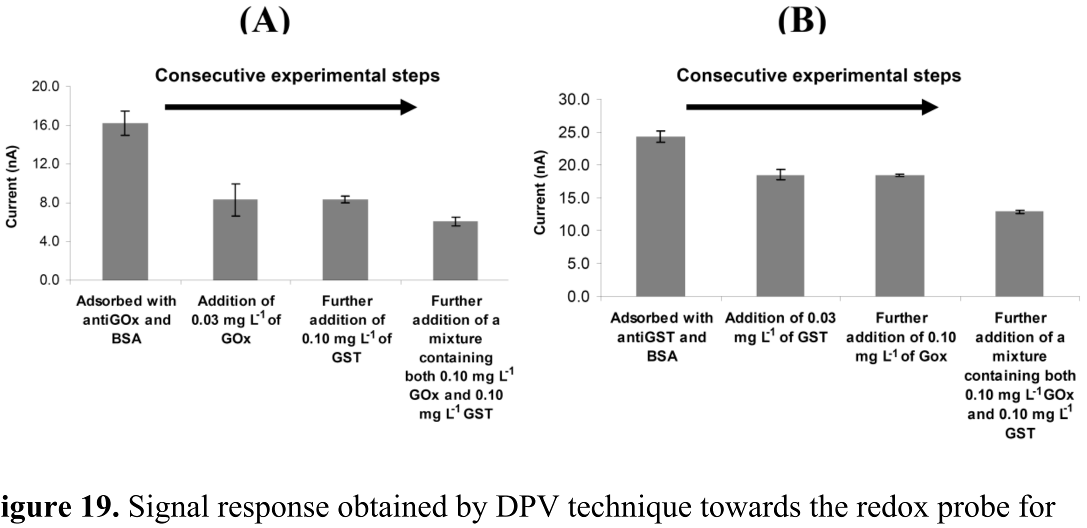

Figure 19. Signal response obtained by DPV technique towards the redox probe for (A) GOx immunosensor and (B) GST immunosensor. Each bar represents the signal response obtained towards the redox probe after adding aliquots of antigen, non-specific antigen and mixture of antigen/non-specific antigen consecutively to a 15mL buffered solution of 1 mM ferrocenemethanol (pH 6.8). Average background noise of

3 consecutive DPV after each step of the experiment was in the range of ± 0.1 to ± 1.6 nA.

Further study on an alumina-IgG-BSA electrode conducted using another protein, glutathione S-transferase (GST) indicated negligible non-specific binding of antigen molecules, when both IgG and BSA were present in the electrode. Figure 19A shows the responses of a GOx immunosensor (alumina-IgG-BSA electrode) towards GOx and non-specific antigen GST. A decrease in signal response of the GOx immunosensor was observed in the presence of 0.03 mg L^{-1} of GOx as expected, compared to a buffer solution without GOx. Subsequent addition of 0.1 mg L^{-1} non-specific antigen GST resulted in no further decrease in signal response of the same GOx immunosensor. Additional decrease in signal response was observed when a solution containing both GOx and GST at concentrations of 0.10 mg L^{-1} was subsequently added.

The experiment was carried out in reverse order using a second GOx immunosensor, by adding the non-specific antigen GST first, followed by the antigen GOx. The GOx immunosensor showed no change in signal response in the presence of GST, but significant change in signal responses in the presence of GOx or GOx–GST mixture. Similarly, using an immunosensor immobilized with anti-GST IgG, negligible signal response change was observed in the presence of non-specific antigen GOx (Figure 19B). The GST immunosensor was immersed sequentially in 0.03 mg L^{-1} GST, 0.10 mg L^{-1} GOx and finally, a mixture containing 0.10 mg L^{-1} GST and GOx. Thus, non-specific binding of GST or GOx if these occurred, resulted in negligible channel blocking effect for the alumina-IgG-BSA electrodes.

3.3. Normalisation of Current Response

Signal responses of an alumina-modified electrode towards the redox probe in the presence of antigen (I_{GOx}) were normalized against the signal response of the same alumina electrode immobilized with IgG (alumina-IgG) ($I_{\mathrm{anti\text{-}GOx}}$), instead of IgG and BSA (alumina-IgG-BSA) ($I_{\mathrm{anti\text{-}GOx/BSA}}$). $I_{\mathrm{anti\text{-}GOx}}$ and $I_{\mathrm{anti\text{-}GOx/BSA}}$ refer to signal responses obtained at the same alumina electrode after the antibody and BSA immobilization step, respectively and in the absence of antigen. Normalization of signal responses against $I_{\mathrm{anti\text{-}GOx}}$ using the ratio of $I_{\mathrm{GOx}}/I_{\mathrm{anti\text{-}GOx}}$ gave reproducible results for different electrodes and good linear logarithmic plots of normalized signal response against concentrations. This is likely due to irreproducible non-specific binding between BSA and IgG close to or at the antigen-binding site of IgG molecules. The BSA molecules bound at these parts of the IgG molecules are readily displaced by the GOx antigen which binds specifically to IgG. This method of data presentation significantly improved the reproducibility of the immunosensor for three different electrodes. For example, the relative standard deviation for three different 60 min etched electrodes prepared under similar conditions ranged from ± 4.1% at 200 ng L^{-1} antigen concentration to ± 13.8% at 10 μg L^{-1} antigen concentration using the normalized signal responses ($I_{\mathrm{GOx}}/I_{\mathrm{anti\text{-}GOx}}$). In contrast, the relative standard deviation were ± 26.4% (200 ng L^{-1}) and ± 15.6% (10μg L^{-1}) respectively when the same data were normalised using $I_{\mathrm{GOx}}/I_{\mathrm{anti\text{-}GOx/BSA}}$ and not $I_{\mathrm{GOx}}/I_{\mathrm{anti\text{-}GOx}}$.

3.4. Study of Channel Diameters

In order to understand the effect of channel diameters on the sensing response of the immunosensor, the alumina overlayer was etched in 3% phosphoric acids for durations of 0, 30 or 60 min. Each alumina-modified electrode was thoroughly rinsed in ultrapure water after the etching process to remove the dissolved alumina, which caused significant electrode fouling problems as well as to remove any remaining phosphoric acid within the alumina nanopores. Figure 20 shows the decreasing signal response of the sensor towards increasing concentrations of GOx antigen for three different alumina-modified electrodes etched for different time durations in phosphoric acid. The 60 min etched electrode exhibited the steepest slope of all the calibration curves.

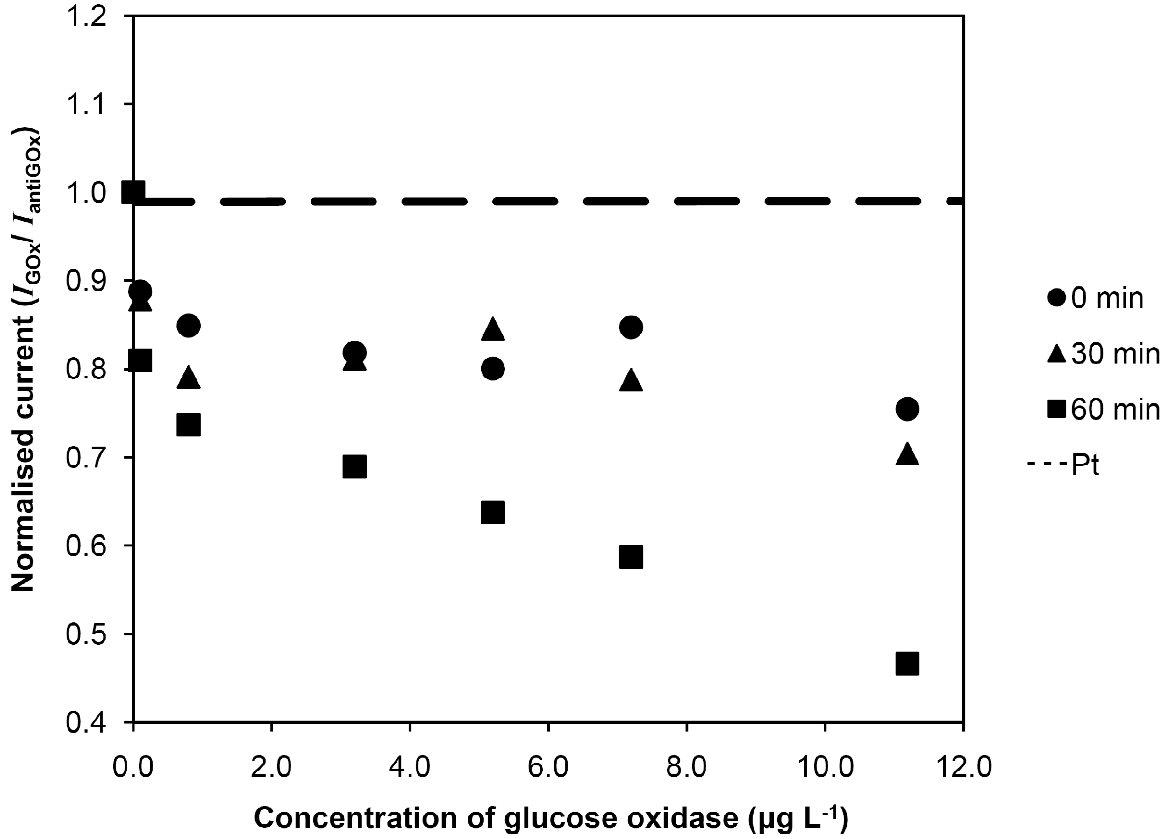

Figure 20. DPV signal response towards the redox probe, ferrocenemethanol for an immunosensor prepared using 0.4 mg L^{-1} anti-GOx and 200 mg L^{-1} BSA over varying concentrations of GOx. Immunosensors were derived from alumina electrodes etched

for 0, 30 and 60 min in 3% phosphoric acid solutions. Concentration of ferrocenemethanol used was 1 mM and all experiments were conducted at 297 K.

Two general trends were observed. First, the decrease in signal response per unit antigen concentration (sensitivity) was highest for electrodes etched at longest time of 60 min. Second, the electrodes etched at 60 min also exhibited the most effective blocking of pore channels at high antigen concentrations, in which its signal response decreased to less than 0.5 times of the initial measured signal response when the channels were unblocked. In contrast, the signal response at high antigen concentrations for the unetched electrode was only ca. 0.8 times of the initial signal response in the absence of antigen.

It was expected that alumina-modified electrodes with pore sizes significantly larger than the IgG and GOx molecules would display poor sensitive response and low resistance towards diffusion of the redox probe at high antigen concentrations. This is considering the dimension of an IgG molecule, which is known to be 14.5 nm × 8.5 nm × 4 nm from X-ray diffraction studies [62] and the average size of a GOx molecule of 14.0 (± 0.3 nm) as determined in phosphate buffered saline (PBS), using dynamic light scattering technique (Malvern Zetasizer Nano ZS). However, SEM studies of the side profiles of alumina overlayers after different duration of etching times further revealed narrow channels extended throughout the alumina overlayer for an unetched alumina-modified electrode (Figure 21). For a 15 min etched alumina-modified electrode, the channels were widened at the side exposed to solution and narrower at the alumina-electrode interface. For the 60 min etched alumina-modified electrode, the alumina overlayer showed two types of layers, a highly porous reticulate layer at the surface with pore sizes at least 10 times larger than either antigen or IgG molecule. The inner layer of the 60 min etched alumina electrode resembled unetched alumina with channel diameters ca. 30–50 nm (Figure 21), the result of slower etching rates at the ‘inner’ part of channels due to depletion and slow mass transfer of acid reagent within the alumina overlayer. Channel diameters within the inner alumina overlayer thus remained relatively unchanged over the varying etching time.

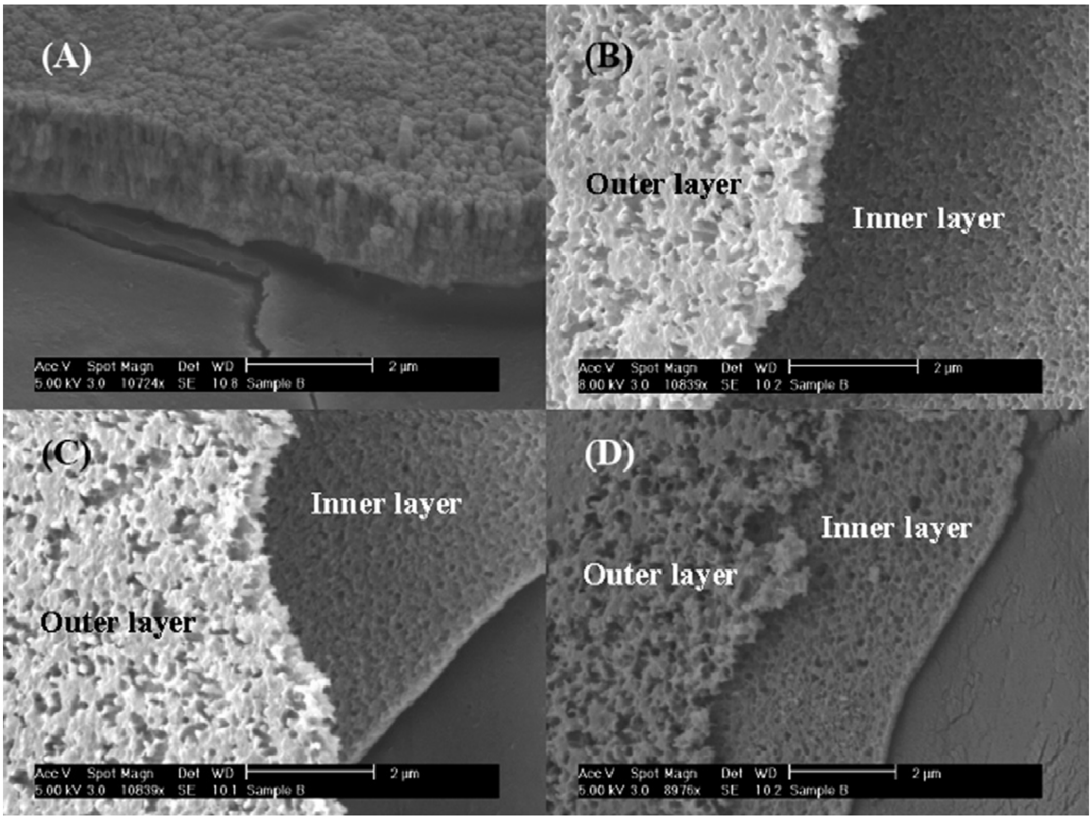

Figure 21. Scanning electron micrographs of side profiles of alumina overlayers etched in 3% phosphoric acid for (A) 15, (B) 30, (C) 45 and (D) 60 min. The pores of the outer films show extensive merging with poorly defined shapes. Pore sizes of the inner film estimated from SEM micrographs were (A) 20–50 nm (B) 25–70 nm (C) 30–75 nm and (D) 30–100 nm. Pore densities of inner films range from 5.9×10^9 to 7×10^9 pores cm^{-2} for (B), (C) and (D).

Besides the change in pore sizes and channel diameters, the other effect of chemical etching on alumina-modified electrodes was a reduction in the ratio of outer surface area to the total internal channel volume of the alumina overlayer. It was possible that binding of antigen molecules to IgG molecules sited along the alumina outer surface occurred, which could not influence the sensor response. Whereas, an extensively etched alumina-modified electrode with reduced ratio of outer surface-to-channel volume likely exhibited sensitive response towards antigen due to majority of antigen-antibody binding occurring along the diffusion path of the redox probe within the channels.

3.5. Electrochemical Studies

During a potential step experiment of an electrochemical reversible redox couple, the faradaic current flow at a planar electrode can be described by a Cottrell-type equation, in which the magnitude of the transient current is inversely related to the square root of time as well as the equilibrium surface concentration ratio of the oxidized and reduced forms of the redox couple after the potential step [25]. The signal response obtained during a differential pulse voltammetric experiment derived from the difference in the faradaic current flow before and after the pulse is thus expressed in the form of the same Cottrell-type equation, with consideration of the equilibrium surface concentration ratios of the oxidized and reduced forms of the redox couple before and after the potential step. For a nernstian system, these concentration ratios are related exponentially to the applied potentials and it can be readily shown at $E = E_{\max}$ (where $E_{\max} = E^{0'} - \Delta E/2$ and ΔE is the pulse height applied during the DPV experiment), the maximum peak height is linearly proportional to concentration of the redox species for an electrochemically reversible system [25]:

$$(\delta i)_{\max} = \frac{nFAD^{1/2}C_{\text{bulk}}}{\pi^{1/2}(\tau - \tau')^{1/2}}\left[\frac{(1-\sigma)}{(1+\sigma)}\right] \qquad (3)$$

where $(\delta i)_{\max}$ is the maximum peak height or DPV signal response, n is 1, F is the Faraday constant, D is the diffusion coefficient of ferrocenemethanol, C_{bulk} is the bulk concentration of ferrocenemethanol, (τ- τ') is the pulse duration, ΔE is the pulse amplitude and $\sigma = \exp(-nF\Delta E/2RT)$ for the oxidation process. Figure 22 shows the plot of maximum peak height $(\delta i)_{\max}$ against $\frac{1-\sigma}{1+\sigma}$ obtained during DPV measurements towards the redox probe over varying pulse heights for unetched and 60 min etched alumina electrodes immobilized with IgG, IgG/BSA or IgG/BSA/antigen. Plots are shown for pulse amplitude values from 0 to 130mV, which demonstrated good linearity, consistent with an electrochemically reversible system, under the experimental conditions described in the caption of the figure. The inset at Figure 22 shows the magnitude of $AD^{1/2}$ derived from the slopes of the plots of $(\delta i)_{\max}$ against $\frac{1-\sigma}{1+\sigma}$. In our immunosensor system, the concentration of ferrocenemethanol was kept constant throughout the experiments. Thus changes in the maximum peak height for the different experiments could only arise due to variation of the electrode active area and/or diffusion coefficient of the redox probe, according to Equation (3).

Figure 22 inset revealed gradual decrease in the magnitude of $AD^{1/2}$ for the IgG and IgG/BSA immobilized 60 min etched alumina electrode, but significant decrease for the IgG/BSA/antigen immobilized 60 min etched alumina electrode. This trend agrees with the result obtained in Figure 17 in which the DPV waveforms similarly revealed significant decrease in the maximum peak height in the presence of antigen. The magnitude of $AD^{1/2}$ values are slightly less than the known diffusion coefficient value of ferrocenemethanol of 1 × 10^{-5} cm^2 s^{-1} and that calculated using the surface area of the 76 µm diameter electrode overlaid by an alumina layer comprising ca. 30 nm size pores of ca. 7 × 10^9 pores cm^{-2} pore density. It is likely due to reduced diffusion coefficient of the redox probe when the channel diameters were narrowed in the presence of antigen due to formation of immunocomplex within the channels, as determined by molecular dynamic stimulation study carried out for system comprising channel size smaller than five times the diameter of the diffusing species [63]. Interestingly, the magnitude of $AD^{1/2}$ obtained at the unetched alumina-modified electrode remained fairly constant when immobilized using IgG, IgG/BSA and IgG/BSA/antigen. This is probably due to ineffective blocking of the channels for the unetched alumina electrode, likely the results of a large number of available binding sites along the outer surface of the unetched alumina overlayer and a smaller channel size in comparison to the etched electrode, which reduce the ease of access by the biological molecules.

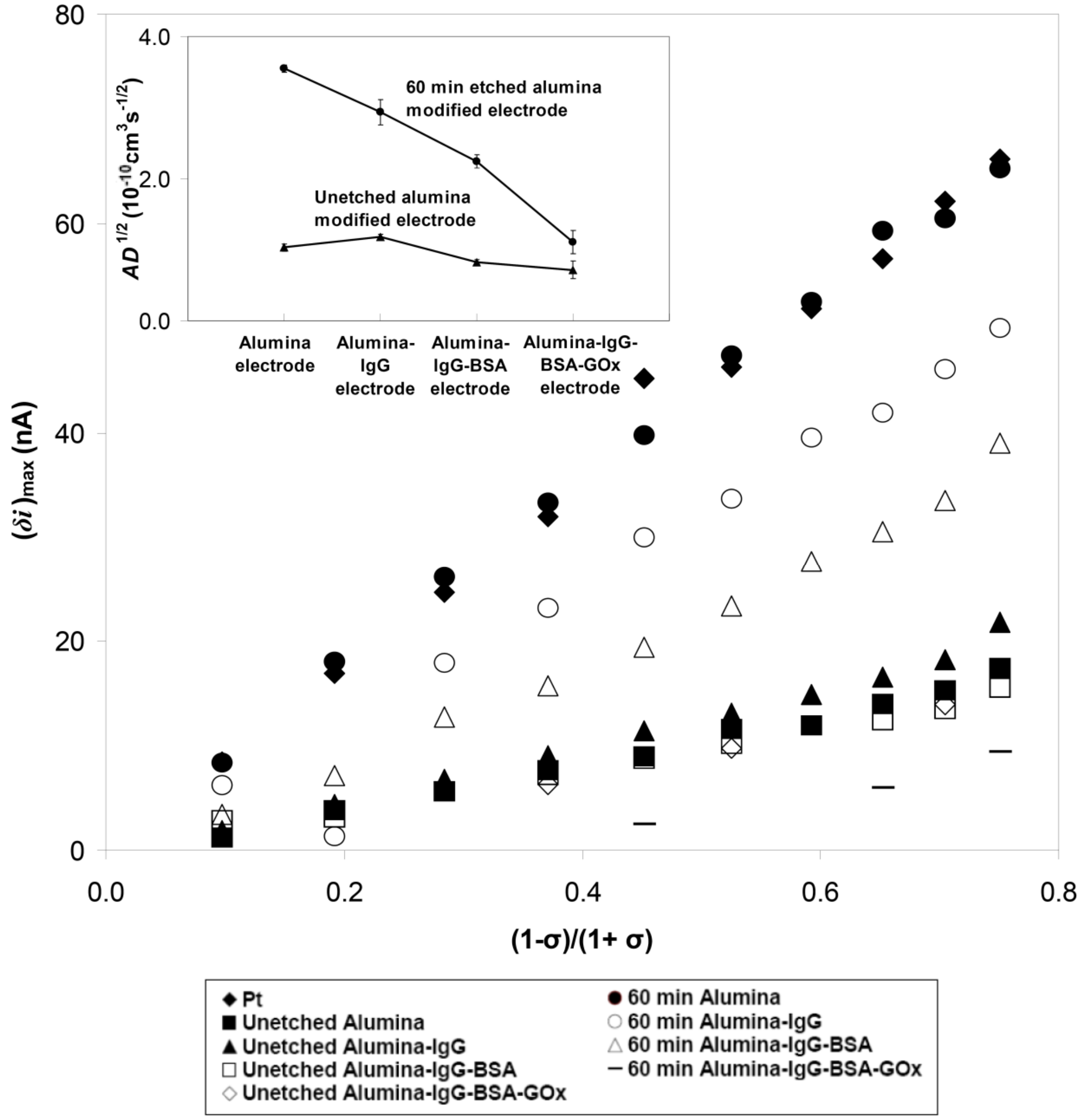

Figure 22. Plots of $(\delta i)_{max}$ against $(1 - \sigma)/(1 + \sigma)$ obtained by varying DPV pulse amplitude from 10 to 130 mV with a pulse width of 50 ms in an unstirred solution containing 1mM ferrocenemethanol at 297 K. Relative standard deviation of $(\delta i)_{max}$ ranges from ± 4.2% for 10 mV pulse amplitude to ± 22.7% for 130 mV pulse amplitude. Inset: variation of $AD^{1/2}$ with respect to types of alumina electrodes immobilized with IgG, IgG/BSA or IgG/BSA/antigen, derived from slopes and slope errors of best-fit lines through the plots presented in this figure.

3.6. Figures of Merit

Measurement of the signal-to-noise ratio revealed a decreasing signal-to-noise (*S*/*N*) ratio, for example, from *S*/*N* = 28 at 200 ng L^{-1} to *S*/*N* = 16 at 50 μg L^{-1} antigen concentration for one of the immunosensor electrodes. This has the advantage of increased sensitivity towards the antigen at low concentrations, unlike most sensors in which the signal-to-noise ratio decreases as concentration of analyte decreases.

Limit of detection was derived from the minimum antigen concentration value which produced a reduction of sensor signal equivalent to three times the background noise at zero antigen concentration. A low-detection limit (LOD) of 100 ng L^{-1} of GOx antigen was achieved using this simple sensing approach with a linear logarithmic concentration dependence range, extending from 200 ng L^{-1} to 11.2 µgL^{-1} (correlation of determination = 0.993). In comparison, commercially available ELISA technique has a higher LOD of ca. 10 µg L^{-1}. Unlike ELISA, where large quantity of antibody (50 µL of 20 mg L^{-1}) is typically used for protein detection, this membrane-based electrochemical immunosensor system requires only ca. 5 µL of 0.4 mg L^{-1} antibody for sensor preparation. The detection limit of this technique is significantly lower compared to other similar immunosensors using static batch system [38, 64, 65].

4. Conclusion

Overall, a membrane-based immunosensor with sensitive response has been developed for the detection of the protein, GOx. An extensively etched alumina membrane overlayer provides the greatest decrease in signal response towards the protein antigen molecules over the concentration range tested. SEM studies also revealed that the 60 min etched alumina layer consist of two types of layers, a highly porous reticulate layer at the surface and an inner layer resembling unetched alumina with channel diameters ca. 30–50 nm. In addition, the prepared immunosensor also has a low detection limit of 100 ng L^{-1} GOx antigen. The same approach may be applicable to detection of other proteins, using appropriate complementary binding immunoglobulin antibodies and this is illustrated in the following chapter.

CHAPTER IV

MEMBRANE-BASED ELECTROCHEMICAL BIOSENSOR – DETECTION OF WEST NILE VIRAL DOMAIN III PROTEIN AND PARTICLES

1. Introduction

Following the successful determination of glucose oxidase enzyme using the developed alumina membrane-based electrochemical immunosensor, it was aimed to made use of the same sensing platform for the detection of West Nile virus domain III (WNV-DIII), which is a specific protein segment of the viral envelope protein and WNV viral particles. Experimental conditions, such as pH, ionic strength of sensing solution and concentration of immunoglobulin M (IgM) utilised for detection, were optimised for the determination of WNV-DIII and the same experimental parameters were subsequently used for detection of WNV particles.

1.1. West Nile Virus

West Nile virus (WNV) was first isolated from a female adult in Uganda in 1937 and had since circulated throughout Africa, Asia, USA, southern Europe, the Middle East and Australia [66]. It had caused over a dozen epidemics of West Nile fever and meningoencephalitis during the past eight decades. The virus normally circulates in natural transmission cycles involving mosquito vectors (usually *Culex* species) and birds, whereas humans and horses are considered incidental or dead-end hosts [67].

As of all flavivirus, the WNV is made up of three structural proteins – a large envelope protein (E), a single nucleocapsid protein (C) and a lipid membrane protein (M). Its genome RNA strand and the protein C form an isometric nucleocapsid, while the M and E proteins, together with the host's membrane, form the envelope that surrounds the nucleocapsids [21] (Figure 23). Protein E also enables receptor binding, host membrane fusion and can elicits a neutralizing antibody response [68]. It is arranged as a homodimer and each monomer has three domains (I, II and III). Among the different domains, domain III is responsible for binding to the host's cell before membrane fusion occurs. Experiments were thus conducted systematically, by first carrying out the detection of WNV-DIII protein, followed by the determination of WNV particles. The domain III protein was also chosen due to its well-studied sequence [69, 70] and its short length of ca. 100 amino acids makes it less susceptible to folding when isolated from the rest of the protein envelope [68].

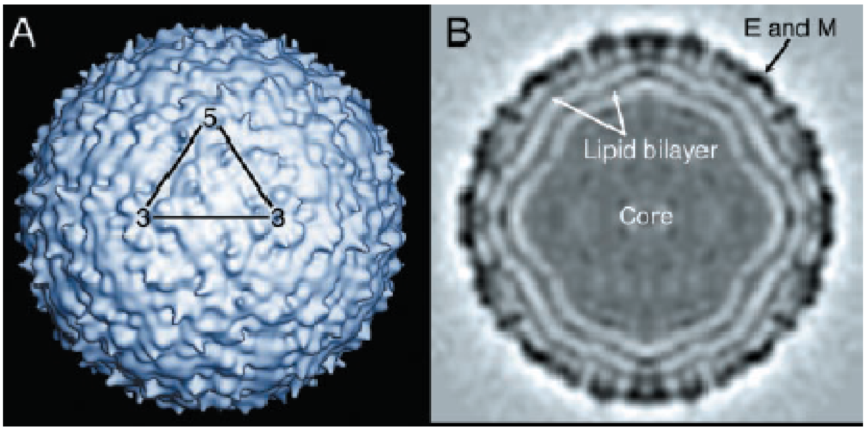

Figure 23. A 17 Å structure of West Nile virus determined by cryo-EM. (**A**) A surface shaded view of the virus. (**B**) A central cross section showing the concentric layers of density [7]. From Mukhopadhyay S., Kim B.-S., Chipman P. R., Rossmann M. G., Kuhn R. J., *Science* **2003**, 302, 248. Reprinted with permission from AAAS.

WNV poses significant public health problems in affected countries. Surveillance and early detection schemes are thus necessary to reduce the spread of the virus from animal vectors to human hosts. The detection of WNV had been typically conducted using immunoassays and reverse transcriptase polymerase chain reaction (RT-PCR) [66, 67, 71-73]. However, these methods are usually labour intensive and time-consuming.

The detection scheme employed for the prepared immunosensor is the same as that employed for determination of GOx. Immunoglobulin M (IgM) antibody raised against WNV-DIII protein was physically adsorbed along the channel walls within the alumina overlayer of an alumina modified electrode. In the presence of WNV-DIII protein, formations of the immunocomplexes occur within the channels of nanosized diameter. The channels thus become blocked in the presence of the protein analyte. The status of blocked and unblocked channels was subsequently detected via a mass transport limiting electro-oxidative current generated by an electrochemical probe, ferrocenemethanol, which diffused through the nano-sized channel to reach the electrochemical sensor at the alumina-electrode interface for redox processes. Again, differential pulse voltammetry was used as the detection technique.

2. Experimental

2.1. Reagents and Materials

Monoclonal anti-West Nile virus (H546, isotype IgM, 275 μg mL^{-1}) was obtained from Microbix Biosystems. Bovine serum albumin (BSA, >98%), ferrocenemethanol (FeMeOH, >99%), sodium dihydrogenphosphate dihydrate and phosphoric acid were purchased from Sigma Aldrich. Sodium chloride (NaCl) was purchased from QRëC. All protein solutions were prepared in 0.1 M phosphate buffer (pH 6.8), unless otherwise stated. All chemicals and solvents used were of analytical grade and were used as received. Ultrapure water (Barnstead Nanopure Ultrapure Water System) was used for preparations of all buffers, unless otherwise stated. Electrodes used were home-made platinum disk electrodes and modified according to the procedures stated in Chapter III section 2.2. West Nile Virus domain III protein and particles were provided by Professor Ng Mah Lee, Mary from the Department of Microbiology, NUS.

2.2. West Nile Virus Domain III Protein and Particles Detection

Detection of WNV-DIII was carried out using the following conditions. 0.2 μg mL^{-1} immunoglobulin M (IgM) solution, 200 μg mL^{-1} BSA solution and 0.25 μg mL^{-1} WNV-DIII solution were first prepared using 0.1 M phosphate buffer (pH 6.8, ionic strength of 1.7M NaCl). IgM was next physically adsorbed onto the alumina modified electrode tip for 1 hour and non-specific binding sites along the channel walls were blocked off subsequently by further adsorption of BSA for 30 min in a solution containing 200 μg mL^{-1} BSA. Both IgM and BSA immobilisation was done by placing 5 μL of the respective protein solution onto the electrode tip. A three-electrode system was then employed for the measurement of faradaic currents of the redox probe, using a silver-silver chloride reference electrode and a 2 mm diameter platinum disk, auxiliary electrode. Detection of WNV-DIII protein antigen was carried using a batch system in which the prepared immunosensor was kept immersed in a sensing solution containing constant concentration of 1 mM ferrocenemethanol, prepared in 100 mM phosphate buffer (pH 6.8, ionic strength of 1.7 M NaCl). Concentration of WNV-DIII in the sensing solution was varied from 0.008 to 0.05 ng mL^{-1} by addition of aliquots from a 0.25 µg mL^{-1} WNV-DIII stock solution containing 1 mM ferrocenemethanol, into the sensing solution. Differential pulse voltammograms (CHI440 potentiostat/ galvanostat, data acquisition software) were obtained at 30 min intervals after addition of each aliquot into the sensing solution. The same was done for the detection of WNV particles.

3. Results and Discussion

3.1. Control Experiments

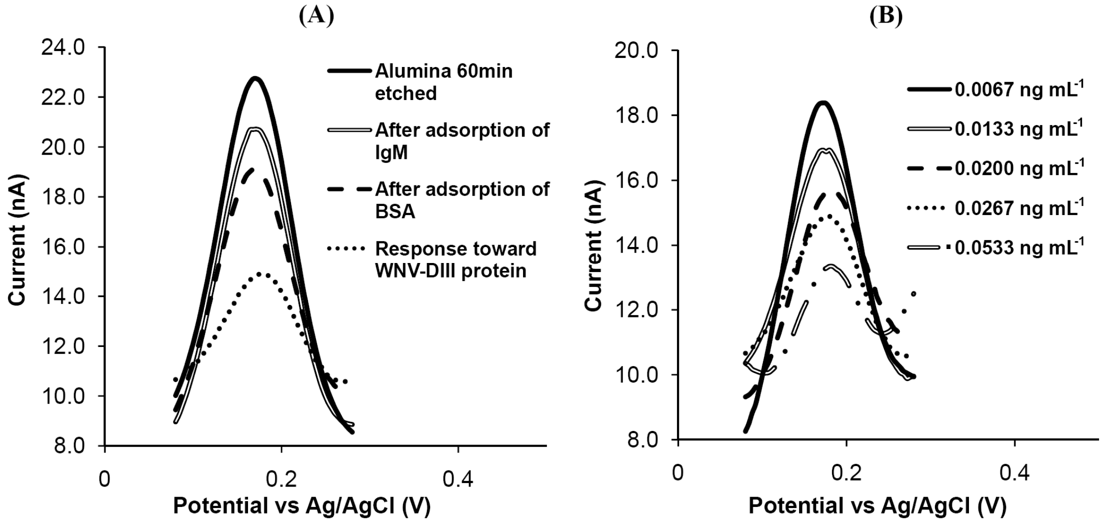

Figure 24. (A) DPV signal response obtained at a 60 min etched alumina electrode immersed in 1 mM ferrocenemethanol, after each step of the sensor preparation procedure. (B) DPV signal response of an immunosensor towards ferrocenemethanol in increasing concentration of WNV-DIII protein, with corresponding decrease in signal response for an immunosensor prepared similarly as in (A).

Figure 24A shows the typical differential pulse voltammograms of ferrocenemethanol obtained at an alumina modified platinum disk electrode after each step of the sensor preparation procedure. The differential pulse voltammetric peak signal responses towards ferrocenemethanol decreased incrementally after IgM, BSA and WNV-DIII protein were adsorbed in consecutive steps onto the alumina overlayers. The DPV peak signal response towards the redox probe was further reduced during successive batch additions of increasing concentrations of protein (Figure 24B). This is again due to adsorption of proteins within the channels "blocking" the diffusion path of redox probe through the channels. Thus the peak signal response of the DPV decreased after each protein adsorption step. Interestingly, the alumina electrode adsorbed with BSA alone exhibited inconsistent and poorly reproducible DPV results. This is likely due to the random formation of dimeric and oligomeric BSA species [74, 75], which "block" the nanosized diameter channels to different extents. In contrast, the prior adsorption of IgM for the IgM/BSA electrode probably reduced the number of available binding sites for formation of oligomeric BSA.

To investigate the influence of this method for analytical sensing of WNV-DIII protein, 4 different electrodes were prepared using IgM (IgM-alumina electrode), BSA (BSA-alumina electrode) and IgM/BSA (IgM-BSA-alumina electrode) or no adsorbed biomolecule (alumina electrode). Figure 25 shows the trend of the normalised DPV signal responses of the electrodes toward ferrocenemethanol during batch addition of increasing concentrations of WNV-DIII protein. The IgM–BSA alumina electrode gives the largest decrease in DPV signal response. This indicates formation of IgM-WNV-DIII immunocomplex is effective towards reducing the diffusion rate of ferrocenemethanol through the nanochannels. For the IgM-alumina, BSA-alumina and alumina electrodes, there are insignificant decreases in the DPV signal responses (Figure 25). This suggests that non-specific binding of WNV-DIII within the channels of the alumina overlayer is less effective in blocking the diffusion path of the redox probe, compared to specific binding between WNV-DIII and its antibody, IgM. It is also possible that the slight decrease in DPV peak signal response is due to surface fouling of the platinum electrode by the protein antigen.

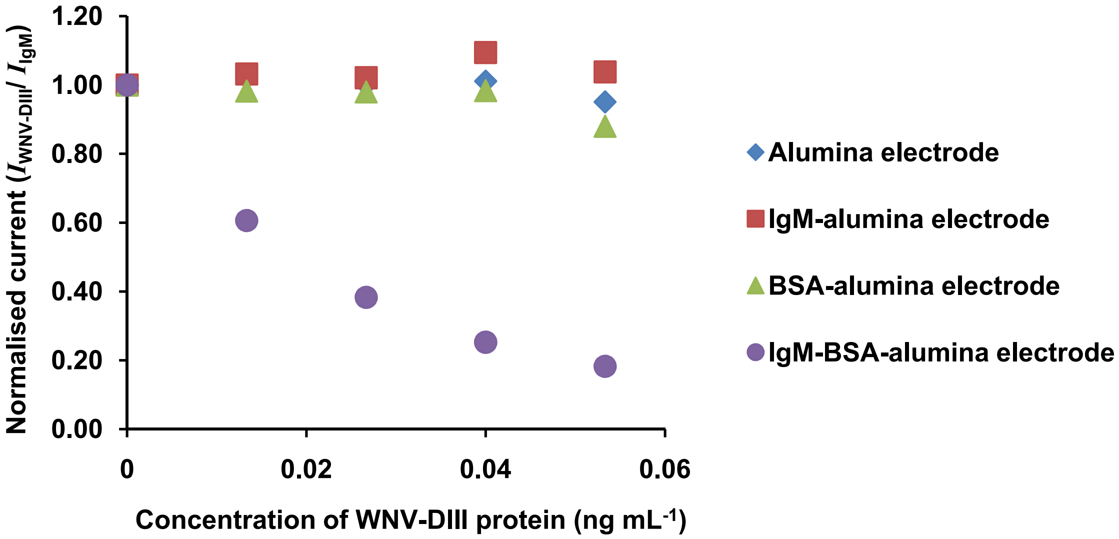

Figure 25. DPV signal responses of four different alumina electrodes prepared using IgM (IgM-alumina electrode), BSA (BSA-alumina electrode) and IgM/ BSA (IgM-BSA-alumina electrode) or no adsorbed biomolecule (alumina electrode). Controls were studied over the antigen concentration range of 0.007 to 0.05 ng mL^{-1} in 1 mM ferrocenemethanol solution at pH 6.8 and an ionic strength of 1.7 M. All alumina electrodes used were etched in 3% phosphoric acid for 60 min. 0.2 µg mL^{-1} IgM solution and 200 mg mL^{-1} BSA solution were used for immobilisation of either or both proteins for the alumina electrodes. All experiments were conducted at 297 K.

3.2. Effect of Antibody Concentration

To understand the effect of IgM antibody loading on the sensor response toward WNV-DIII antigen, IgM-BSA-alumina electrodes were prepared from 0.1 to 0.4 μg mL^{-1} IgM solutions and used for WNV-DIII detection (Figure 26). Using a higher IgM concentration of 0.4 μg mL^{-1}, the prepared electrode exhibited a small, linear concentration range from 0.007 ng mL^{-1} to 0.030 ng mL^{-1} and low detection limit of WNV-DIII antigen. This is probably due to higher loading of IgM antibody within the nanochannels, which led to more antigen molecules being retained within the nanochannels at each antigen concentration under equilibrium condition and hence the lower limit of detection. However the initial high loading of IgM molecules within the nanochannels had blocked off most of the alumina pores, resulting in a low initial signal response after all immunosensor preparation steps. The extent at which the signal response can be depressed without compromising the signal-to-noise ratio at the highest concentration of antigen detected is therefore lower, resulting in a narrow linear range.

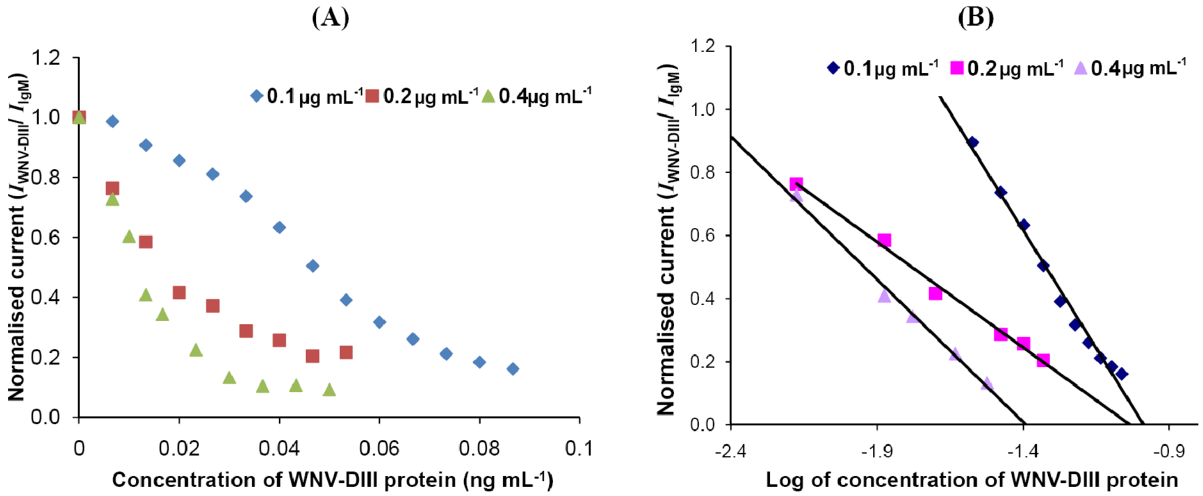

Figure 26. Plots of normalised current against (A) concentration and (B) log of concentration of WNV-DIII protein for different concentrations of IgM used. When a high concentration of 0.4 μg mL^{-1} IgM was used, a lower limit of detection and a narrow linear range was obtained. At lower concentration of 0.1 μg mL^{-1} IgM, a higher limit of detection and a wide linear range was achieved. Thus, to have a

compromise between these two figures of merit, 0.2 μg mL^{-1} IgM was utilised. Sensing solution was 1 mM ferrocenemethanol in 100 mM phosphate buffer (pH 6.8) with an ionic strength of 1.7 M. All alumina electrodes used were etched in 3% phosphoric acid for 60 min.

In contrast, when a low IgM concentration of 0.1 μg mL^{-1} was used to prepare the immunosensor, the electrode exhibited a wider linear range (0.027 ng mL^{-1} to 0.087 ng mL^{-1}) and a higher limit of detection. Due to the initial lower loading of IgM molecules onto the alumina membrane and within the alumina nanopores, the immunosensor can be used to detect over a wider range of antigen concentration due to its initial high signal response after all immunosensor preparation steps. However, the lower loading of IgM molecules also meant that less antigen molecules can be retained within the nanochannels at each antigen concentration under equilibrium condition and hence the higher limit of detection. To compromise between having a wide linear range and an acceptable limit of detection, an optimized 0.2 μg mL^{-1} IgM solution was therefore used as the loading solution for preparation of the WNV-DIII sensor.

3.3. Effect of pH on Adsorption of IgM onto the Alumina Overlayer and Sensor Response

pH of sensing solutions has a strong influence on the stability of proteins such as antibody and antigens. At too low or high pH, antibodies can be denatured, resulting in a change of its three dimensional structure [76], which in turn affects the effective binding to its specific antigen. Determination of optimal pH of the sensing solution for the detection of proteins is thus necessary. For the following investigations, pH of the phosphate buffer solutions used was varied from 6.2 to 8.2, since alumina is stable in the pH range of about 4 to 9 [77] and the buffering capacity of phosphate buffer is effective only at the buffer range of pKa 7.2 (± 1).

Figure 27A shows the effect of pH on the immobilisation of IgM onto the alumina electrode. The percentage decrease in DPV signal responses increased when pH increased from 6.2 to 7.6, indicating a higher loading of IgM molecules onto the alumina electrode. However at pH 8.2, the DPV signal response decreased to a lesser extent. This is likely due to the influence of pH on the overall charge densities of IgM and alumina. At pH 8.2, IgM with an isoelectric point of 8.0 [78] is negatively charged and surface charge density of alumina is also negative at pH higher than 7.2 [79]. Thus at pH 8.2, there will be electrostatic repulsion between the alumina film and negatively charged IgM molecules, resulting in a lower amount of IgM molecules being adsorbed onto alumina, which is reflected in the reduced percentage decrease in DPV signal response. At pH 6.2, 6.8 and 7.6, IgM is positively charged, considering its isoelectric point (pI) of 8.0. At pH value of less than 7.2, alumina has an overall positive surface charge density, which becomes less positive as pH increases and becomes neutral at pH 7.2 [79]. The electrostatic repulsion between the positively charged IgM molecules and alumina thus decreases from pH 6.2 to 7.6. As a result, the percentage decrease in DPV signal responses increased when pH increased from 6.2 to 7.6, indicating a higher amount of IgM molecules being adsorbed onto the alumina.

The different extent of IgM loading onto the alumina electrodes due to pH changes can affect the sensitivity of the IgM-BSA-alumina electrodes (Figure 27B). Sensitivity at each pH value was determined from the gradient of the plots of normalised current against log of concentration of WNV-DIII protein. The gradient values obtained at pH 6.2, 6.8, 7.6 and 8.2 were -0.61 (± 0.04), -0.64 (± 0.03), -0.76 (± 0.06) and -0.42 (± 0.03) respectively. A more negative gradient signifies a greater decrease in signal response at a given analyte concentration and thus higher sensitivity. Since a higher loading of IgM molecules allows more antigen molecules to be retained within the nanochannels at each antigen concentration under equilibrium conditions, it is therefore not surprising for the IgM-BSA-alumina electrodes to be more sensitive as pH increases from 6.2 to 7.6 and to be less sensitive at pH 8.2, following the trend of IgM loading onto the alumina overlayer as pH is varied.

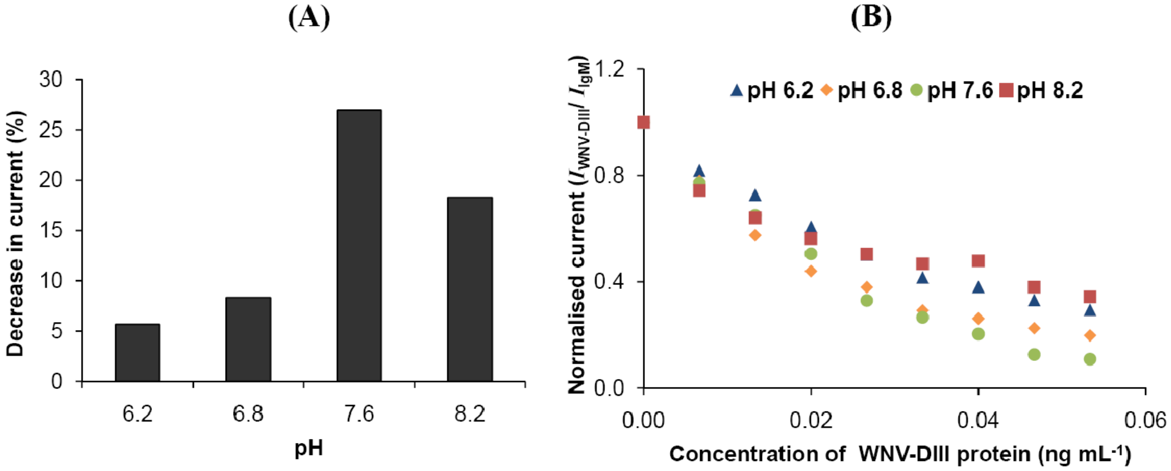

Figure 27. (A) Percentage decrease in observed current upon IgM immobilization at various pH values. The larger decrease in observed current indicates higher loading of IgM molecules onto the surface of the alumina membrane and within the alumina nanopores. (B) DPV signal responses towards redox probe in the presence of increasing antigen concentration, using alumina electrode adsorbed with IgM from solutions of different pH and in sensing solutions of different pH. 1 mM ferrocenemethanol, prepared in 100 mM phosphate buffer with 1.7 M ionic strength solutions was used as the sensing solution.

From the values of the gradient, it is obvious that the most sensitive detection of WNV-DIII was achieved at pH 7.6. However, the difference in the coefficient of determination (0.962 at pH 7.6 and 0.993 at pH 6.8) and results obtained from data fitting into equation (4) derived from a Langmuir-type isotherm (Section 3.6) supports the choice of pH 6.8 as the optimal pH instead.

3.3. Effect of Ionic Strength on Sensor Response

Figure 28 shows the sensor response against WNV-DIII antigen concentrations in three sensing solutions of different ionic strengths. The desired ionic strength of phosphate buffered ferrocenemethanol solution was adjusted using sodium chloride salt. From Figure 28, it is clear that at low ionic strength of 0.5 M and high ionic strength of 3.5 M, the decrease in DPV signal response was minimal. In contrast, at ionic strength of 1.7 M, the largest sensitivity towards the viral protein was achieved.

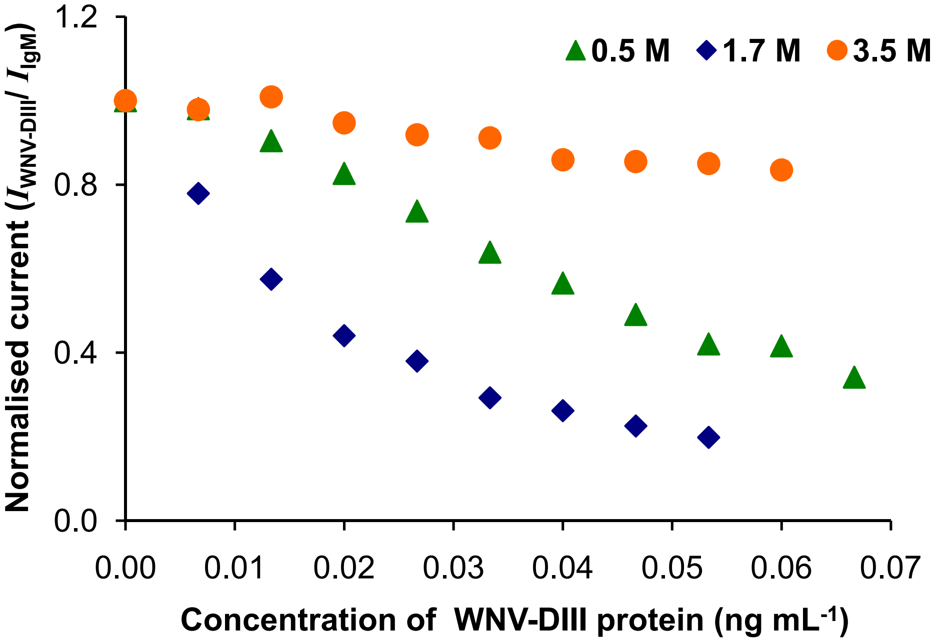

Figure 28. DPV signal responses towards redox probe, prepared in phosphate buffers of different ionic strengths, in the presence of increasing antigen concentration using alumina electrode adsorbed with IgM from solutions of different ionic strengths. 1

mM ferrocenemethanol, prepared in 100 mM phosphate buffer (pH 6.8) was used as the sensing solution. Sodium chloride salt was employed to control of ionic strengths of the prepared buffers.

The reason for lower sensitivity of the alumina-IgM-BSA electrode towards WNV-DIII is probably due to the ‘salting out’ of proteins at high salt concentrations [80] of sizes larger than the surface pore sizes of the alumina overlayer. The extent of immunocomplex formation is subsequently reduced within the channels, resulting in a decrease in the degree of blocking of the nanopores. Thus, the redox probe can readily access the platinum electrode through the alumina overlayer, without much hindrance. Interestingly, at the lower 0.5 M ionic strength, low sensitivity of the alumina-IgM-BSA electrode towards WNV-DIII was similarly observed. It is likely that the reduced total surface charges on alumina at lower ionic strengths at pH 6.8 [79] disfavoured the physical adsorption of IgM along the surface of the alumina channel walls, resulting in reduced loading of IgM molecules onto the alumina overlayer and hence, a prepared immunosensor of lower sensitivity. An intermediate ionic strength of 1.7 M was found to give optimal sensitive response towards WNV-DIII protein.

3.4. Effect of Channel Diameters

The effect of channel diameters on the sensing response of the immunosensor for WNV-DIII detection was conducted by etching alumina electrodes in 3% phosphoric acid for 0, 30 and 60 min. Etching time beyond 60 min caused disintegration of the alumina overlayer. The unetched (0 min) alumina electrode gave large signal response fluctuations (Figure 29). In contrast, the 30 and 60 min etched alumina electrodes gave incremental decreasing signal responses (Figure 29). Similar to results obtained for detection of GOx, the decrease in signal response per unit antigen concentration (sensitivity) was highest for electrodes etched at longest time of 60 min. They also exhibited the most effective blocking of pore channels at high antigen concentrations.

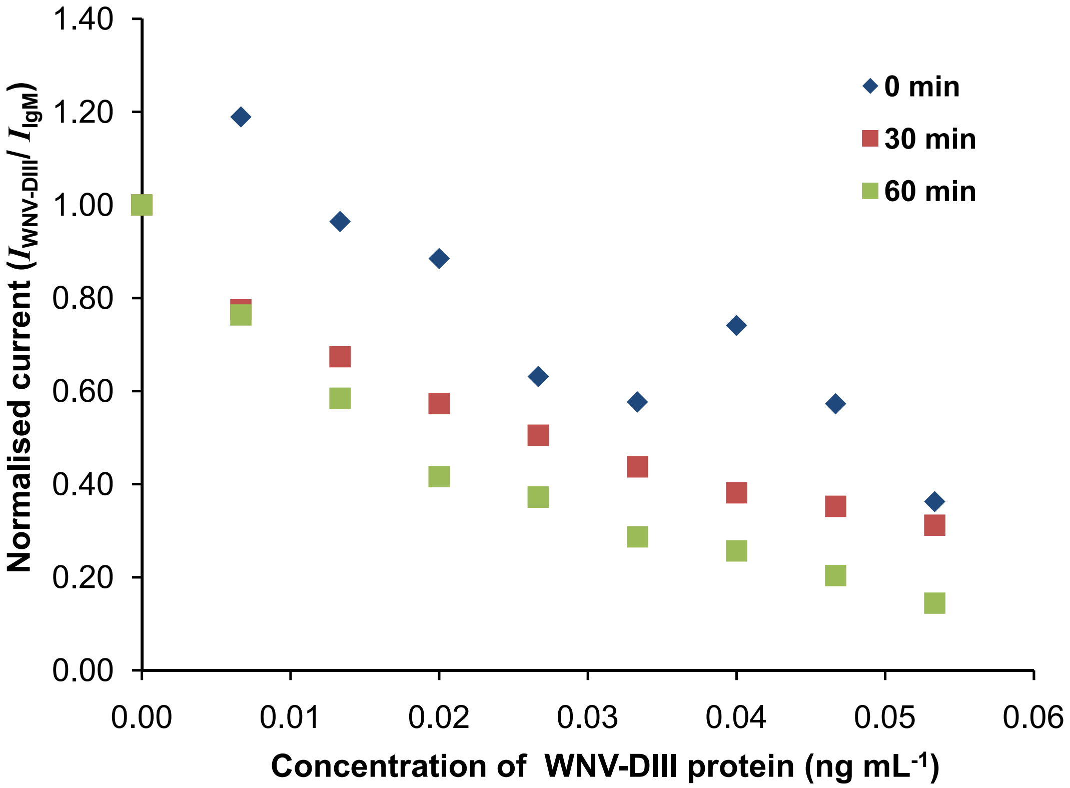

Figure 29. DPV signal response towards the redox probe for an immunosensor prepared using 0.2 µg L^{-1} IgM and 200 mg L^{-1} BSA over varying concentrations of WNV-DIII protein. Immunosensors were derived from alumina electrodes etched for 0, 30 and 60 min in 3% phosphoric acid solutions. Sensing solution was 1 mM ferrocenemethanol, prepared in pH 6.8 phosphate buffer with ionic strength of 1.7 M.

The reason for the fluctuating current response towards redox probe for the unetched alumina electrode was probably due to non-specific adsorption of the antigen within the channels of the alumina overlayer surface. Antibody IgM is a large pentameric molecule with molecular size of 900kDa [81] and estimated width of 29 nm [62], while the pores along the surface of the unetched alumina overlayer have average diameters of 20 nm. The IgM molecules are thus likely to be immobilised along the surface of the alumina overlayer, instead of within the pores. However, the smaller WNV-DIII protein (10.7 kDa) can be adsorbed along the surface and within the pores of the alumina overlayer. Non-specifically adsorbed WNV-DIII protein can easily desorbed from the alumina pores, leading to an erratic signal response.

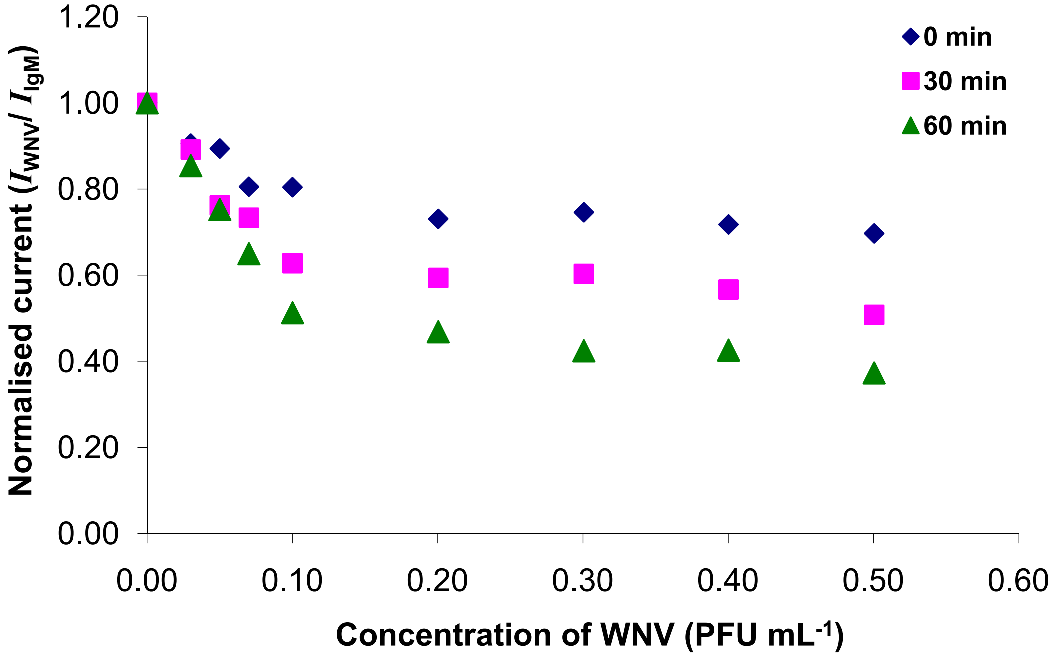

Figure 30. DPV signal response towards the redox probe for an immunosensor prepared using 0.2 µg L^{-1} IgM and 200 mg L^{-1} BSA over varying concentrations of WNV particles. Immunosensors were derived from alumina electrodes etched for 0, 30 and 60 min in 3% phosphoric acid solutions. Sensing solution was 1 mM ferrocenemethanol, prepared in pH 6.8 phosphate buffer with ionic strength of 1.7 M.

A similar experiment conducted using whole virus particles with dimension ca. 50 nm showed similar incremental decrease in the DPV signal responses for the 30 min and 60 min etched alumina electrodes in the presence of increasing concentration of WNV particles (Figure 30). However, the signal response obtained for the unetched (0 min) alumina electrode was not as erratic. Considering the size of IgM molecules (29 nm), WNV particles (50 nm) and nanopores (20 nm), it is likely the 20% decrease in DPV signal response is due to the specific binding of the IgM and WNV particles immobilised along the surface and not within the alumina nanopores. Under this condition, low sensitivity cannot be achieved though specific binding between IgM and WNV particles can occur. From both sets of results, it is evident that the 60 min etched alumina electrode is the most sensitive and effective for WNV-DIII protein and WNV particles determination.

3.5. Stability and Reproducibility of Sensor Response

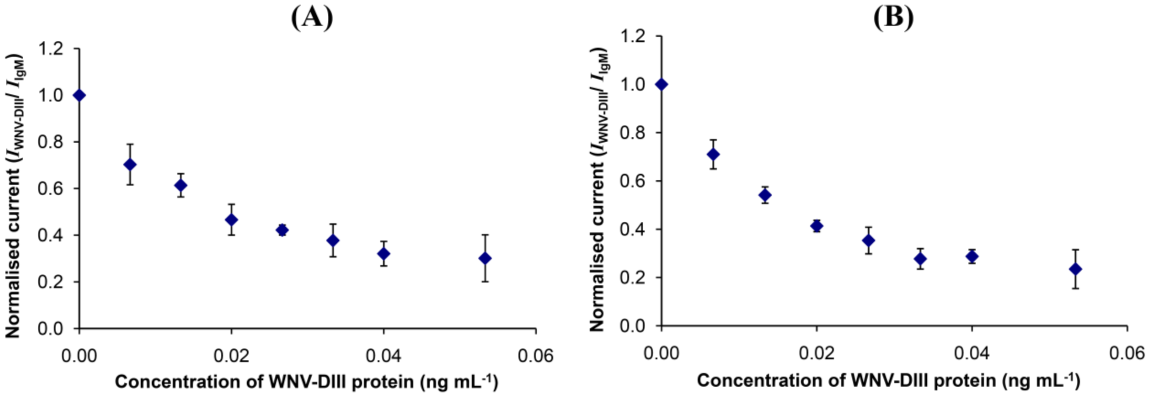

Figure 31. Reproducibility (A) across different batches of sputtered electrodes and (B) within a single batch of electrodes sputtered with aluminum simultaneously. Standard deviations in the range of 2% to 10% and a low limit of detection of 4 ng mL^{-1} were obtained.

Signal responses of the alumina modified electrodes towards the redox probe in the presence of antigen were normalised against the signal response of alumina electrode immobilised with IgM (alumina-IgM), instead of alumina electrode immobilised with IgM and BSA (alumina-IgM-BSA), which had been similarly done for data obtained for the determination of GOx in the previous chapter. The former method gave reproducible results for different electrodes and good linear logarithmic plots of normalised signal response against concentrations. This is likely due to irreproducible non-specific binding between BSA and IgM close to or at the antigen binding site which the BSA molecules are readily removed and subsequently displaced by the protein antigen which binds specifically to IgM. This method of data presentation significantly improved the reproducibility of the immunosensor for 3 different electrodes, which was critical to its applicability. Reproducibility of the fabricated alumina electrodes utilized for WNV-DIII detection was investigated across different batches and within a batch of prepared electrodes. All alumina electrodes were etched in 3% phosphoric acid for 60 min before immobilization of both IgM and BSA.

Calibrations employing alumina electrodes from different fabricated batches resulted in standard deviations ranging from 2% to 8%, while that conducted using alumina electrodes of the same fabricated batch resulted in standard deviations ranging from 2% to 10% (Figure 31) across the concentration range of WNV-DIII protein investigated. These slight deviations could be due to the differences in sputtered aluminum overlayer thickness or anodization that led to slight differences in pore sizes. Since IgM molecules were physically adsorbed onto the alumina overlayer, differences in IgM molecular orientation may also have contributed to differences in the observed signal responses. However, standard deviations of the calibrations are within acceptable range and a limit of detection of 4 ng mL^{-1} (S/N = 3) was obtained for detection of WNV-DIII protein.

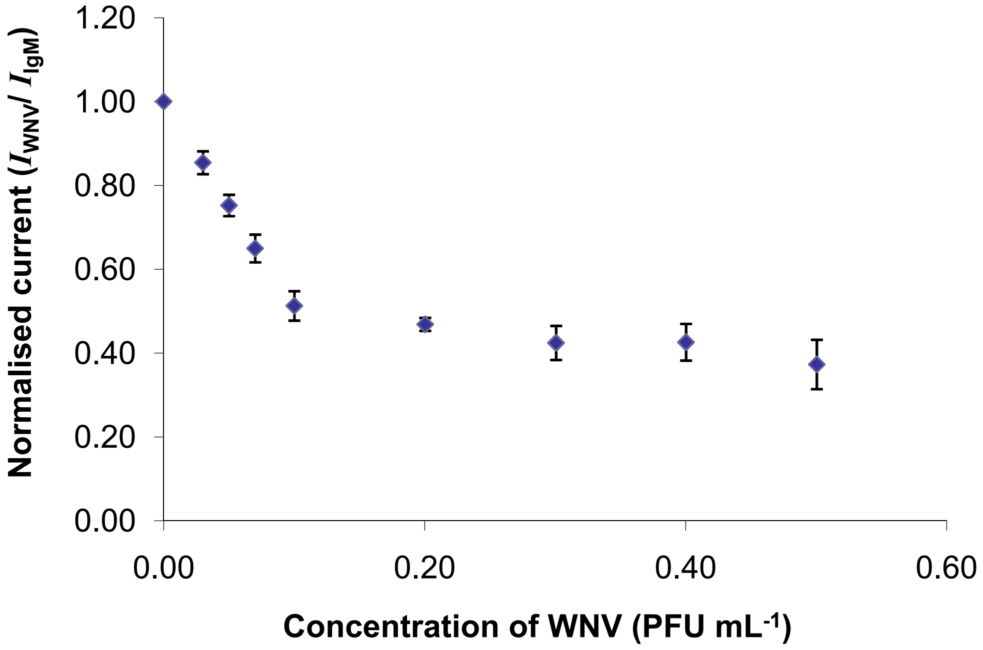

Figure 32. Reproducibility of the prepared IgM-BSA-alumina electrodes applied in the detection of WNV particles. Standard deviations in the range of 2% to 6% and a low limit of detection of ca. 0.02 PFU mL^{-1} (2 viral particles mL^{-1}) were obtained.

Figure 32 shows the signal responses of three similarly prepared alumina electrodes applied for the determination of WNV particles. Standard deviations ranging from 2% to 6% were obtained for signal responses across the concentration of 0.03 to 0.50 plague forming unit (PFU) mL^{-1} WNV particles. Considering the lowest PFU that can be detected with a signal-to-noise ratio of 3, the limit of detection of the immunosensor was estimated to be 0.02 PFU mL^{-1} (ca. 2 viral particles mL^{-1}).

3.6. Fitting of Data

Logarithmic plots of immunoassay experimental data which include log-log and logit-log are commonly used for deriving linear plots for calibration purposes [82]. Similarly in this work, plots of the normalized DPV signal response against logarithmic function of concentration yield good linearity for data derived under the optimized conditions (Figure 33).

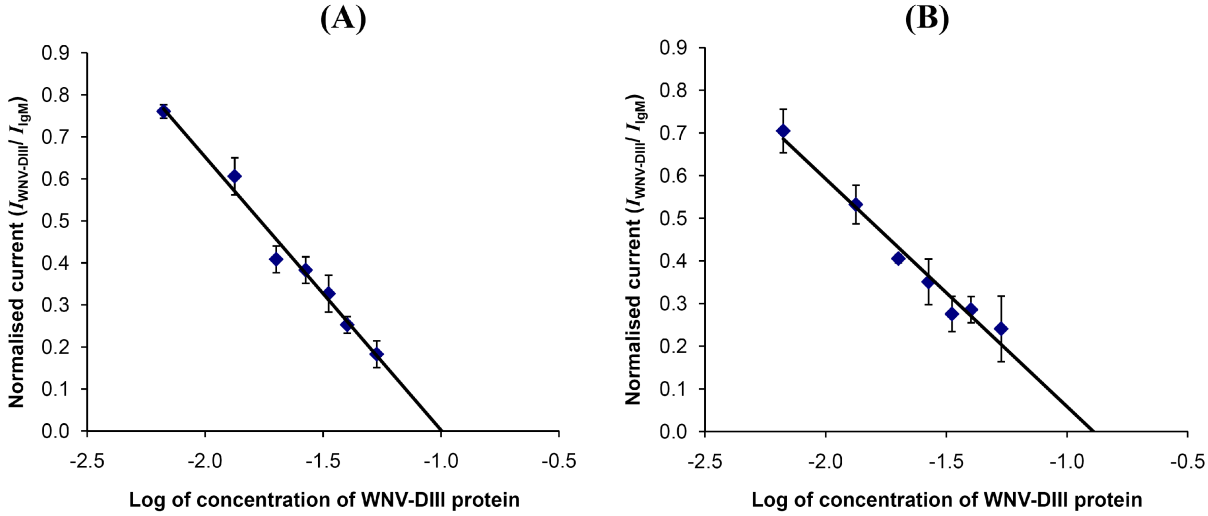

Figure 33. Plots of the normalized DPV signal response against logarithmic function of WNV-DIII protein concentration (A) within a single batch and (B) across different batches of fabricated electrodes. Calibration plots were obtained using alumina modified electrodes etched for 60 min in 3% phosphoric acid. Sensing solution was 1 mM ferrocenemethanol, prepared in pH 6.8 phosphate buffer with ionic strength of 1.7 M.

However, these mathematical plots do not adequately explain the physicochemical processes occurring within the system. To correlate the antigen detection mechanism with the detection signal response, a simple model is described as follows:

$$IgM_S + P \leftrightarrow IgM_S\text{-}P$$

where IgM_S refers to the surface bound immunoglobulin M within a channel, P is the WNV-DIII protein and IgM_S-P refers to the immunocomplex formed between the antibody and antigen within the channel. Herein, formation of immunocomplex between protein and IgM bound to alumina surfaces outside the channels was not considered. Since only one monolayer of protein molecules can form immunocomplexes to the surface-bound IgM molecules, the well described Langmuir-type isotherm can be used to describe the binding process as follows:

$$\theta = \frac{K_b[P]}{(1 + K_b[P])} \qquad (4)$$

where θ is the fraction of filled effective binding sites and each effective binding site refers to one surface bound IgM unit within the channel. $[P]$ is concentration of WNV-DIII protein and K_b refers to the equilibrium binding constant between IgM and WNV-DIII.

The observed DPV peak signal response was derived from the mass transfer-limiting oxidation process of the redox probe at the platinum electrode. Under the condition in which no formation of immunocomplex occurs within the channel, the DPV peak signal response, I_{IgM} is the maximum. In the presence of antigen, the formation of immunocomplex within the channel reduces the rate of diffusional mass transfer of the redox probe moving through the channels towards the platinum electrode under the alumina overlayer [63]. Therefore, it is assumed that each filled binding site within the channel causes a proportionally linear incremental decrease in the DPV signal response towards the redox probe. Thus, the experimentally determined normalized DPV signal response $\frac{I_{\mathrm{IgM-WNV}}}{I_{\mathrm{IgM}}}$ can be related to fraction of filled binding sites θ as follows:

$$k\theta = 1 - \frac{I_{\text{IgM-WNV}}}{I_{\text{IgM}}} \qquad (5)$$

where $\left(1 - \frac{I_{\text{IgM-WNV}}}{I_{\text{IgM}}}\right)$ is the decrease in the normalized DPV signal and k is the proportionality constant.

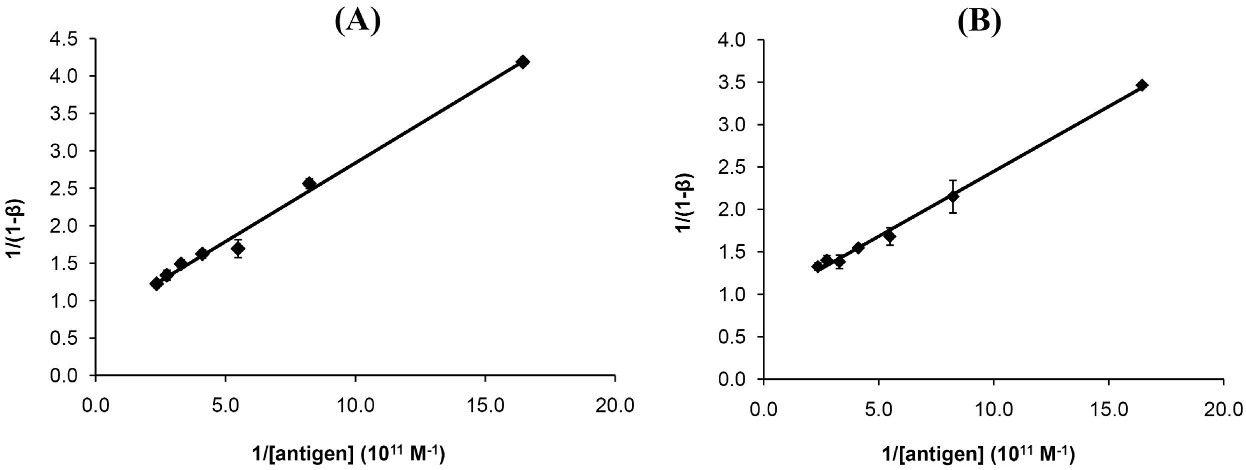

Figure 34. Langmuir fitting of reproducibility plots of WNV-DIII detection (A) within a single batch and (B) across different batches of electrodes. Calibration plots were obtained using alumina modified electrodes etched for 60 min in 3% phosphoric acid. Sensing solution was 1 mM ferrocenemethanol, prepared in pH 6.8 phosphate buffer with ionic strength of 1.7 M. Note that $\frac{1}{1\text{-}\beta} = \frac{1}{1 - \frac{I_{\text{IgM-WNV}}}{I_{\text{IgM}}}}$.

From equations (4) and (5), the relation between normalized DPV peak signal response and concentration of WNV-DIII protein is expressed as follows:

$$1 - \frac{I_{\text{IgM-WNV}}}{I_{\text{IgM}}} = \frac{kK_{\text{b}}[P]}{(1 + K_{\text{b}}[P])} \qquad (6)$$

Rearrangement into its reciprocal form gives:

$$\frac{1}{1-\frac{I_{\mathrm{IgM-WNV}}}{I_{\mathrm{IgM}}}}=\frac{1}{kK_{\mathrm{b}}[P]}+\frac{1}{k} \qquad (7)$$

Figure 34 shows the double reciprocal plots of $\frac{1}{1-\frac{I_{\mathrm{IgM-WNV}}}{I_{\mathrm{IgM}}}}$ against $\frac{1}{[P]}$ using the same experimental data shown in Figure 31. Good linearity with coefficients of determination of 0.992 and 0.984 were obtained for all IgM-BSA-alumina electrodes within the same fabricated batch and between different batches respectively.

Table 2. K and r^2 values obtained from Langmuir plots of WNV-DIII protein calibration plots obtained upon variation of different parameters investigated.

Parameter investigated	**Variations**	**K_b (10^{11})**	**k**	**r^2**
pH of buffered electrolyte	pH 8.2	8.5	0.74	0.981
	pH 7.6	3.8	1.30	0.962
	pH 6.8	3.5	1.36	0.993
	pH 6.2	2.9	1.16	0.986
Ionic strength of electrolyte	1.7M	4.5	1.20	0.974
	0.5M	0.9	0.81	0.978
	3.5M	0.3	1.04	0.965
Etching time	0 min	11.7	0.24	0.006
	30 min	3.5	1.09	0.999
	45 min	13.4	0.72	0.940
	60 min	4.1	1.27	0.982
Reproducibility	Within batch	3.5	1.36	0.992
	Across batches	6.0	1.09	0.996

Table 2 summarized the values of K_b and k derived from the reciprocal plots under different pH, ionic strengths of electrolyte and etching times of the alumina overlayer. Fitting of the data obtained from varying etching time, ionic strength and pH further supports the selection of 60 min etching time, pH 6.8 and 1.7 M ionic strength as the optimal conditions for detection of WNV-DIII utilizing our alumina electrode. Data fitting yield linear plots of the highest r^2 values of 0.994, 0.993 and 0.993 within each set of data at 60 min etching time, pH 6.8 and 1.7 M respectively.

3.6. Detection of WNV particles in Blood Serum

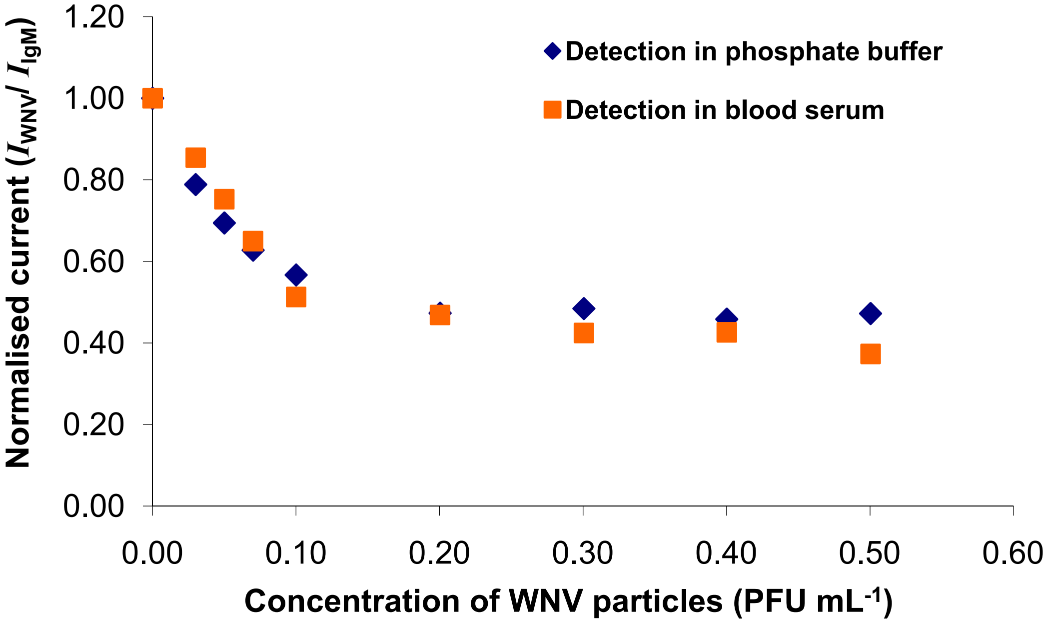

Figure 35. Comparison of DPV signal response of the prepared immunosensor in the detection of WNV particles in 100 mM phosphate buffer (pH 6.8, ionic strength of 1.7 M) and blood serum.

In order to evaluate the potential application of the prepared immunosensor in real sample detection of WNV particles, determinations were conducted using blood serum, instead of phosphate buffered solution. Figure 35 shows the decrease in DPV signal response of an IgG-BSA-alumina electrode when applied in viral particles detection using spiked blood serum samples. The DPV signal responses obtained for detection conducted in blood serum were very similar to that obtained for detection conducted in phosphate buffer, indicating minimal inference from the array of proteins present in the blood serum. When DPV signal responses from 3 similarly prepared IgM-BSA-alumina electrodes were compared, standard deviations ranging from 6% to 15% were obtained in the WNV particles concentration range of 0.03 to 0.50 PFU mL^{-1}. It was not surprising that the standard deviations obtained was higher compared to that achieved when detection was conducted in phosphate buffer (2% to 6%) due to the presence of a high concentration of other interfering proteins. However, the standard deviations were lower than 20%, indicating high selectivity of the prepared immunosensor and this is greatly favourable for real sample detection.

4. Conclusion

A membrane-based electrochemical immunosensor, sensitive towards WNV-DIII and viral particles has been developed. The sensor is based on the principle of channel blocking by the protein antigen within a nanoporous alumina matrix. A low detection limit of 4 ng L^{-1} and 0.02 PFU mL^{-1} (ca. 2 viral particles mL^{-1}) was achieved for WNV-DIII and particles, respectively. In addition, detection of WNV particles in spiked blood serum demonstrated the potential application of the immunosensor in real sample detection. The same technique is likely to be applicable to other viral proteins and small molecular weight proteins by choosing the appropriate specific binding immunoglobulin antibodies and similar electrode fabrication and preparation conditions.

CHAPTER V

ELECTROANALYTICAL STUDIES OF IMMUNOGLOBULIN-BOUND GLUCOSE OXIDASE

1. Introduction

Development of new methodologies and materials for the immobilization of biological molecules is an exciting and important research area in bioanalytical, environmental and biomedical applications, including biosensors, bioaffinity chromatography, bioreactors, besides being useful for fundamental biochemical and biophysical studies [83]. In electrochemical biosensors, a large number of matrices have been shown to be suitable for the entrapment of biological molecules [83-85]. Typically, biological molecules are entrapped within these matrices by mixing the solutions containing biological molecules and the matrix components and subsequently applied as a coating over the sensing electrode. Other methods include direct physical mixing of the enzyme molecules into electrode materials such as carbon paste [86]. Physical entrapment of biological molecules during electrodeposition of conductive polymers [87] and metals [88] are also convenient single step methods that are rapid and readily controlled.

Monolayers and multi-layers of immunoglobulin G (IgG) structures have been routinely used in enzyme-linked immunoassay analysis (ELISA) and electrochemical immunoassay techniques [42-44, 89, 90]. The use of immunoglobulin monolayer as immobilization matrix for enzymes is not new and had been applied for the detection of glucose in flow injection systems [91, 92]. Glucose oxidase bound to its specific antibody was found to be stable and active [93]. In this work, the enzyme activity of surface adsorbed IgG-bound glucose oxidase enzyme using scanning electrochemical microscopy was studied and the feasibility of using IgG as the immobilization matrix for glucose oxidase (GOx) in an electrochemical biosensor had been demonstrated in another thesis [94]. The activity of surface-bound IgG-GOx was investigated on two different surfaces – gold and glass. Glucose oxidase enzyme was chosen since it is one of the most studied enzymes in enzyme-based biosensors.

1.1. Scanning Electrochemical Microscopy

Scanning electrochemical microscopy (SECM) is a scanning probe microscopy technique which relies on faradaic currents to provide information on the electrochemical activity of surfaces [95]. An electrochemically sensitive disk ultramicroelectrode (UME) probe tip is moved over a surface to monitor the presence of redox active species generated by electrochemical, enzymatic or catalytic processes occurring at the surface. The current generated at the ultramicroelectrode probe tip is monitored either as a function of distance (feedback modes) or held at a potential close to the surface in order to detect the surface electrogenerated species (collection modes) [95]. In the feedback mode, SECM is useful in probing heterogeneous kinetics of surfaces, including enzymes-coated surfaces [96] under the condition in which the surface bound redox enzyme oxidizes or reduces a redox mediator in the presence of excess amount of enzyme substrate. The rate at which the redox mediator is generated at the surface is measured by keeping the ultramicroelectrode probe tip at a suitable potential which either reduces or oxidizes the mediator.

If the UME probe tip is far (greater than several tip diameters) from the substrate, the steady state current depends only on the characteristics of the mediator and the electrode itself. The surface does not communicate with the electrode tip and the steady-state-diffusion controlled oxidation current $i_{T,\infty}$ of a reduced species is given by:

$$i_{T,\infty} = 4nFDCa$$

where F is the Faraday constant, n is the number of electrons transferred in the tip reaction, D is the diffusion coefficient of reduced species (R), C is the bulk concentration of R and a is the ultramicroelectrode radius. At closer distance, the surface begins to intercept both redox forms of the mediator. For insulating or non-reactive substrates, the surface blocks R from diffusing to the probe tip and the steady-state current decreases from $i_{T,\infty}$. Currents lower than $i_{T,\infty}$ demonstrate a negative feedback communication between the probe tip and the surface. For conducting surface poised at a potential sufficient to reverse the tip reaction, the substrate intercepts the oxidized mediator species (O) produced at the probe tip and reduces it back to R. The probe tip current i_T derived from the oxidation of R, will be greater than the steady state current $i_{T,\infty}$ due to the regeneration of the reduced mediator species R at the substrate surface. This is known as 'positive feedback'.

Using the feedback mode, an immobilized enzyme regenerates the mediator species, R and the rate of the enzyme reaction could be monitored by measuring directly the substrate current. For enzymes with high enzymatic activities, the SECM current will demonstrate a positive feedback. On the other hand, a slow or hindered enzyme reaction will result in an overall negative feedback response, although this negative feedback current is expected to be larger than that observed for a pure insulator. At very close distance between the tip and surface where there is insignificant lateral diffusion of mediator, the current measured at the probe tip is derived entirely from the reduction or oxidation of the redox mediator regenerated at the enzyme-coated solid surface. Thus, the heterogeneous kinetics of the surface-bound enzyme could be derived from the probe tip current.

1.2. Catalysis by Glucose Oxidase

Glucose oxidase catalyses the oxidation of β-D-glucose to D-glucono-δ-lactone via a multistep reaction. If natural oxygen is used as the mediator, it functions as a two electron acceptor and the overall process can be summarised in the following equations [97]:

$$\beta\text{-D-glucose} + \text{glucose-FAD} \leftrightarrow \text{Glucose oxidase-FADH}_2 + \delta\text{-D-gluconolactone}$$

$$\text{Glucose oxidase-FADH}_2 + O_2 \rightarrow \text{Glucose oxidase-FAD} + H_2O_2$$

Upon reaction with β-D-glucose, glucose oxidase rapidly forms an enzyme-substrate complex, followed by an electron transfer that results in the reduction of the FAD cofactor to $FADH_2$. This is believed to proceed via a hydride transfer mechanism. The second equation oversimplifies the actual mechanism, where the reduced glucose oxidase-$FADH_2$ undergoes activation, before being oxidised by oxygen and is converted back to glucose oxidase-FAD. Oxygen, itself is reduced to hydrogen peroxide and released.

Besides natural oxygen, ferrocene derivatives such as ferrocenemethanol have also been used to probe the kinetics of glucose oxidase enzyme [98]. When applied in SECM studies, there is the continuous regeneration of ferrocene from ferrocinium ion by the reduced glucose oxidase enzyme. The reaction sequence is similar to that when glucose oxidase reacts with oxygen and is as follows [98]:

$$\beta\text{-D-glucose} + \text{glucose-FAD} \leftrightarrow \text{Glucose oxidase-FADH}_2 + \delta\text{-D-gluconolactone}$$

$$\text{Glucose oxidase-FADH}_2 + 2\text{Fecp}_2\text{R}^+ \rightarrow \text{Glucose oxidase-FAD} + 2\text{Fecp}_2\text{R} + 2\text{H}^+$$

$$2\text{Fecp}_2\text{R} \leftrightarrow 2\text{Fecp}_2\text{R}^+ + 2e^-$$

The catalytic cycle of glucose oxidase thus replenishes the supply of ferrocene to the UME at a faster rate than the diffusion of ferrocene towards the surface of the UME, driven by concentration gradient. As a result, the activity of glucose oxidase immobilised on a substrate surface can be probed via SECM.

2. Experimental

2.1. Reagents and Materials

The buffer used was 0.1 M KH_2PO_4/K_2HPO_4, pH 7.0, prepared from 0.1 M KH_2PO_4 (ACS reagent, 99.0%) and 1 M KOH solutions. D-(+) glucose (99.5%), glucose oxidase (GOx, EC 1.1.3.4; from *Aspergillus Niger*, 215 U mg^{-1}, 186000 g mol^{-1}), anti-glucose oxidase (monoclonal antibody produced in mice, 150000 g mol^{-1}), ferrocenemethanol (97%) were purchased from Sigma Aldrich and were used as received. Solutions containing glucose were prepared at least 24 hr before the experiment to allow complete mutarotation of α- and β-D-glucose. All solutions used for electroanalytical studies were prepared using the buffer solution (pH 7.0) and deoxygenated with argon.

2.2. Instrumentation

Photometric measurements were performed in 1 cm quartz cell using a Shimadzu UV spectrophotometer 2450. A CH instruments (Austin, Texas) model 900B scanning electrochemical microscope was used to perform the electrochemical measurements. pH measurements were carried out using a Metrohm 744 pH meter.

2.3. Methodology

2.3.1. SECM Probe Approach Measurements

Approach curves were obtained using a 10 μm diameter ultramicroelectrode (UME) (CH Instruments). The ultramicroelectrode probe tip was first manually positioned in contact with the solid substrate surface and subsequently retracted to a position of 100 μm above the substrate surface. During approach curve measurements, the probe tip was moved at a rate of 2.5 μm s^{-1} and held at a potential of 600 mV versus a silver-silver chloride reference electrode. The run was stopped when the UME probe tip had travelled the full distance of 100 μm. Line scans across the IgG-bound enzyme spot to measure the enzyme activity at a fixed distance of 20 μm away from solid substrate surface was additionally carried out. No significant difference in the feedback response across the spot, except expectedly at the edge of spot was observed, which confirmed that there was negligible local change in the distribution of modified sites within the IgG-bound enzyme spot. All SECM measurements were carried out within the first 15 min after the IgG-GO coated solid substrate was placed in the solution of the SECM cell.

2.3.2. Preparation of Glass and Gold Substrate

Microscope slides were cut into pieces of 1.5 cm × 0.9 cm and cleaned with dichloroethane, ethanol, acetone and finally rinsed with deionized water. The gold substrates used were polished, bounded, mounded 100Å Cr + 1000Å gold crystal (CH Instrument). All gold substrates were treated with piranha solution (3:1 volume H_2SO_4 to H_2O_2) at 70°C for 30 seconds before use.

2.3.3. Immobilization of Immunoglobulin G and Glucose Oxidase

For SECM studies, 0.4 µl of IgG solution was carefully spotted onto a glass slide or gold substrate. Physical adsorption of IgG onto the solid substrate was carried out for 30 min before rinsing with buffer solution (pH 7.0). 0.4 µl of GOx solution was then applied to the IgG spot on the solid substrates to form the IgG-bound GOx immunocomplex over a 30 min duration, followed by rinsing.

2.3.4. Measurement of Immunoglobulin G and Glucose Oxidase Surface Coverage

UV measurements of IgG and GOx solutions of concentrations ranging from 1 to 4 μg mL^{-1} were obtained and absorptivity of both proteins were calculated using Beer-Lambert law. 2.5 μg mL^{-1} IgG solution was added into the absorption cell containing the solid substrate. The solution's absorbance was measured at 280 nm wavelength before and after 30 min adsorption time. The amount of IgG adsorbed onto the substrate surface was calculated from the difference in absorbance before and after immobilisation. To measure the amount of GOx bound to IgG, 4 μg mL^{-1} GOx solution was added to the same substrate immediately after the IgG immobilisation procedure. The UV absorbance method for measuring surface coverage was carried out for both glass and gold substrates. All surface coverage values on glass substrates were subsequently corrected and referenced to the more precise and accurate quartz crystal microbalance (QCM) measurements on gold substrate to correct for the loss of protein materials during transfer of solution between the adsorption cell and the measurement cuvette, besides protein adsorption along the walls of the adsorption cell.

QCM measurements of IgG and enzyme surface coverage on gold substrates were carried out as follows. A polished, bounded, mounded 100 Å Ti + 1000 Å gold quartz crystal was immersed in piranha solution (3: 1 sulfuric acid to hydrogen peroxide) for 30 seconds and rinsed thoroughly before use. The gold quartz crystal was equilibrated in 0.1 M phosphate buffer solution (pH 7.0) until the frequency remained relatively constant. The solution was changed to an IgG solution of 0.5 μg mL^{-1} concentration and the change in frequency was recorded once it reached a relatively constant value. Subsequent addition of GOx solution into the adsorption cell containing the IgG-coated quartz crystal was carried out to determine the surface coverage of IgG-bound enzyme. The same was repeated for IgG solutions in the concentration range of 10 to 150 μg mL^{-1}.

For leaching studies, the gold or glass substrate was first immobilised with both IgG-GOx complex using solutions of the same concentrations as described above. The substrate was subsequently placed in a 10 mL buffer and aliquots of the buffer solution were taken at 10 min intervals from 0 to 90 min for measurement of absorbance at 280 nm. As a control, the same procedure was carried out for a gold or glass substrate immobilised only with IgG.

3. Results and Discussion

3.1. Apparent Heterogeneous Rate Constant and Turnover Numbers of Immunoglobulin G-Bound Glucose Oxidase

SECM was used to measure the apparent heterogeneous rate constant k'_f, of the enzyme-mediator reaction for GOx enzyme bound to surface adsorbed IgG. Gold and glass substrate surfaces were used to immobilize the IgG and GOx molecules since these surfaces are routinely used for adsorbing enzymes [99-102]. Surface adsorbed GOx on gold and glass substrates were similarly attempted but gave highly irreproducible results due to significant desorption of GOx during the SECM experiments. Figure 36 shows the schematic of the SECM feedback mode used in probing a substrate surface physically adsorbed with IgG-bound GOx immunocomplex.

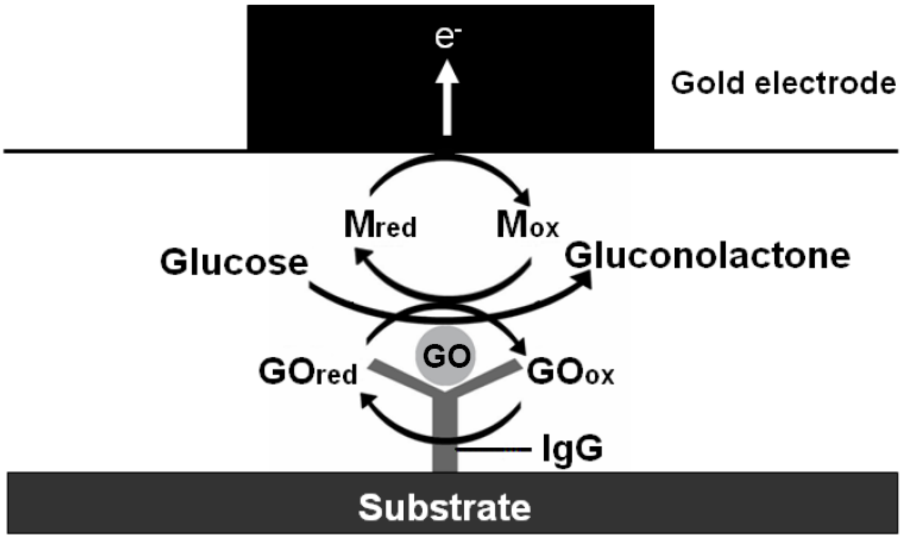

Figure 36. Schematic of the SECM feedback mode.

The probe tip current responses obtained for an insulating substrate and a highly conducting substrate (diffusion-limiting case) derived during SECM feedback modes can be described using the following equations, respectively [103]:

$$I_{\mathrm{T}}^{\mathrm{ins}}(L) = \frac{1}{0.292 + \frac{1.5151}{L} + 0.6553\exp(\frac{-2.4035}{L})} \qquad (8)$$

$$I_{\mathrm{T}}^{\mathrm{c}}(L) = \frac{0.78377}{L} + 0.3315\exp(\frac{-1.0672}{L}) + 0.68 \qquad (9)$$

where $I_{\mathrm{T}}^{\mathrm{c}}(L)$ and $I_{\mathrm{T}}^{\mathrm{ins}}(L)$ are the normalized ultramicroelectrode probe currents for diffusion-controlled regeneration of a redox mediator on a conducting and insulating substrate respectively, at a normalized probe tip-substrate separation, $L = d/a$; d is the probe tip-substrate separation and a is the ultramicroelectrode radius. Between these two extremes, the steady-state feedback current response is limited by the substrate current $I_{\mathrm{s}}^{\mathrm{k}}$ derived from the 'turnover' (regeneration) of the mediator at an electrochemically active substrate surface. The magnitude of substrate current can be calculated from the difference between the probe tip feedback current response of the substrate and an insulating substrate, normalized with respect to the highly conducting substrate (diffusion-limiting) case, as follows [103]:

$$\frac{I_{\mathrm{s}}^{\mathrm{k}}}{I_{\mathrm{T}}^{\mathrm{c}}} = \frac{I_{\mathrm{T}} - I_{\mathrm{T}}^{\mathrm{ins}}}{I_{\mathrm{T}}^{\mathrm{c}} - I_{\mathrm{T}}^{\mathrm{ins}}} \qquad (10)$$

Using equations (8), (9) and (10), I_s^k values were derived from the SECM approach curves and plotted against normalized distance. Figure 37 shows the normalized substrate current I_s^k obtained for GOx bound to physically adsorbed IgG on both gold and glass substrates, which were of intermediate magnitudes between 2 and 0.5. This indicates the surface activities of GOx occurred halfway between the ‘conducting’ (diffusion limited) and ‘insulating’ cases.

The approximate analytical solutions for heterogeneous reactions over the intermediate kinetic region have been described by the following equation [103]:

$$I_{\mathrm{s}}^{\mathrm{k}} = \frac{0.78377}{L(1+\frac{1}{\Lambda})} + \frac{[0.68 + 0.3315\exp(\frac{-1.0672}{L})]}{[1 + \mathrm{F}(L,\Lambda)]} \qquad (11)$$

where $\Lambda = k'_{\mathrm{f}}d/D_{\mathrm{R}}$, k'_{f} is the apparent heterogeneous rate constant (cm s^{-1}), $\kappa = k'_{\mathrm{f}}a/D$, D_{R} is the diffusion coefficient of the reduced mediator in water and $\mathrm{F}(L, \Lambda) = (11/\Lambda + 7.3)/(110-40L)$.

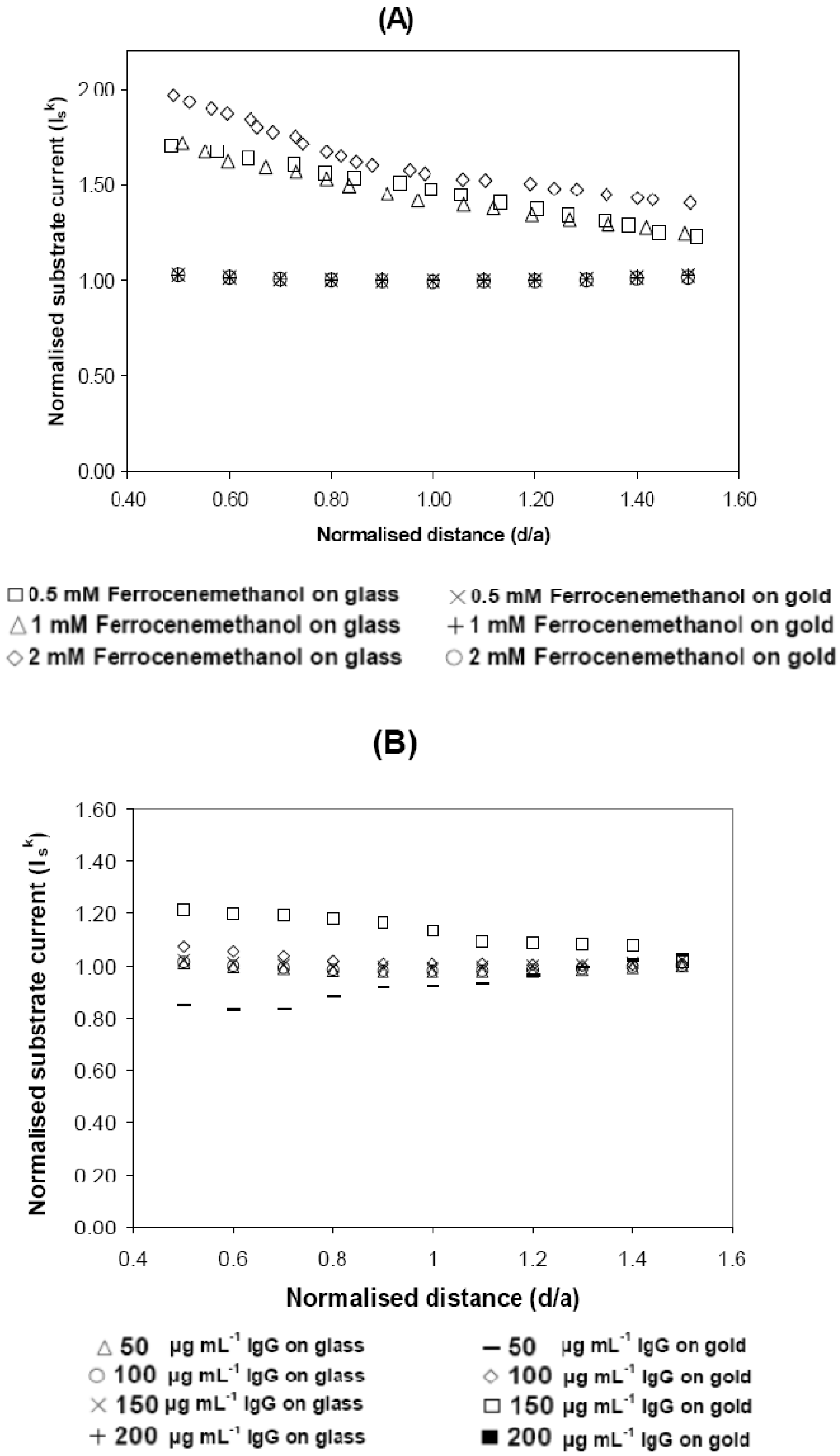

Figure 37. Plots of normalized substrate current against normalized distance, *L* for different concentrations of (A) ferrocenemethanol mediator and (B) IgG for glucose oxidase enzyme bound to surface adsorbed IgG on gold and glass substrates.

The curves in Figure 37 were fitted to equation (11) using non-linear regression in order to find the heterogeneous rate constant, k'_f, for $0.5 \leq L \leq 1.5$. Table 3 presents the best fitted k'_f values for GOx bound to surface adsorbed IgG on gold and glass substrates.

To find the turnover number of the mediator under saturated enzyme concentration condition, the substrate current, I_s^k was first expressed as the rate of production of the reduced form of mediator (dc_R/dt) by the enzyme-mediator reaction under steady-state condition [95]. The rate of production (in mol cm^{-2}) of the reduced form of mediator by the enzyme-mediator reaction can be derived from the generalised steady-state two-reactant enzyme rate equation for a heterogeneous reaction, as follows [95]:

$$I_s^k = \mathrm{nFA}\,\frac{dc_R}{dt} \tag{12}$$

$$\frac{\mathrm{d}c_\mathrm{R}}{\mathrm{d}t} = \frac{k_\mathrm{cat}\Gamma_\mathrm{enz}}{\frac{K_\mathrm{M,glc}}{c_\mathrm{glc}} + \frac{K_\mathrm{M,O}}{c_\mathrm{O}} + 1} \tag{13}$$

where the kinetic constants K_M are the corresponding Michaelis-Menten constants for glucose (glc) and oxidized mediator (O). $k_\mathrm{cat}\Gamma_\mathrm{enz}$ represents the maximum rate for the enzyme-mediator reaction, where k_cat is the maximal turnover number of the immobilized enzyme GOx and Γ_enz is the surface coverage of the enzyme.

Under condition of large excess glucose concentration, the two-reactant rate equation is reduced to the Michaelis-Menten type expression [104, 105]:

$$\frac{\mathrm{d}c_{\mathrm{R}}}{\mathrm{d}t} = \frac{k_{\mathrm{cat}}\Gamma_{\mathrm{enz}}c_{\mathrm{O}}}{K_{\mathrm{M,O}} + c_{\mathrm{O}}} \qquad (14)$$

These kinetic parameters in the generalized enzyme kinetics, equation (14), were compared with the corresponding apparent heterogeneous rate constants k'_{f} derived from SECM data. For example, equation (14) reduces to $\frac{\mathrm{d}c_{\mathrm{R}}}{\mathrm{d}t} = \frac{k_{\mathrm{cat}}\Gamma_{\mathrm{enz}}c_{\mathrm{O}}}{K_{\mathrm{M,O}}}$ where $k'_{\mathrm{f}} = (k_{\mathrm{cat}}\Gamma_{\mathrm{enz}})/K_{\mathrm{M,O}}$ for first order reaction when $c_{\mathrm{O}} << K_{\mathrm{M}}$. Thus, the turnover numbers for the enzyme-mediator reaction of GOx bound to IgG adsorbed on gold and glass substrates could be derived (Table 3). The turnover numbers of the IgG immobilized enzyme, k_{cat} ranged from 475 to 740 s^{-1} and 103 to 354 s^{-1} for gold and glass substrate respectively. However, it was not possible to measure the kinetics of surface adsorbed GOx in the absence of IgG due to significant desorption of GOx from the substrate surfaces during the experiments. In comparison to the turnover number of unbound GOx in the presence of natural mediator, O_2, the turnover numbers of surface bound IgG-bound GOx immunocomplexes on gold and glass were lower than that of the native enzyme (800 s^{-1}) [106]. In a previous work [94], it was demonstrated that the second order homogeneous rate constant k_{S} for the reaction between $\mathrm{Med}_{\mathrm{ox}}$ and GOx was lower for IgG-bound GOx compared with free GOx.

This trend was consistent with several studies in which the turnover numbers of immobilized enzymes were significantly lower than that of the native enzyme [92, 95, 96, 107]. For example, Bard observed a k_{cat} value that was 3 orders of magnitude lower than the intrinsic k_{cat} value for solubilised GOx, when they immobilized GOx within hydrogel membranes [95]. In another study involving urease, k_{cat} value of the entrapped enzyme was 70-fold lower than that of the solubilised enzyme [108]. Enzyme turnover number of sol-gel encapsulated alcohol dehydrogenase was drastically reduced to 1.8×10^2 s^{-1}, from a reported k_{cat} value of 8.4×10^5 s^{-1} for the same enzyme/cofactor/substrate system in a pH 9 buffered solution [107]. The same was observed for bovine carbonic anhydrase II encapsulated in sol-gel silica glass [109]. Its turnover number diminished to ca. 2% of the corresponding value for the dissolved enzyme, upon entrapment. It has been suggested that the smaller turnover number may be due to deactivation of the enzyme during the immobilization and chemical modification of additional functional groups [96].

Another possible reason for decreased enzyme activity could be caused by random orientation of the enzyme on the electrode surface, leading to blocked binding site of the enzyme which prevented access for the enzyme substrate [92]. In contrast, the lowest turnover numbers of IgG-bound GOx physically adsorbed on gold and glass substrate were 60 % and 10 % of the turnover number of native enzyme respectively, whereas the highest turnover number was ca. 90 %. Similarly, the homogeneous rate constant k_s of IgG-bound GOx was ca. 25% of the k_s value of free GOx measured using cyclic voltammetry described elsewhere [94]. These changes in the kinetic parameters were much less significant compared with those observed for other immobilization methods.

Table 3. Average apparent rate constants and turnover number for heterogeneous glucose oxidase-mediator reaction at different concentrations of mediator and IgG.

Substrate	**[FeMeOH]/ mM**	**Apparent rate constant[a] k'_f/ cm s^{-1}**	**%RSD**	**Turnover number[b,c] k_{cat} / s^{-1}**	**%RSD**
Gold	0.5	1.38×10^{-2}	3.1	479	15.3
	1	1.38×10^{-2}	3.1	480	15.3
	2	1.37×10^{-2}	2.9	475	15.3
Glass	0.5	3.30×10^{-2}	2.0	206	20.3
	1	3.17×10^{-2}	8.1	196	21.7
	2	5.69×10^{-2}	2.6	354	20.4

Substrate	**[IgG]/ µg mL^{-1}**	**Apparent rate constant[a] k'_f/ cm s^{-1}**	**%RSD**	**Turnover number[b,d] k_{cat} / s^{-1}**	**%RSD**
Gold	50	1.01×10^{-2}	8.1	352	17.1
	100	1.44×10^{-2}	2.0	499	15.2
	150	2.13×10^{-2}	2.0	740	15.1
Glass	50	1.29×10^{-2}	2.6	103	20.3
	100	1.31×10^{-2}	2.6	104	20.3
	150	1.35×10^{-2}	3.1	108	20.4

[a] Apparent rate constants are obtained by fitting values of I_s^k and L to equation (11) using non-linear regression. Refer text for details. Diffusion coefficient of ferrocenemethanol = 7.25×10^{-6} cm^2 s^{-1}.

[b] Turnover numbers were calculated from where K_M = 50.3 µM [110].

[c] Γ_{enz}(gold) = 1.5 (± 0.2) × 10^{-12} mol cm^{-2} and Γ_{enz}(glass) = 6.3 (± 1.3) × 10^{-12} mol cm^{-2}.

[d] Γ_{enz}(gold) = 0.8 ± 0.1 × 10^{-12} mol cm-^{2}, 1.5 ± 0.2 × 10^{-12} mol cm-^{2} and 2.1 ± 0.3 × 10^{-12} mol cm-^{2} for 50, 100 and 150 µg mL^{-1} IgG respectively, and Γ_{enz}(glass) = 6.3 (± 1.3) × 10^{-12} mol cm^{-2} for all three IgG concentrations. Surface coverage of IgG-bound GOx on gold surfaces were determined using quartz crystal microbalance (CH Instruments). UV absorbance measurements carried out on protein solutions before and after adsorption, were used to determine the surface coverage of IgG-bound GOx on gold and glass substrates. Enzyme surface coverages on glass substrates were subsequently corrected using the QCM measurements on gold substrate as reference.

Table 3 shows that the apparent heterogeneous rate constant k'_f remained constant for the gold substrate, but increased for the glass substrate as the mediator concentration increased. It was not surprising that mediator concentration did not affect k'_f for the gold substrate since the Michaelis-Menten constant for the oxidized mediator $K_{M,O}$ (50.3 µM) [111] was at least ten times smaller than the mediator concentrations used in the experiments. Conversely, the increase in k'_f values for glass substrate under varying mediator concentration indicated that the enzymatic reaction was limited by the enzyme-mediator reaction. It is known that a densely-packed IgG monolayer gives a surface coverage ranging from 200 to 550 ng cm^{-2}, depending on orientation of IgG molecules [112]. In addition, for the IgG-bound GOx adsorbed on gold and glass substrates, the amount of enzyme bound to one molecule of IgG was between 0.8 to 1.2, determined using quartz crystal microbalance (CH Instruments) and UV-visible spectroscopy. Therefore, the enzyme surface coverage on gold (1.5 (± 0.2) × 10^{-12} mol cm^{-2}) and glass (6.3 (± 1.3) × 10^{-12} mol cm^{-2}) substrates corresponded closely to one monolayer coverage and 1-6 times monolayer coverage of IgG on gold and glass, respectively.

It was possible the amount of GOx molecules oxidized by the mediator during the SECM measurements was limited by the amount of mediator molecules entrapped between the UME probe tip and substrate, due to slow diffusion of mediator with the multilayer IgG-bound GOx structure on glass substrate. The effect of slow diffusion on the k_{cat} values was estimated by calculating the diffusion coefficient of the mediator within the IgG multilayer structure as follows. A diffusion term k_{d} was added into equation (14) in the reciprocal form and subsequent comparison with the substrate current gave the relation:

$$k'_{\mathrm{f}} = \frac{k_{\mathrm{cat}}\Gamma_{\mathrm{enz}}}{\dfrac{k_{\mathrm{cat}}\Gamma_{\mathrm{enz}}}{k_{\mathrm{d}}} + K_{\mathrm{M,O}}} \qquad (15)$$

for a pseudo first order reaction when $c_{\mathrm{O}} << K_{\mathrm{M}}$ where k_{d} is the diffusion rate constant of mediator comprising the solution diffusion ($k_{\mathrm{d,soln}}$) and diffusion within the

IgG-GOx multi-layer film ($k_{\mathrm{d,film}}$) in the form of $k_{\mathrm{d}} = \dfrac{k_{\mathrm{d,soln}} k_{\mathrm{d,film}}}{k_{\mathrm{d,soln}} + k_{\mathrm{d,film}}}$. Using equation (15), the values of k_{d} were found in the range of 0.07 to 0.08 for all mediator and IgG concentrations obtained on glass substrates except when the mediator concentration was 2 mM, k_{d} was significantly higher at 1.2. From the k_{d} values and an approximated 90 nm thick IgG multi-layer structure (assuming 6 IgG layers and each IgG layer was ca. 15 nm thick), the diffusion coefficient of mediator within this IgG multi-layer structure was estimated to be 6.1 (± 1.2) × 10^{-7} $\mathrm{cm^2\ s^{-1}}$. This compares favorably with magnitudes of reduced diffusion coefficients of ferrocene derivatives in polymer films [113]. The large k_{d} value obtained in the 2 mM mediator concentration clearly indicates a non-mass transport limiting process at high mediator concentration. It is likely at the high mediator concentration, more GOx molecules could be accessed by the mediator molecules within the multilayer structure during SECM measurements.

In contrast, as the IgG concentration increased from 50 to 150 μg $\mathrm{mL^{-1}}$, k'_{f} values for gold substrate increased, but remained constant for glass substrate. The amount of IgG loading on both gold and glass substrates was measured using quartz crystal microbalance (QCM, CH Instruments) and UV absorbance. QCM results showed that as IgG concentration was increased from 0.5 to 150 μg $\mathrm{mL^{-1}}$, the amount of IgG loaded onto the gold surface increased from 3.3 (± 0.4) x 10^{-14} to 1.5 (± 0.2) x 10^{-12} mol $\mathrm{cm^{-2}}$, in the regime of sub-monolayer to monolayer coverage. However, UV absorbance measurements of IgG solutions before and after adsorption of IgG on glass substrates revealed the amount of adsorbed IgG remained constant at ca. 6.3 (± 1.3) × 10^{-12} mol $\mathrm{cm^{-2}}$, which was in the regime of multilayer coverage. It was possible the enzyme-mediator reaction for the gold substrate was limited by the low surface loading of GOx due to sub- and monolayer coverage of IgG. Thus, the k'_f values for surface bound IgG-GOx immunocomplexes on gold substrate increased at higher IgG concentrations. It was equally possible that the difference between the trends in k'_f values for gold and glass substrates could arise from differences in surface roughness. It has been demonstrated that surface roughness could influence the kinetics of protein loading, hence the amount of protein adsorbed [114, 115]. In addition, under situations of high surface roughness, close-packing of IgG may not always apply [115].

In the following, the value of second order homogeneous rate constant k_S obtained from cyclic voltammetry experiments [88] was compared with apparent heterogeneous rate constant k'_f derived using SECM for the gold substrate. It should be noted that there is a mistake in the reported values in reference [88] due to using v in unit of mV s^{-1}, instead of V s^{-1}. Recalculation of k_f using the correct slope relation of $k_f RT/nF$ and in unit of V s^{-1} gives k_S for free GOx (1.0 (± 0.05) x 10^4 L mol^{-1} s^{-1}) and IgG-bound GOx (2.4 (± 0.05) x 10^3 L mol^{-1} s^{-1}) at pH 7.0 and 25 ^{0}C. Assuming the IgG-bound GOx enzyme activity remained unaffected by physical adsorption of IgG-bound GOx on the solid substrates, the hypothetical heterogeneous rate constant k'_f (hyp) can be obtained using k'_f (hyp) = $\Gamma_{enz} k_S$. The k'_f (hyp) value of IgG-bound GOx derived from k_S was 3.6 (± 0.1) × 10^{-6} cm s^{-1} using the experimentally determined value of Γ_{enz} on gold substrate (1.5 (± 0.2) × 10^{-12} mol cm^{-2}). Interestingly, this k'_f (hyp) value was significantly less than the heterogeneous k'_f values at Table 3, obtained from SECM measurements. This strongly suggests the enzyme-mediator reaction rate of IgG-bound GOx was influenced by the surface adsorption of IgG to the solid substrate. It was likely the surface adsorbed IgG molecules were not all arranged via end-on arrangement, so some of the IgG-bound GOx enzyme could interact with the solid substrate surface [116]. It is known that GOx undergo conformational changes when bound to solid substrate surfaces [99]. Similar to other enzymes, changes in their secondary and tertiary structures upon surface adsorption, could lead to changes in the enzyme kinetics [117-120].

In order to determine whether the IgG-GOx adsorbed layers on gold and glass substrates were stable over long time, desorption of the IgG-GOx complexes from the substrates was monitored using UV-visible spectroscopy. The gold or glass substrate was first immobilised with IgG-GOx complex, rinsed and subsequently immersed in phosphate buffer. Buffer aliquots were subsequently obtained at 10 min intervals and the absorbance was measured. No desorption of the GOx enzyme or IgG-GOx complex occurred during the first 20 min. Between 20 to 30 min, rapid leaching of GOx enzyme or IgG-GOx complex from the IgG-GOx coated glass and gold substrates were observed. At longer period from 40 to 90 min, the absorbance of the buffer aliquot reached a constant plateau value, which indicated no further leaching after 40 min. The same trend was observed for both IgG coated gold or glass substrates. The absorbance values obtained after 40 min for the IgG-GOx coated substrates were ca. 2 times more than the controls with only IgG coated substrates as expected since the IgG-GOx complex and IgG were desorbed respectively. SECM measurements confirmed that the IgG-bound GOx on both gold and glass substrates remained active at the end of 90 min immersion time in pH 7 phosphate buffer when no further leaching occurred. The apparent heterogeneous rate constant, k'_f values for gold and glass substrates after 90 min immersion in buffer solution were 5.38×10^{-3} and 5.29×10^{-3} cm s^{-1} for gold and glass substrates. The corresponding turnover numbers (k_{cat}) for gold and glass substrates calculated using the lower surface coverage values after leaching, were 373 (± 65) and 127 s^{-1} (± 28) respectively.

3.2. Glucose detection

To find out whether the surface adsorbed IgG-bound GOx immunocomplexes on electrode could function as a glucose sensor, the current response of a glucose sensor prepared using a home-made gold electrode (electrode diameter = 0.01 mm) and physically adsorbed with IgG-bound GOx immunocomplexes was measured as shown in another thesis [94] (Figure 38A). In addition, the current response of the IgG-bound GOx electrode was compared with another electrode fabricated using covalently attached IgG, subsequently bound with glucose oxidase enzyme. A control electrode using surface adsorbed GOx without IgG was similarly prepared. All three electrodes gave current response towards glucose. Curve fitting of all three current response curves gave apparent Michaelis K_m(glucose) value of 7 (± 1), 13 (± 1) and 99 (± 3) mM for physically adsorbed GOx, physical adsorbed IgG-bound GOx and covalently immobilized IgG-bound with GOx (Figure 38B). Apparent Michaelis K_m(glucose) values obtained for physically adsorbed GOx and adsorbed IgG-bound GOx were lower than the reported value for free enzyme from *A. Niger* [121]. This clearly indicates the immobilized GOx via surface adsorbed IgG was non-denaturing [122]. The K_m(glucose) value for covalently immobilized IgG-bound with GOx was significantly higher, suggesting the covalently immobilized IgG could have affected the enzyme characteristics in which the GOx became less responsive towards low concentration of glucose.

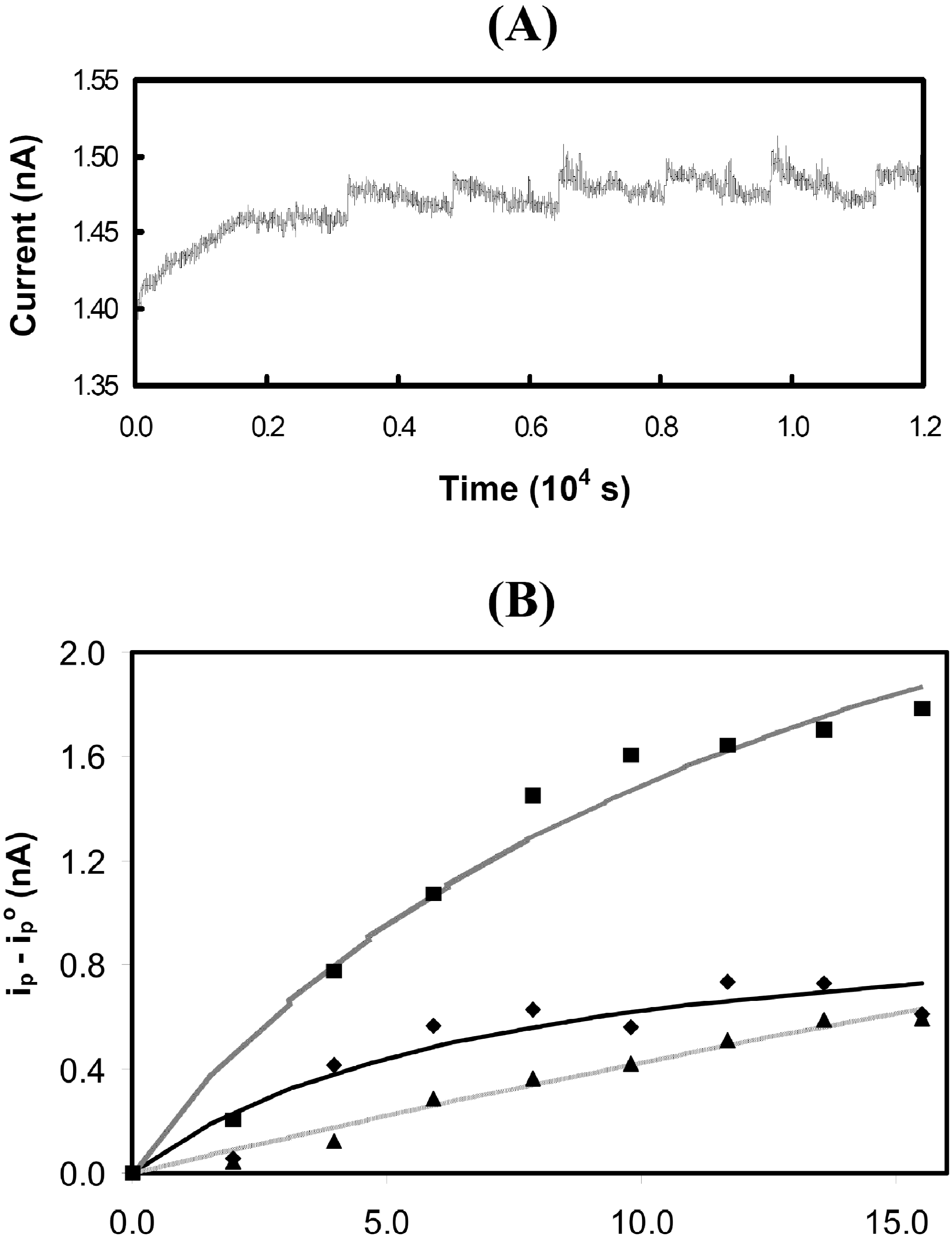

Figure 38. (A) Steady-state amperometry obtained at a glucose sensor prepared using GOx bound to a monolayer of IgG adsorbed on gold electrode. 2.0 mM D-glucose was successively added to 0.5 mM ferrocenemethanol solution in 0.1 M pH 7.0 phosphate buffer and the sensor potential was held constant at +0.35 V. (B) Sensor response towards glucose for electrodes coated with (♦) GOx directly adsorbed on gold, (■) GOx bound to monolayer of IgG adsorbed on gold substrate and (▲) GOx bound to monolayer of IgG covalently bound to gold substrate. The solid lines are best fitted curves to the generalized Michaelis-Menten type equation for biosensor

$i - i_0 = \frac{k_{cat}[glc]}{K_{m,glc} + [glc]}$ using non-linear regression. *i* is the peak current response obtained using cyclic voltammetry and i_0 is the peak current response at zero concentration of glucose. k_{cat} is the enzyme turnover number, [*glc*] is the concentration of substrate, glucose and $K_{m,glc}$ is the apparent Michaelis constant.

4. Conclusion

SECM studies indicated turnover numbers of 475 to 740 s^{-1} and 103 to 354 s^{-1} for IgG-bound GOx adsorbed on a gold and glass substrate respectively, using ferrocenemethanol as mediator. IgG was also successfully applied as an alternative immobilization method for GOx in a glucose biosensor. The same approach is potentially applicable in other enzyme-based biosensors.

CHAPTER VI

CONCLUSION AND FURTHER RESEARCH

The major portion of this thesis dealt with the fabrication and development of an alumina membrane-based immunosensor. In the first section, the anodization of aluminum to alumina is described and explained. Alumina electrodes were fabricated using two different techniques, namely sub-surface and pipette anodization. Results from electrochemical studies and scanning electron microscopy (SEM) studies supported the construction of a barrier layer free alumina membrane on the home-made platinum wire electrode tips using the developed, novel pipette anodization technique. This is significant since the absence of a barrier layer will allow redox probes to reach the platinum wire electrode surface beneath the membrane and facilitate rapid electron transfer. In addition, barrier layer free alumina membranes formed using this technique can be used directly for electrodeposition of materials such as carbon, gold and platinum, for the fabrication of electrode nanoarrays and nanotubes. The step involving the removal of alumina barrier layer can be omitted, thus reducing the amount of work required.

The alumina modified platinum disk electrodes were subsequently used to develop immunosensors, specifically detecting glucose oxidase. The fundamental idea is to immobilise a sub-monolayer or monolayer of immunoglobulin G along the nanochannel walls of the porous alumina, followed by the immobilization of bovine serum albumin (BSA) to block unspecific adsorption sites. After which the alumina-modified platinum disk electrode was used for antigen detection, in the presence of the redox probe. Upon binding the complementary antigen to the immunoglobulin G, formation of the antigen–antibody (Ag–Ab) complexes blocked the approach of ferrocenemethanol towards the exposed platinum surface beneath the porous alumina layer and the extent of blockage was measured using differential pulse voltammetry. This resulted in a signal-off immunosensor, where the signal response decreases as the concentration of analyte increases.

However, no more than 100% of the signal can be suppressed by target binding in a signal-off immunosensor and hence, the dynamic range of the sensor is limited. This can be overcome by the use of a sandwich assembly system, commonly applied in immunoassays as well as other various biosensors [123-125]. In this system, the antigen is bound to a secondary antibody after binding to the first antibody, immobilised onto the sensor substrate. The secondary antibody is usually conjugated to an enzyme and the reduction of the appropriate enzyme substrate added into the system will generate side products, which can be detected electrochemically or optically [126, 127]. The amount of reaction product detected can subsequently be related to the concentration of antigen present for quantitative analysis. A more direct method would to employ of a secondary antibody conjugated to a light sensitive or fluorescent molecule and making use of a optical detection system [128].

Nevertheless, the developed signal-off immunosensor demonstrated high selectivity for glucose oxidase and control experiments confirmed the reliability of the detection scheme. A low detection limit of 100 ng mL^{-1} was achieved for glucose oxidase and this was 100 times lower than those provided by commonly used immunoassay techniques. The successful development of this immunosensor prompted further application for the determination of West Nile Virus domain III protein and West Nile viral particles. A 60 min etched alumina electrode was found to exhibit the most sensitive response and most effective blocking effect. The optimal sensing solution was found to be 100mM phosphate buffer of pH 6.8 and ionic strength of 1.7 M. The same experimental conditions were used, when the prepared immunosensor was employed for the detection of West Nile Viral particles, which is usually detected using reverse transcription polymerase chain reaction (RT-PCR) techniques [71, 129]. A low detection limit of 7 ng mL^{-1} and ca. 3 viral particles mL^{-1} were found for both West Nile Virus domain III protein and viral particles, respectively. The determination of West Nile viral particles in blood serum was also conducted and results indicated minimal interference from the wide array of protein existing in the serum. The high selectivity of the developed immunosensor is again demonstrated and the immunosensor can potentially be applied in real sample detection. However, the results should be compared to an established technique such as enzyme-linked immunosorbent assay (ELISA) to ensure high accuracy of the results. Due to the difficulties encountered in culturing WNV-DIII protein and WNV particles as well as time constraints, ELISA was not conducted currently and may be possible in the near future.

Work is on-going to investigate the mechanism or real-time effect of the blockage of the alumina nanopores by the antibody-antigen immunocomplex, which subsequently hinders the pathway of the redox probe to the electrode surface for redox processes. 60 min etched alumina electrodes were demonstrated to be the most effective and sensitive for detection of glucose oxidase, West Nile Virus domain III protein and West Nile viral particles. However, the extent of blocking differs for all three types of analytes and real-time studies of binding of the antigen to the antibody should shed some light on the intrinsic behaviour of the antibody-antigen binding as well as the effect of immunocomplex formation on the diffusional behaviour of redox probe, ferrocenemethanol into the alumina nanochannels. Continuous collection of differential pulse voltammetry data during the 30 min allowed for antibody-antigen binding did not reveal much information about the blocking process. Thus, other similarly sensitive techniques have to be employed. It is aim to make use of AC voltammetry for this further work. This technique had been used to probe various electron transfer mechanisms [130-135] and should be more suitable for real-time studies.

In addition, attempts to remove the immobilised biomolecules from the alumina membrane using urea and high concentrations of sodium chloride were futile. Given the inability to reuse the alumina electrodes and the high portability of chip devices, it would be advantageous to deviate from single electrodes construction and develop screen-printed electrodes for the developed immunosensor. The ability to include a counter electrode and a reference electrode into the design of such devices will eliminate the use of external electrodes. Having all required electrodes miniaturised into a single screen-printed electrode can also allow the use of a small sample cell and thus drastically reduce the amount of sample required [136, 137].

In addition, covalent bonding of immunoglobulin molecules to the alumina overlayer can be conducted to investigate its effect on the detection of the different analytes. Immunoglobulin's molecules can also be aligned in a particular direction on a substrate by first conducting absorption or covalent bonding of protein A, followed by the binding of immunoglobulin to these proteins. Protein A binds to immunoglobulin molecules via its Fc domain, leading its Fab arms free to bind to antigen molecules [138]. This approach had been attempted in the development of other biosensors and results proved that the aligned immunoglobulin molecules provided higher binding capability, thus conferring higher sensitivity to the sensing platforms [138, 139].

Furthermore, if most of the pores of the alumina can be masked such that only a few or one nanopores remain exposed to the sensing solution, detection of single molecule may be possible. To work toward this direction, attempts were made to etch the platinum wire into a fine tip with sodium nitrite, before sealing in epoxy glue to construct an ultramicroelectrode of nanometer dimensions. A nanometer disk electrode when overlaid with an alumina membrane may be capable for single molecule detection, if a nanopore is directly above the electrode surface and the same blocking detection scheme is carried out. However, platinum wire etching conducted in sodium nitrite was not reproducible and the fine tip breaks off easily before or during sealing of the wire in epoxy glue. Polishing of electrode tips manually using silica carbide paper to expose the sealed platinum wire, is also not an ideal method to construct platinum disk electrodes of similar nanometer dimensions. As such, a screen-printed electrode design, mentioned previously, may be more probable and useful.

The last section described the use of scanning electrochemical microscopy (SECM) to investigate the apparent heterogeneous electron transfer coefficient and activity of glucose oxidase bound to immunoglobulin G. Turnover numbers of 475 to 740 s^{-1} and 103 to 354 s^{-1} were obtained for immunoglobulin G -bound glucose oxidase adsorbed on a gold and glass substrate respectively, using ferrocenemethanol as mediator. Immunoglobulin G was also successfully applied as an alternative immobilization method for glucose oxidase in a glucose biosensor as indicated in another thesis. The result of this investigation can complement other sensor studies utilising immunoglobulin G-bound glucose oxidase [91, 92] as well as other SECM studies involving enzymes [96], in which complete kinetic calculations and data analysis is lacking.

CHAPTER VII

BIBLIOGRAPHY

1. Furneaux R. C., Ribgy W. R., Davidson A. P., *Nature* **1989**, 337, 147.
2. Knaack S. A., Redden M., Onelliona M., *The American Journal of Physics* **2004**, 72, 856-9.
3. Petrovic S., *The Chemical Educator* **2000**, 5, 231-5.
4. Fort R. C. *Mechanism of Chorismate Mutase Activity - V*. http://chemistry.umeche.maine.edu/CHY431/Chorismate5.html (Accessed 25 April 2008).
5. Goodsell D. S. http://mgl.scripps.edu/people/goodsell/pdb/pdb77/pdb77_1.html (Accessed 29 April 2008).
6. Cypress. *Pulsed Voltammetry Techniques*. http://www.cypresssystems.com/Experiments/pulsetechniques.html (Accessed 2 May 2008).
7. Mukhopadhyay S., Kim B.-S., Chipman P. R., Rossmann M. G., Kuhn R. J., *Science* **2003**, 302, 248.
8. Thevenot D. R., Toth K., Durst R. A., Wilson G. S., *Pure Applied Chemistry* **1999**, 71, 2333.
9. Mehrab M., Mustafe A., *Analytical Sciences* **2004**, 20, 1113-26.
10. Guilbault G. G., Pravda M., Kreuzer M., O'Sullivan C. K., *Analytical Letters* **2004**, 37, 1481-96.
11. Luppa P. B., Sokoll L. J., Chan D. W., *Clinica Chimica Acta* **2001**, 314, 1-26.

12. Stradiotto N. R., Yamanaka H., Zanoni M. V. B., *Journal of Brazilian Chemical Society* **2003**, 14, 159-73.

13. Huczko A., *Applied physics* **2000**, 70, 365-76.

14. Lakshmi B. B., Dorhout P. K., Martin C. R., *Chemistry of Materials* **1997**, 9, 857-62.

15. Masuda H., Fukuda K., *Science* **1995**, 268, 1466-8.

16. Toh C. S., Kayes B. M., Nemanick E. J., Lewis N. S., *Nano Letters* **2004**, 4, 767-70.

17. Chu S. Z., Inoue S., Wada K., Hishita S., *J Electrochem Soc* **2004**, 151, C38-C44.

18. Vrublevsky I., Parkoun V., Sokol V., Schreckenbach J., *Applied Surface Science* **2004**, 236, 270-7.

19. Jagminas A., Kurtinaitiene M., Angelucci R., Valincius G., *Applied Surface Science* **2006**, 252, 2360-7.

20. Wang J., *Analytical Electrochemistry*, 2nd Edition 2nd Edition, New York, John Wiley & Sons, Inc., **2000**, 209.

21. Chu S.-Z., Wada K., Inoue S., Isogai M., Yasumori A., *Advanced Materials* **2005**, 17, 2115-9.

22. Cannes C., Kanoufi F., Bard A. J., *J Electroanal Chem* **2003**, 547, 83-91.

23. Dijksma M., Boukamp B. A., Kamp B., van Bennekom W. P., *Langmuir* **2002**, 18, 3105-12.

24. Dimitri E., Khoshtariya D. E., Dolidze T. D., Vertova A., Longhi M., Rondinini S., *Electrochem Comm* **2003**, 5, 241-5.

25. Bard A. J. a. F., L. R., *Electrochemical Methods: Fundamentals and Applications*, Second Second, John Wiley and Sons, **2000**, 236.

26. Lohrengel M. M., *Materials Science and Engineering: R: Reports* **1993**, 11, 243-94.
27. Munoz A. G., *Corrosion Science* **2005**, 47, 2307-20.
28. Schmickler W., Schultze J. W., *Modern Aspects of Electrochemistry*, 17 17, **2005**.
29. Schultze J. W., Lohrengel M. M., *Electrochimica Acta* **2000**, 45, 2499-513.
30. Thompson G. E., Furneaux R. C., Wood G. C., *Corrosion Science* **1978**, 18, 481-98.
31. Fukuda Y., Fukushima T., *Bulletin of Chemical Society of Japan* **1980**, 53, 3125-30.
32. Nicholson R. S., *Analytical Chemistry* **1965**, 37, 1351-5.
33. Wada K., Shimohira T., Yamada M., Baba N., *Journal of Materials Science* **1986**, 21, 3810.
34. Kanamori Y., Hane K., Sai H., Yugami H., *Applied Physics Letters* **2001**, 78, 142-3.
35. Amatore C., Saveant J. M., Tessier D., *J Electroanal Chem* **1983**, 147, 39-51.
36. Baeumner A. J., Schlesinger N. A., Slutzki N. S., Romano J., Lee E. M., Montagna R. A., *Analytical Chemistry* **2002**, 74, 1442-8.
37. Booth S., Baleriola C., Rawlinson W. D., *Journal of Medical Virology* **2006**, 78, 619-22.
38. Okochi M., Ohta H., Taguchi T., Ohta H., Matsunaga T., *Electrochimica Acta* **2005**, 51, 952-5.
39. Vetcha S., Abdel-Hamid I., Artanasov P., Ivnitski D., Wikkins E., Hjelle B., *Electroanalysis* **2000**, 12, 1034-8.

40. Tudorache M., Co M., Lifgren H., Emneus J., *Analytical Chemistry* **2005**, 77, 7156-62.

41. Volland H., Neuburger L. M., Schultz E., Grassi J., Perraut F., Creminon C., *Analytical Chemistry* **2005**, 77, 1896-904.

42. Wu L., Chen J., Du D., Ju H., *Electrochimica Acta* **2006**, 51, 1208-14.

43. Palecek E., Kizek R., Havran L., Billova S., Fojta M., *Analytica Chimica Acta* **2002**, 469, 73-83.

44. O'Connor M., Kim S. N., Killard A., Forster R. J., Smyth M. R., Papadimitrakopoulos F., Rusling J. F., *Analyst* **2004**, 129, 1176-80.

45. Invitrogen. *Catalog of Proteomics and Protein Biochemistry Products*. http://probes.invitrogen.com/lit/catalog/1/sections/7830.html (Accessed 5 October 2006).

46. Diggle J. W., Downie T. C., Goulding C. W., *Chemical Reviews* **1969**, 69, 365-405.

47. O'Sullivan J. P., Wood G. C., *Proceedings of the Royal Society A: Mathematical, Physical & Engineering Sciences* **1970**, 317, 511-43.

48. Kang H.-S., Chang Y.-H., Lee C.-W., *Korean Journal of Chemical Engineering* **2000**, 17, 266-72.

49. Shan D., He Y., Wang S., Xue H., Zheng H., *Analytical Biochemistry* **2006**, 356, 215-21.

50. Kanungo M., Kumar A., Contractor A. Q., *Analytical Chemistry* **2003**, 75, 5673-9.

51. Zhao K., Song H., Zhuang S., Dai L., He P., Fang Y., *Electrochem Comm* **2007**, 9, 650-70.

52. Nematollahi D., Mohammad R., *Sensors* **2003**, 3, 534-43.

53. Uosaki K., kazaki K., Kita H., *Analytical Chemistry* **1990**, 62, 652-6.

54. Xian Y., Liu M., Cai Q., Li H., Lu J., Jin L., *Analyst* **2001**, 126, 871-6.

55. Koh G., Agarwal S., Cheow P. S., Toh C.-S., *Electrochimica Acta* **2007**, 52, 2815–21.

56. Burton D. R., *Molecular Immunology* **1985**, 22, 161-206.

57. Werner T. C., Bunting J. R., Cathou R. E., *The Proceedings of the National Academy of Sciences USA* **1972**, 69, 795-9.

58. Sandin S., Ofverstedt L.-G., Wikstro¨m A.-C., Wrange O., Skoglund U., *Structure* **2004**, 12, 409-15.

59. Malmsten M., *Colloids and Surfaces B: Biointerfaces* **1995**, 3, 297-308.

60. Kamyshny A., Magdassi S., *Colloids and Surfaces B: Biointerfaces* **1997**, 9, 147-55.

61. Buijs J., VandenBerg P. A. W., Lichtenbelt J. W. T., Norde W., Lyklema J. J., *Journal of Colloid and Interface Science* **1996**, 178, 594-605.

62. Roberts C. J., Williams P. M., Davies J., Dawkes A. C., Sefton J., Edwards J. C., Haymes A. G., Bestwick C., Davies M. C., Tendler S. J. B., *Langmuir* **1995**, 11, 1822-6.

63. Tang Y. W., Szalai I., Chan K.-Y., *Journal of Physical Chemistry A* **2001**, 105, 9616-23.

64. Tang D., Yuan R., Chai Y., Fu Y., Dai J., Liu Y., Zhong X., *Biosensors and Bioelectronics* **2005**, 21, 539-48.

65. Wilson M. S., Rauh R. D., *Biosensors and Bioelectronics* **2004**, 19, 693–9.

66. Hunt A. R., Hall R. A., Kerst A. J., Nasci R. S., Savage H. M., Panella N. A., Gottfried K. L., Burkhalter K. L., Roehrig J. T., *Journal of Clinical Microbiology* **2002**, 40, 2023-30.

67. Malan A. K., Martins T. B., Hill H. R., Litwin C. M., *Journal of Clinical Microbiology* **2004**, 42, 727-33.

68. Volk D. E., Beasley D. W. C., Kallick D. A., Holbrook M. R., Barrett A. D. T., Gorenstein D. G., *The Journal of Biological Chemistry* **2004**, 279, 38755-61.

69. Beasley D. W. C., Barrett A. D. T., *Journal of Virology* **2002**, 76, 13097-100.

70. Kanai R., Kar K., Anthony K., Gould L. H., Ledizet M., Fikrig E., Marasco W. A., Koski R. A., Modis a. Y., *Journal of Virology* **2006**, 80, 11000-8.

71. Lanciotti R. S., Kerst A. J., Nasci R. S., Godsey M. S., Carl J M., Savage H. M., Komar N., Panella N. A., Allen B. C., Volpe K. E., Davis B. S., Roehrig J. T., *Journal of Clinical Microbiology* **2000**, 38, 4066-71.

72. Gancz A. Y., Campbell D. G., Barker I. K., Lindsay R., Hunter B., *Emerging Infectious Disease* **2004**, 10, 2204-6.

73. Prince H. E., Lape'-Nixon M., Moore R. J., Hogrefe W. R., *Journal of Clinical Microbiology* **2004**, 42, 12-5.

74. Wen J., Arakawa T., Philo J. S., *Analytical Biochemistry* **1996**, 240, 155-66.

75. Chang C.-S., Suen S.-Y., *Journal of Membrane Science* **2006**, 275, 70-81.

76. Wright G. G., Schomaker V., *The Journal of Biological Chemistry* **1948**, 175, 169-77.

77. Chu S. Z., Wada K., Inoue S., Todoroki S., *J Electrochem Soc* **2002**, 149, B321-B7.

78. Liang H., Reich C. F., Pisetsky D. S., Lipsky P. E., *Scandinavian Journal of Immunology* **2001**, 54, 551-63.

79. Todorovic Z., Milonjic S. K., *Journal of the Serbian Chemical Society* **2004**, 69, 1063-72.

80. Collins K. D., *Methods* **2004**, 34, 300-11.

81. Wilhelm P., Pilz I., Palm W., Bauer K., *European Journal of Biochemistry* **1978**, 84, 457-63.

82. Plikyatis B. D., Turner S. H., Gheesling L. L., Carlone G. M., *Journal of Clinical Microbiology* **1991**, 29, 1439-46.

83. Rusling J. F., Zhang Z. Designing Functional Biomolecular Films on Electrodes. In: Rusling JF, ed. Biomolecular Films: Design, Function, and Applications, Vol. Basel: Marcel Dekker, 2003:1-64.

84. Karube I., Nomura Y., *Journal of Molecular Catalysis B: Enzymatic* **2000**, 10, 177-81.

85. Liang J. F., Li Y. T., Yang V. C., *Journal of Pharmaceutical Science* **2000**, 89, 979-90.

86. Wang J., Ciszewski A., Naser N., *Electroanalysis* **1992**, 4, 777-82.

87. Bartlett P. N., Birkin P. R., *Synthetic Metals* **1993**, 61, 15-21.

88. Remirez C. P., Caruana D. J., *Electrochemical Communications* **2006**, 8, 450-4.

89. Li J., Wang H., Deng T., Wu Z., Shen G., Yu R., *Biosensors and Bioelectronics* **2004**, 20, 841-7.

90. Farace G., Lillie G., Hianik T., Payne P., Vadgama P., *Bioelectrochemistry* **2002**, 55, 1-3.

91. Farooqi M., Sosnitza P., Saleemuddin M., Ulber R., Schepert T., *Applied Microbiology and Biotechnology* **1999**, 52, 373-9.

92. Limoges B., Marchal D., Mavre F., Saveant J.-M., *Journal of American Chemical Society* **2006**, 128, 2084-92.

93. Jan U., Husain Q., Saleemuddin M., *Biotechnology and Applied Biochemistry* **2001**, 34, 13-7.

94. Wivanius R. *Electrochemical Biosensors* [M.Sc.]. Singapore: National University of Singapore, **2007**, 122.

95. Pierce D. T., Unwin P. R., Bard A. J., *Analytical Chemistry* **1992**, 64, 1795-804.

96. Zhao C., Wittstock G., *Analytical Chemistry* **2004**, 76, 3145-54.

97. Paisley U. o. *Glucose oxidase - mechanism of action*. http://www-biol.paisley.ac.uk/marco/Enzyme_Electrode/chapter3/chapter3_page7.htm (Accessed 26 April 2008).

98. Cass A. E., Davis G., Francis G. D., Hill H. A., Aston W. J., Higgins I. J., Plotkin E. V., Scott L. D., Turner A. P., *Analytical Chemistry* **1984**, 56, 667-71.

99. Szucs A., Hitchens G. D., Bockris J. O. M., *Journal of Electroanalytical Chemistry* **1989**, 136, 3748-55.

100. Ligler F. S., Bhatia S., Shriver-lake L. C., Georger J., Calvert J., Dulcey C. Surface modification to create regions resistant to adsorption of biomolecules. Vol. USA: Navy US. (US) and Geo Centers Inc. (US), 1995:10.

101. Quinto M., Ciancio A., Zambonin P. G., *Journal of Electroanalytical Chemistry* **1998**, 448, 51-9.

102. Moridera N., Yamamoto M., Okumura W., Sugawara M., *Analytical Sciences* **2007**, 23, 39-44.

103. Wei C., Bard A. J., Mirkin M. V., *Journal of Physical Chemistry* **1995**, 99, 16033-42.

104. Parker J. W., Schwartz C. S., *Biotechnology and Bioengineering* **1987**, 30, 724-35.

105. Atkinson B., Lester D. E., *Biotechnology and Bioengineering* **1974**, 16, 1299-320.

106. Weibel M. K., Bright H. J., *JOurnal of Biological Chemistry* **1971**, 246, 2734-44.

107. Williams A. K., Hupp J. T., *Journal of American Chemical Society* **1998**, 120, 4366-71.

108. Brennan J. D., Rupcich N. Multicomponent Protein Microarrays. Vol. Canada: Univ, Mcmaster (CA), 2003:44.

109. Badjic J. D., Kostic N. M., *Chemistry of Materials* **1999**, 11, 3671-9.

110. Yokoyama K., Kayanuma Y., *Anal Chem* **1998**, 70, 3368-76.

111. Yokoyama K., Kayanuma Y., *Analytical Chemistry* **1998**, 70, 3368-76.

112. Buijs J., Hlady V., *Current Opinion in Biotechnology* **1996**, 7, 72-7.

113. Howells A. R., Zambrano P. J., Collinson M. M., *Analytical Chemistry* **2000**, 72, 5265-71.

114. Stalgren J. J. R., Eriksson J., Boschkova K., *Journal of Colloid and Interface Science* **2002**, 253, 190-5.

115. Murali S., *Bulletin of Materials Science* **2000**, 23, 159-63.

116. Cheow P.-S., Liu L., Toh C.-S., *Surface and Interface Analysis* **2007**, 39, 601-10.

117. Baron M. H., Revault M., Servagent-Noinville S., Abadie J., Quiquampoix H., *Journal of Colloid and Interface Science* **199**, 214, 319-32.

118. Noinville S., Revault M., Baron M.-H., *Biopolymers (Biospectroscopy)* **2002**, 67, 323-6.

119. Zoungrana T., Findenegg G. H., Norde W., *Journal of Colloid and Interface Science* **1997**, 190, 437-48.

120. Zardeneta G., Mukai H., Marker V., Milam S. B., *Journal of Oral and Maxillofacial Surgery* **1996**, 54, 873-8.

121. Swoboda B. E. P., Massey V., *JOurnal of Biological Chemistry* **1965**, 240, 2209-15.

122. Ekanayake E. M. I. M., Preethichandra D. M. G., Kaneto K., *Biosensors and Bioelectronics* **2007**, 23, 107-13.

123. Zhua P., Shelton D. R., Karns J. S., Sundaram A., Li S., Amstutz P., Tang C.-M., *Biosensors and Bioelectronics* **2005**, 21, 678-83.

124. Baeumner A., Jones C., Wong C., Price A., *Analytical and Bioanalytical Chemistry* **2004**, 378, 1587-93.

125. Zaytseva N., Montagna R. A., Baeumner A. J., *Analytical Chemistry* **2005**, 77, 7520-7.

126. Li Y. J., Xie W. H., Fang G. J., *Analytical and Bioanalytical Chemistry* **2008**, 390, 2049-57.

127. Fähnrich K. A., Pravda M., Guilbault G. G., *Biosensors and Bioelectronics* **2003**, 18, 73-82.

128. Carter R. M., Blake R. C., Nguyen T. D., Bostanian L. A., *Biosensors and Bioelectronics* **2003**, 18, 69-72.

129. Kauffman E. B., Jones S. A., II A. P. D., Ngo K. A., Bernard K. A., Kramer L. D., *Journal of Clinical Microbiology* **2003**, 41, 3661-7.

130. Tatsumi H., Katanoa H., *Journal of Electroanalytical Chemistry* **2008**, 614, 61-6.

131. Duncana H., Lasia A., *Electrochimica Acta* **2007**, 52, 6195-205.

132. Ahmadia A., Norouzib P., Ganjalib M. R., *Progress in Organic Coatings* **2006**, 56, 227-33.

133. Anastassiou C. A., Ducros N., Parker K. H., O'Hare D., *Analytical Chemistry* **2006**, 78, 4383-9.

134. Haddox R. M., Finklea H. O., *Journal of Physical Chemistry B* **2004**, 108, 1694-700.

135. Shiu K.-K., Zhang Y., Wong K.-Y., *Journal of Electroanalytical Chemistry* **1995**, 389, 105-14.

136. Kelso E., McLean J., Cardosi M. F., *Electroanalysis* **2000**, 12, 490-4.

137. Azek F., Grossiord C., Joannes M., Limoges B., Brossier P., *Analytical Biochemistry* **2000**, 284, 107-13.

138. Wang H., Liu Y., Yang Y., Deng T., Shen G., Yu R., *Analytical Biochemistry* **2004**, 324, 219-26.

139. Anderson G. P., Jacoby M. A., Ligler F., King K. D., *Biosensors and Bioelectronics* **1997**, 12, 329-36.

CHAPTER VII

APPENDIX I - PUBLICATIONS

Part of this research work had been submitted for the degree of Bachelor of Science (Hons). These include the description of the novel pipette anodization and the effect of alumina channel diameters on the detection of glucose oxidase in Chapter I and II respectively. However, all other data provided in this thesis, including the electrochemical investigation of the alumina barrier layer and scanning electron microscopy studies in Chapter I as well as control experiments, selectively studies and electrochemical studies in Chapter II were completed after the award of the degree of Bachelor of Science (Hons).

The research discussed in this thesis had been presented at the following conferences.

1) Koh Guiwan, Lim Hui Si, Ng Mah Lee Mary, Toh Chee-Seng, Development of a Novel Electrochemical Immunosensor for West Nile Virus, Oral Presentation, ACS Division of Analytical Chemistry Pittcon, March 2 – 7, 2008, New Orleans, Louisiana, USA
2) Koh Guiwan on behalf of Dr Toh Chee-Seng, Immunoglobulin-Nanoporous Alumina Materials for Novel Electrochemical Immunosensors, Oral Presentation, American Chemical Society Meeting & Exposition, March 26 – 30, 2006, Atlanta, Georgia, USA

In addition, Chapter I, Chapter II and Chapter V of this thesis had been published in the following journal articles respectively:

1) Koh Guiwan, Shuchi Agarwal, Cheow Pui-Sze, Toh Chee-Seng, Characterization of the barrier layer of nanoporous alumina films prepared using two different contact configurations, *Electrochimica Acta*, 2007, 52 , 2815-2821
2) Koh Guiwan, Shuchi Agarwal, Cheow Pui-Sze, Toh Chee-Seng, Development of a membrane-based electrochemical immunosensor, *Electrochimica Acta*, 2007, 53, 803–810
3) Koh Guiwan, Ridha Wivanius, Woo Ming Shue Michelle, Toh Chee-Seng, Electroanalytical Studies of Immunoglobulin-bound Glucose Oxidase, *Journal of Electrochemical Society*, Accepted

Descriptions of the work in Chapter I and II were also briefly mentioned in the following book chapter.

1) Koh Guiwan and Toh Chee-Seng, Nanoscale Bioanalysis using Electrochemical Methods in Encyclopedia of Nanoscience and Nanotechnology, 2nd Edition, H. S. Nalwa, Editor, American Scientific Publishers, Valencia, 2008

A manuscript describing the determination of West Nile Virus domain III and particles utilising the developed membrane-based electrochemical immunosensor is also in preparation.

CHAPTER XI

APPENDIX II - GRANTED COPYRIGHT PERMISSIONS

Permission 1

This is a License Agreement between Guiwan Koh ("You") and Nature Publishing Group ("Nature Publishing Group"). The license consists of your order details, the terms and conditions provided by Nature Publishing Group, and the payment terms and conditions.

License Number	1942690518736
License date	May 05, 2008
Licensed content publisher	Nature Publishing Group
Licensed content publication	Nature
Licensed content title	The formation of controlled-porosity membranes from anodically oxidized aluminium
Licensed content author	R. C. Furneaux, W. R. Rigby, A. P. Davidson
Volume number	
Issue number	
Pages	
Year of publication	1989
Portion used	Figures / tables
Requestor type	Student
Type of Use	Thesis / Dissertation
Total	0.00 USD
Terms and Conditions	

Terms and Conditions for Permissions

Nature Publishing Group hereby grants you a non-exclusive license to reproduce this material for this purpose, and for no other use, subject to the conditions below:

1. NPG warrants that it has, to the best of its knowledge, the rights to license reuse of this material. However, you should ensure that the material you are requesting is original to Nature Publishing Group and does not carry the copyright of another entity (as credited in the published version). If the credit line on any part of the material you have requested indicates that it was reprinted or adapted by NPG with permission from another source, then you should also seek permission from that source to reuse the material.

2. Permission granted free of charge for material in print is also usually granted for any

electronic version of that work, provided that the material is incidental to the work as a whole and that the electronic version is essentially equivalent to, or substitutes for, the print version. Where print permission has been granted for a fee, separate permission must be obtained for any additional, electronic re-use (unless, as in the case of a full paper, this has already been accounted for during your initial request in the calculation of a print run). NB: In all cases, web-based use of full-text articles must be authorized separately through the 'Use on a Web Site' option when requesting permission.

3. Permission granted for a first edition does not apply to second and subsequent editions and for editions in other languages (except for signatories to the STM Permissions Guidelines, or where the first edition permission was granted for free).

4. Nature Publishing Group's permission must be acknowledged next to the figure, table or abstract in print. In electronic form, this acknowledgement must be visible at the same time as the figure/table/abstract, and must be hyperlinked to the journal's homepage.

5. The credit line should read:

   Reprinted by permission from Macmillan Publishers Ltd: [JOURNAL NAME] (reference citation), copyright (year of publication)

   For AOP papers, the credit line should read:

   Reprinted by permission from Macmillan Publishers Ltd: [JOURNAL NAME], advance online publication, day month year (doi: 10.1038/sj.[JOURNAL ACRONYM].XXXXX)

6. Adaptations of single figures do not require NPG approval. However, the adaptation should be credited as follows:

   Adapted by permission from Macmillan Publishers Ltd: [JOURNAL NAME] (reference citation), copyright (year of publication)

7. Translations of 401 words up to a whole article require NPG approval. Please visit http://www.macmillanmedicalcommunications.com for more information. Translations of up to a 400 words do not require NPG approval. The translation should be credited as follows:

   Translated by permission from Macmillan Publishers Ltd: [JOURNAL NAME] (reference citation), copyright (year of publication).

We are certain that all parties will benefit from this agreement and wish you the best in the use of this material. Thank you.

Permission 2

Permission is granted – subject to the conditions outlined below – for the following:

Figure from:
Jessensky O., Muller F., Gosele U., Applied Physics Letters 1998, 72, 1173-5.

To be used in the following manner:

Reproduced in your thesis for submission to the National University of Singapore.

1. The American Institute of Physics grants you the right to reproduce the material indicated above on a one-time, non-exclusive basis, solely for the purpose described. Permission must be requested separately for any future or additional use.

2. This permission pertains only to print use and its electronic equivalent, including CD-ROM or DVD.

3. The following copyright notice must appear with the material (please fill in the information indicated by capital letters): "Reprinted with permission from [FULL CITATION]. Copyright [PUBLICATION YEAR], American Institute of Physics." Full citation format is as follows: Author names, journal title, Vol. #, Issue #, Page #, Year of publication. For an article, the copyright notice must be printed on the first page of the article or book chapter. For figures, photographs, covers, or tables, the notice may appear with the material, in a footnote, or in the reference list.

4. This permission does not apply to any materials credited to sources other than the copyright holder.

5. If you have not already done so, please attempt to obtain permission from at least one of the authors. The author's address can be obtained from the article.

Please let us know if you have any questions.

Sincerely,
Susann Brailey

Office of the Publisher, Journals and Technical Publications
Rights & Permissions
American Institute of Physics
Suite 1NO1
2 Huntington Quadrangle
Melville, NY 11747-4502
516-576-2268 TEL
516-576-2450 FAX
rights@aip.org

Permission 3

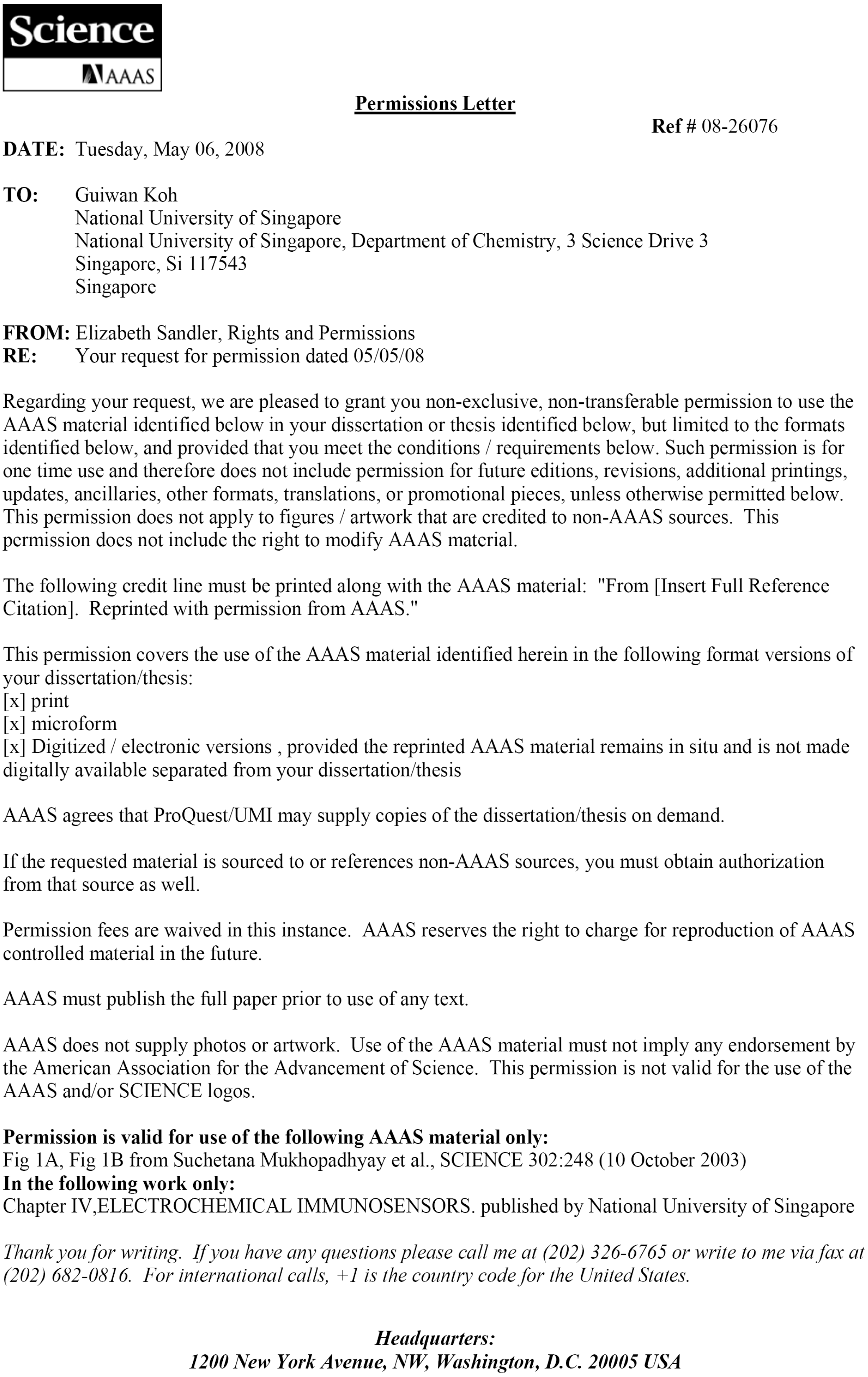

Science
AAAS

Permissions Letter

Ref # 08-26076

DATE: Tuesday, May 06, 2008

TO: Guiwan Koh
National University of Singapore
National University of Singapore, Department of Chemistry, 3 Science Drive 3
Singapore, Si 117543
Singapore

FROM: Elizabeth Sandler, Rights and Permissions
RE: Your request for permission dated 05/05/08

Regarding your request, we are pleased to grant you non-exclusive, non-transferable permission to use the AAAS material identified below in your dissertation or thesis identified below, but limited to the formats identified below, and provided that you meet the conditions / requirements below. Such permission is for one time use and therefore does not include permission for future editions, revisions, additional printings, updates, ancillaries, other formats, translations, or promotional pieces, unless otherwise permitted below. This permission does not apply to figures / artwork that are credited to non-AAAS sources. This permission does not include the right to modify AAAS material.

The following credit line must be printed along with the AAAS material: "From [Insert Full Reference Citation]. Reprinted with permission from AAAS."

This permission covers the use of the AAAS material identified herein in the following format versions of your dissertation/thesis:
[x] print
[x] microform
[x] Digitized / electronic versions , provided the reprinted AAAS material remains in situ and is not made digitally available separated from your dissertation/thesis

AAAS agrees that ProQuest/UMI may supply copies of the dissertation/thesis on demand.

If the requested material is sourced to or references non-AAAS sources, you must obtain authorization from that source as well.

Permission fees are waived in this instance. AAAS reserves the right to charge for reproduction of AAAS controlled material in the future.

AAAS must publish the full paper prior to use of any text.

AAAS does not supply photos or artwork. Use of the AAAS material must not imply any endorsement by the American Association for the Advancement of Science. This permission is not valid for the use of the AAAS and/or SCIENCE logos.

Permission is valid for use of the following AAAS material only:
Fig 1A, Fig 1B from Suchetana Mukhopadhyay et al., SCIENCE 302:248 (10 October 2003)
In the following work only:
Chapter IV,ELECTROCHEMICAL IMMUNOSENSORS. published by National University of Singapore

Thank you for writing. If you have any questions please call me at (202) 326-6765 or write to me via fax at (202) 682-0816. For international calls, +1 is the country code for the United States.

Headquarters:
1200 New York Avenue, NW, Washington, D.C. 20005 USA